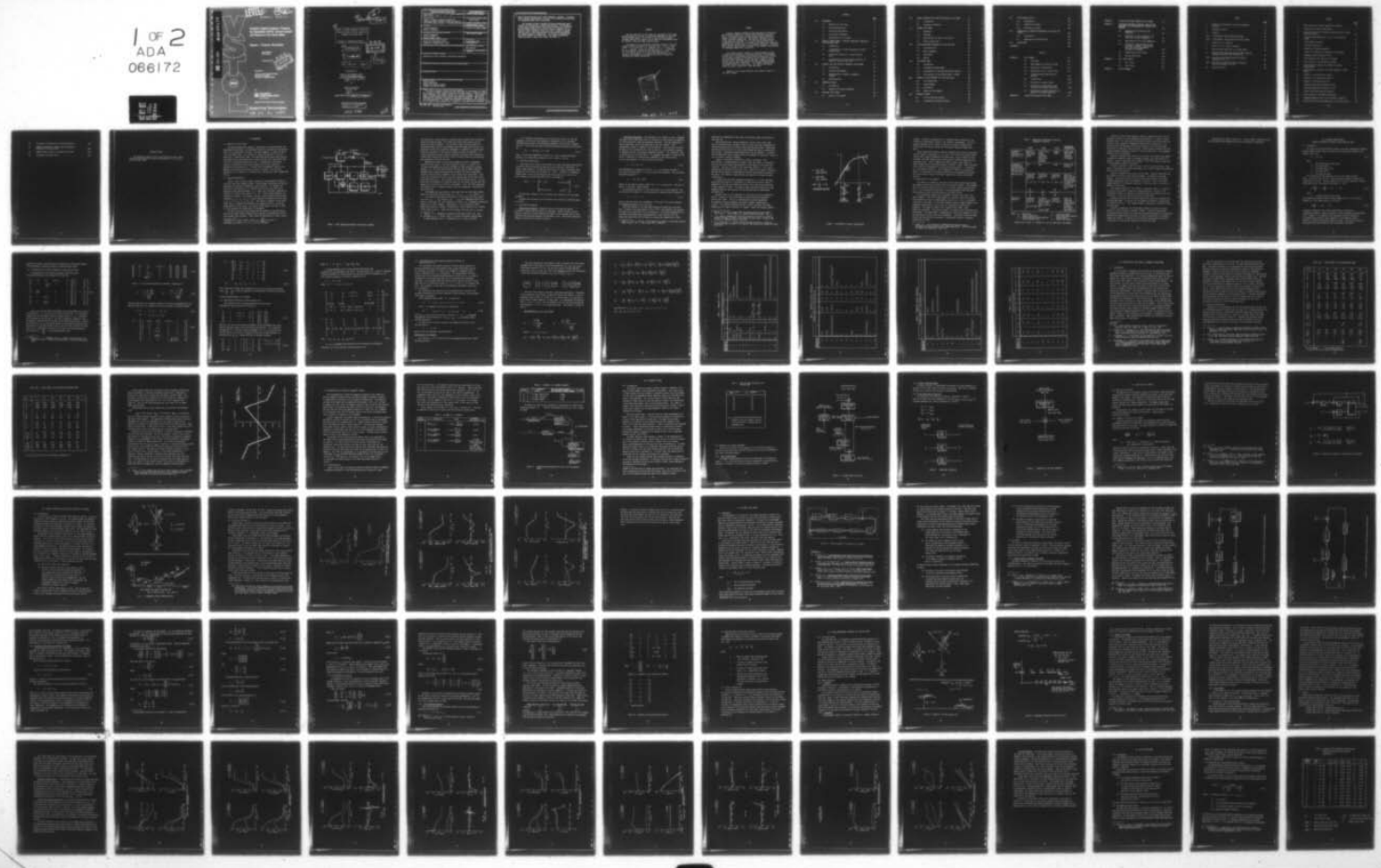
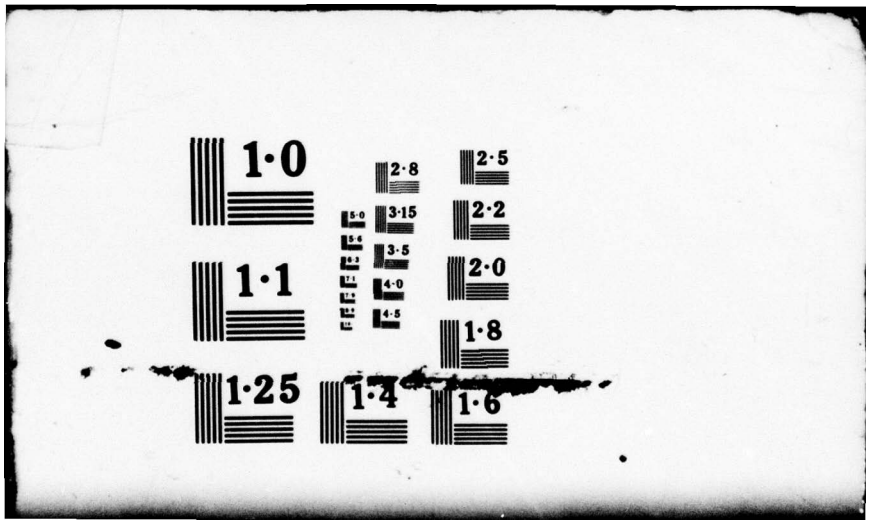
AD-A066 172 VOUGHT CORP DALLAS TEX F/G 1/2
VOLAR: A DIGITAL COMPUTER PROGRAM FOR SIMULATING VSTOL AIRCRAFT--ETC(U)
DEC 78 J WOLKOVITCH, B B BRASSELL N62269-77-R-0389
UNCLASSIFIED 2-32000/8R-41672-VOL-1 NADC-77123-30-VOL-1 NL

1 OF 2
ADA
066172




1·0
1·1
1·25
1·4
1·6
1·8
2·0
2·2
2·5
2·8
3·15
3·5
4·0
4·5

DDC FILE COPY
AD A066172

LEVEL II

NADC Report No. 77123-30, Vol. I

VOLAR: A Digital Computer Program for Simulating VSTOL Aircraft Launch and Recovery from Small Ships

Volume I - Program Description

Julian Wolkovitch
Billy B. Brassell

DDC
RECEIVED
MAR 22 1979
C

14 December 1978

Performed for:

NAVAL AIR DEVELOPMENT CENTER
Warminister, Pennsylvania
Contract No.: N 62269-77-R-0389

by

VOUGHT CORPORATION
an LTV company

Approved for Public Release: Distribution Unlimited

R&D

Supporting Technologies

79 03 21 013

(18) NADC Report No. (19) 77123-30, Vol. 1

(6)

VOLAR: A Digital Computer Program for Simulating VSTOL Aircraft Launch and Recovery from Small Ships.

Volume I. Program Description.

DDC
RECEIVED
MAR 22 1979
C

(10) Julian Wolkovitch
Billy B. Brassell

(11) 14 December 1978

(12) 129 p.

(9) Final Rept.,

Performed for:

Naval Air Development Center
Warminster, Pennsylvania
Contract No: N 62269-77-R-0389
(15)

by

Vought Corporation
Dallas, Texas

(14)
Vought Report No. 2-32000/8R-41672, Vol. 1

This document has been approved for public release and sale; its distribution is unlimited.

392 990

B

SECURITY CLASSIFICATION OF THIS PAGE (When Data Entered)

REPORT DOCUMENTATION PAGE		READ INSTRUCTIONS BEFORE COMPLETING FORM
1. REPORT NUMBER NADC-77123-30, Vol. I	2. GOVT ACCESSION NO.	3. RECIPIENT'S CATALOG NUMBER
4. TITLE (and Subtitle) VOLAR: A Digital Computer Program for Simulating VSTOL Aircraft Launch and Recovery From Small Ships; Volume I, Program Description		5. TYPE OF REPORT & PERIOD COVERED Final Report 6. PERFORMING ORG. REPORT NUMBER 2-32000/8R-41672, Vol. I
7. AUTHOR(s) Julian Wolkovitch Billy B. Brassell		8. CONTRACT OR GRANT NUMBER(s) N 62269-77-R-0389 new
9. PERFORMING ORGANIZATION NAME AND ADDRESS Vought Corporation P.O. Box 225907 Dallas, Texas 75265		10. PROGRAM ELEMENT, PROJECT, TASK AREA & WORK UNIT NUMBERS
11. CONTROLLING OFFICE NAME AND ADDRESS Naval Air Development Center Warminster, Pennsylvania 18974		12. REPORT DATE 14 December 1978 13. NUMBER OF PAGES 119
14. MONITORING AGENCY NAME & ADDRESS(if different from Controlling Office)		15. SECURITY CLASS. (of this report) Unclassified 15a. DECLASSIFICATION/DOWNGRADING SCHEDULE

16. DISTRIBUTION STATEMENT (of this Report)

Approved for public release; distribution unlimited.

17. DISTRIBUTION STATEMENT (of the abstract entered in Block 20, if different from Report)

18. SUPPLEMENTARY NOTES

19. KEY WORDS (Continue on reverse side if necessary and identify by block number)

VSTOL Aircraft
Flight Simulation
Human Pilot Analytic Models
Guidance and Control Theory

20. ABSTRACT (Continue on reverse side if necessary and identify by block number)

A digital computer program has been developed for simulating the launch and recovery of VSTOL aircraft operating from small ships. Volume I of this report describes the program, Volume II is the user's manual. The program, known as VOLAR (Vought Launch and Recovery Dynamics Program), employs the computational technique of nonlinear covariance propagation. This permits the time histories of the means and variances of all system state variables to be computed from a single run, as opposed to the Monte Carlo technique,

DD FORM 1 JAN 73 1473 EDITION OF 1 NOV 65 IS OBSOLETE
S/N 0102-014-6601 |

SECURITY CLASSIFICATION OF THIS PAGE (When Data Entered)

which requires multiple runs, plus subsequent averaging. Typically, VOLAR requires approximately 7 percent of the computer time required for comparable Monte Carlo simulations.

The program includes a general airframe mathematical model suitable for helicopters or fixed-wing aircraft. The airwake of a small ship is also modeled and ship motion models are included. Two alternative models of the human pilot are supplied, one is based on verbal adjustment rules, the other is based on optimal control theory, utilizing performance index parameters deduced from manned simulator experiments. The program is demonstrated for AV-8A recovery on a small ship. The trends predicted by VOLAR are shown to agree with flight test data.

FOREWORD

The work described in this report was sponsored by the Flight Dynamics Branch of Air Vehicle Technology Department of the Naval Air Development Center. Mr. Ronald L. Nave served as project engineer and technical monitor for the Naval Air Development Center Mr. Carmen J. Mazza was NADC program manager.

The authors wish to thank the following individuals for their prompt response to requests for technical data: Mr. R. L. Nave; Lt/Col. J. D. Dillow; Mr. R. O. Anderson, Mr. S. J. Craig, and Dr. V. J. Lebacqz. Thanks are also due to Mr. R. L. Fortenbaugh who developed the ship motion and airwake models, and to Mr. R. B. Hughes and Mr. W. C. Waits who made extensive and valuable contributions to programming the analytic models and developed the COMPASS subroutines.



79 03 21 013

SUMMARY

A digital computer program has been developed for simulating the launch and recovery of VSTOL aircraft operating from small ships. The program, known as VOLAR (Vought Launch and Recovery Dynamics Program), employs the computational technique of non-linear covariance propagation. This permits the time histories of the means and variances of all system state variables to be computed from a single run, as opposed to the Monte Carlo technique, which requires multiple runs, plus subsequent averaging. Typically, VOLAR requires approximately 7 percent of the computer time required for comparable Monte Carlo simulations.

The program includes a general airframe mathematical model suitable for helicopters or fixed-wing aircraft. The airwake of a small ship is also modeled and ship motion models are included. Two alternative models of the human pilot are supplied, one is based on verbal adjustment rules, the other is based on optimal control theory, utilizing performance index parameters deduced from manned simulator experiments. The program is demonstrated for AV-8A recovery on a small ship. The trends predicted by VOLAR are shown to agree with flight test data.

Volume I of this report describes the program, Volume II is the user's manual.

CONTENTS

		Page
1.0	BACKGROUND	1
	1.1 Objective of this Study	1
	1.2 System Representation	1
	1.3 Statistical Descriptors	4
	1.4 Calculation Procedures	4
	1.5 Organization of this Report	8
2.0	AIRCRAFT DYNAMIC MODEL: AIRCRAFT EQUATIONS OF MOTION IN STATE-VARIABLE FORM	12
	2.1 Introduction	12
	2.2 Transformation of Lateral Equations to State-Variable Form	13
	2.3 Longitudinal Equations in State-Variable Form	15
	2.4 Transformation of Cross-Coupled Equations of Motion to State-Variable Form	17
3.0	AIRCRAFT DATA AND STABILITY AUGMENTER SYSTEM MODEL	24
	3.1 Introduction	24
	3.2 AV-8A and AV-8B Models	25
	3.3 Representation of Stability Augmenter Systems	30
	3.4 AV-8A Autopilot	30
4.0	ATMOSPHERIC MODEL	33
	4.1 Introduction	33
	4.2 Summation of Airwake Components	34
5.0	CLASSICAL PILOT MODEL	38
	5.1 Types of Pilot Model	38

6.0 EXAMPLE APPROACH FOR AV-8A WITH CLASSICAL PILOT MODEL . 41

6.1 Introduction 41

6.2 Discussion of Results 43

7.0 OPTIMAL PILOT MODEL 48

7.1 Background 48

7.2 The Model 51

7.3 Modifications for Multi Axis Control 61a

7.4 Visual Landing Aids 61a

8.0 AV-8A LONGITUDINAL APPROACH IN A LOW SEA-STATE . . . 62

8.1 Task Description 62

8.2 Model Components 62

8.3 Ship Motion 66

8.4 Results 67

9.0 SHIP MOTION MODEL 79

9.1 Introduction 79

9.2 The RAOH Ship Motion Model 79

9.3 Approximation of the RAOH Ship Motion Spectra . 80

9.4 Incorporation of Ship Motion Model in VOLAR. . 84

10.0 EXAMPLE OF AV-8A RECOVERY IN A HIGH SEA-STATE. . . . 89

10.1 Task Description. 89

10.2 Element Models 89

10.3 Ship Motion 91

10.4 Results of the Example. 93

11.0 PROXIMITY EFFECTS 95

11.1 List of Proximity Effects. 95

11.2 Simulation of Proximity Effects. 97

12.0 MISCELLANEOUS TOPICS 99

12.1 Introduction 99

12.2 Probability Ellipses 99

12.3 Simulation of Launch 101

13.0 CORRELATION OF SIMULATED APPROACHES WITH FLIGHT TEST RESULTS 103

13.1 Introduction 103

13.2 Comparison with VOLAR Results 105

14.0 CONCLUSIONS 106

REFERENCES 107

VOLUME II

APPENDIX A. USER'S MANUAL. A-1

A.1 Philosophy A-2

A.2 Some Comments on the Use of VOLAR . . A-2

A.3 Description of Subroutines. A-3

A.4 Description of the I and R Arrays . . A-7

A.5 The Main Program (Description of Options). A-9

A.6 Program Flow A-60

A.7 Discussion of Control Cards A-60

A.8 Discussion of Input Deck for the Classical Pilot Model Simulation. . . A-64

A.9 Discussion of an Input Deck for the Optimal Pilot Model Simulation A-69

APPENDIX B. LISTING FOR CLASSICAL PILOT MODEL B-1

APPENDIX C. LISTING FOR OPTIMAL CONTROLLER PILOT MODEL . . C-1

APPENDIX D. DESCRIBING FUNCTIONS OF GENERAL SINGLE-VALUED NONLINEARITIES REPRESENTABLE BY STRAIGHT-LINE SEGMENTS D-1

D.1 Decomposition into Odd and Even Components D-2

D.2 Separation of the Nonlinearity into Even, Odd, and Bias Components . . . D-3

D.3 Approximation to the Even Components . D-4

D.4 Routines for Computing Describing Functions of General Single-Valued Nonlinearities Represented by Straight-Line Segments D-6

D.5 Common Block Initialization D-9

D.6 Routine Description D-12

APPENDIX E. THE I AND R ARRAYS E-1

E.1 The I Array. E-2

E.2 The R Array. E-5

APPENDIX F. LIST OF SYMBOLS F-1

TABLES

		Page
1.	Comparison of Nonlinear Covariance Propagation Programs	9
2.	Transposed F-Matrix.	20
3.	G-Matrix	23
4(a).	"Single-Model" AV-8B Longitudinal Model	26
4(b).	"Single-Model" AV-8B Lateral-Directional Model.	27
5.	AV-8A & B S.A.S. Dynamics.	31
6.	AV-8A & B S.A.S. Control Authority.	32
7.	Wind-Over-Deck Conditions for Airwake Model.	34
8.	Candidate Ship Speed-Wave Direction-Wave Spectrum Parameters-Wind-Over-Deck Combinations	81
9(a).	Equivalent Ship Motion Response Parameters: Longitudinal (at C.G.).	85
9(b).	Equivalent Ship Motion Response Parameters: Lateral-Directional (at C.G.)	86
10.	Proximity Effects	96

FIGURES

		Page
1.	VSTOL Launch and Recovery System Block Diagram. . . .	2
2.	Illustration of Quasi-Linearization	7
3.	Nonlinear Variation of AV-8B Yaw Acceleration (N') Versus Sideslip Velocity	29
4.	Simplified Representation of S.A.S. for Fly-By-Wire System	32
5.	Airwake Model Flow Chart	35
6.	Turbulence Simulation	36
7.	Summation of Airwake Components.	37
8.	Lateral Pilot Model for AV-8A Hover and Low-Speed. . .	40
9.	Commanded Lateral Approach Profile.	42
10.	AV-8A Approach with Classical Pilot Model	44
11.	Block Diagram of the Optimal Pilot Model.	49
12.	Block Diagram of Optimal Pilot Model with Padé Approximation	53
13.	Block Diagram of Optimal Pilot Model Employed in VOLAR Program.	54
14.	Elements of the Generalized F-Matrix	61
15.	Elements of the Generalized G-Matrix	61
16.	Schematic of AV-8A Landing Task.	63
17.	Commanded Longitudinal Approach Profile	64
18.	Simulated Approaches with Optimal Pilot	69
19.	Typical Ship Motion Response Spectrum.	83
20.	Block Diagram for Ship Motion Simulation.	87
21.	Commanded Approach Profile for Sea-State 5 Condition. .	90
22.	Modified Pilot Altitude Command Due to Ship Heave Motion	92

23. Flow Chart for Simulation of Proximity Effects. . . . 98

24. Compact Presentation: Mean Values and Degree of Randomness of Two Variables 100

25. Example VOLAR Printout of Probability Ellipses. . . . 102

26. LPD Dynamic Interface Chart 104

EXECUTIVE GUIDE

The reader who wishes to get a quick overview of this report without going into details should read Sections 14, 1, 13, 6, 8, and 10 in that order.

1.0 BACKGROUND

1.1 Objective of this Study

The study reported here supports a broad group of related research and development efforts which are ultimately directed at enlarging the operational limits of sea-based VSTOL aircraft. Particular emphasis is placed on operations from small ships. It is desired to assess the feasibility of such operations in quantitative terms. For some applications these terms describe the probability of safe operation of a given airplane from a particular type of ship in a specified wind and sea state. Alternatively, quantitative stability and control criteria may be sought which yield a specified probability of safe operation. In either case a mathematical model of the dynamics of the launch and recovery system is required. The principal objectives of this report are to develop such a system model and to demonstrate its use.

1.2 System Representation

Figure 1 shows the major dynamic elements of our mathematical model of the VSTOL launch and recovery system. The positional coordinates and velocity components of interest are denoted as state variables. For example, the position of the airplane c.g. in inertial space at any given time may be denoted by three state variables x, y, z, which are conveniently expressed as elements of a column state vector $\{x, y, z\}^T$*. Other system parameters are adjoined as necessary. For example, the ship inertial position and velocity components x_s, y_s, z_s, $\dot{x}_s$, $\dot{y}_s$, $\dot{z}_s$ can be adjoined to augment the state vector to $\{x, y, z, x_s, y_s, z_s, \dot{x}_s, \dot{y}_s, \dot{z}_s\}^T$. The number of elements of the state vector that is required to characterize the complete system is called the dimensionality of the system. The overall system model is written in terms of state variables for convenience in programming.

The most significant inputs come from the atmospheric and sea motions, which at any given instant produce certain changes or perturbations of ship and airplane state variables. Other inputs are manifested as "noise" within

*Throughout this report column vectors, e.g., $\begin{bmatrix} x \\ y \\ z \end{bmatrix}$ are written as transposed row vectors, e.g., $\{x, y, z\}^T$ to save space.

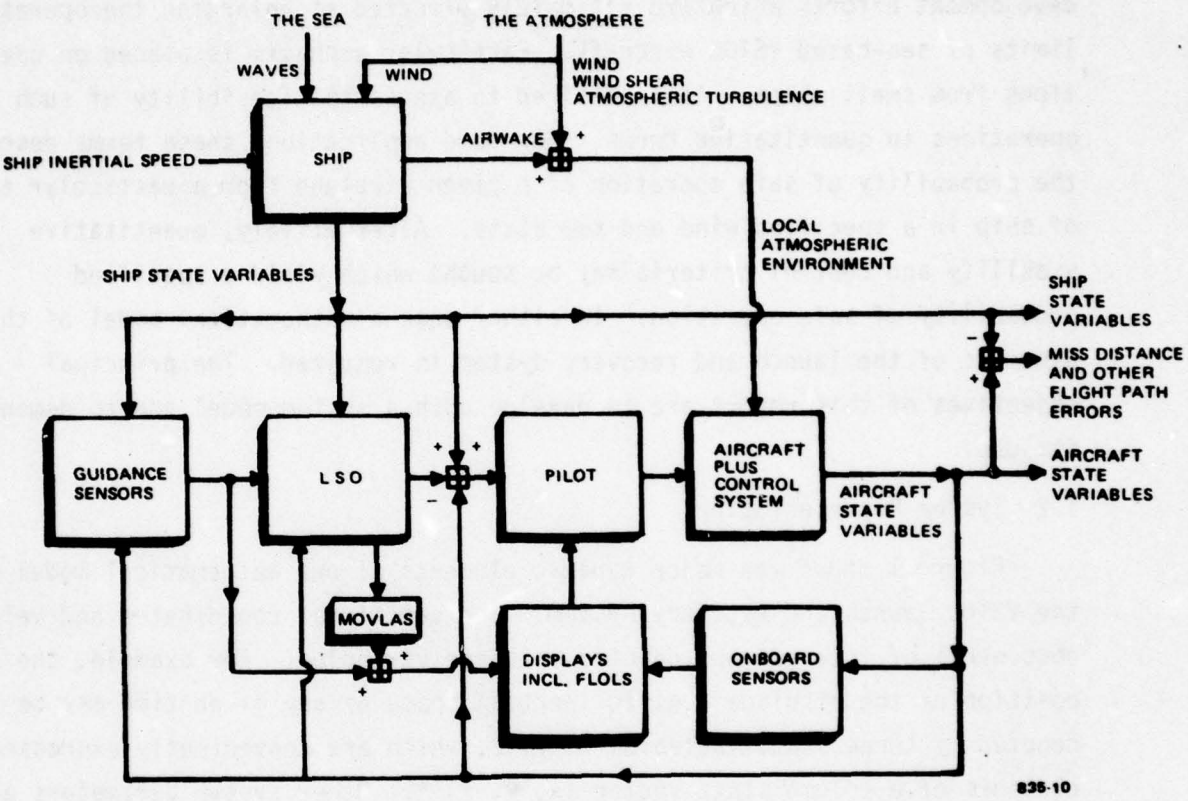


FIGURE 1 VSTOL LAUNCH AND RECOVERY SYSTEM BLOCK DIAGRAM

the system, e.g., noisy sensors of airplane state variables such as angle-of-attack and sideslip angle. For simplicity, these noise sources are not explicitly shown in Figure 1. The principal inputs (wind and waves) are correlated because the sea state depends upon the steady wind and the r.m.s. magnitude of the wind fluctuations (atmospheric turbulence) is approximately linearly proportional to the mean wind speed, as shown in Reference 1. A further correlation results from the wind/ship interaction which produces an airwake which affects the airplane in the vicinity of the ship, particularly when approaching from the lee side.

Mathematical models of each system element are given in subsequent sections of this report. The block diagram of Figure 1 is general, and includes some elements which may be omitted from some launch and recovery systems, e.g., the LSO (Landing Signals Officer) and the MOVLAS (Manually Operated Visual Landing and System) which permits the LSO to communicate visually with the pilot in addition to his verbal radio instructions. Such pilot aids enlarge the portion of the total system state vector that can be perceived by the pilot. This portion is called the display vector. Its size quantifies the complexity and sophistication of the display and indicates the capability of the pilot to sense his environment. Thus, for night approaches the display vector is generally smaller than for approaches in conditions of good visibility.

The mathematical description of the system requires two further vectors. These are firstly the control vector $\{u\} = \{\delta_1, \delta_2, \ldots\ldots \delta_n\}^T$, where $\delta_1, \delta_2, \ldots\ldots\delta_n$ are the aircraft control deflections, and secondly the noise vector $\{w\} = \{w_1, w_2, \ldots\ldots w_m\}^T$ where $w_1, w_2, \ldots\ldots w_m$, are independent white noise sources. Physically all noise sources are colored, e.g., atmospheric turbulence, sensor noise, pilot "remnant" (Reference 2). It is customary to model these noise sources as outputs of hypothetical filters forced by $\{w\}$, instead of the actual noise w', where the prime denotes that the noise is colored.

---

1. Houbolt, J. C., Atmospheric Turbulence, AIAA Paper 72-219, Jan. 1972.
2. Kleinman, D. L., S. Baron, and W. H. Levison, An Optimal Control Model of Human Response, Part I. Automatica, Vol. 6, 1970, p 357-369.

It is frequently convenient to split the control vector {u} into two components, one derived from feedbacks of components of {x}, the other representing open-loop or pre-programmed components, which can be included with {w}. This allows the system linearized dynamical equations to be written as:

$$\dot{\{x\}} = [F(t)]\{x\} + [\Gamma(t)]\{w\} \tag{1.1}$$

where {x} has been augmented to include {u} , and F includes additional equations, not stated here, relating {x} to {u} and {w'} to {w}.

1.3 Statistical Descriptors

Since some of the inputs to the system are random, meaningful quantitative results can only be obtained through the use of statistical quantities. A scalar random quantity x is typically described by its mean or expected value denoted as $\bar{x}$ or E(x) and its variance, $E\ (x - \bar{x})^2$. Similarly a n-component random vector {x} may be characterized by a mean vector E{x}, and a n x n matrix known as the covariance matrix P({x}), defined as:

$$P(\{x\}) = E \begin{bmatrix} (x_1 - \bar{x}_1)^2, \ldots\ldots & (x_1-\bar{x}_1)(x_n-\bar{x}_n) \\ (x_n-\bar{x}_n)\ (x_1-\bar{x}_1), \ldots\ldots & (x_n-\bar{x}_n)^2 \end{bmatrix} \tag{1.2}$$

The principal diagonal of P({x}) defines the variances of all the state variables.

The mean and covariance can be obtained in two distinctly different ways, as follows.

1.4 Calculation Procedures

Monte Carlo Simulation: Repeated runs are performed with sample statistical inputs, and the results are averaged. Several hundred runs are typically required to ensure adequate confidence in the averages used to form the means and covariance matrices as functions of time. Monte Carlo simulation imposes no restriction on system linearity.

Covariance Propagation: The advantage of this method is that it computes the means and the covariance matrix as functions of time without the necessity for running multiple cases and subsequent averaging. Only two computations need be performed, one for the mean and one for the variance. Thus considerable savings of computer time are possible. Starting with an initial estimate of the covariance matrix P at the time t_o, P at successive instants is computed from the "covariance propagation equation". For simplicity, this is quoted below for the case when u = 0, assuming the system is linear and the noise is comprised of a deterministic component b, plus white noise w. For this case equation 1.1 can be written as follows,

$$\dot{x} = Fx + \Gamma w + \Gamma b \tag{1.3}$$

The parentheses are dropped for brevity. F, Γ, are matrices and both F and Γ may be time-varying; x, w, b are vectors as previously. The covariance propagation equation is

$$\dot{P} = FP + PF^T + \Gamma Q \Gamma^T \tag{1.4}$$

where Q is the spectral density matrix of w, i.e. $E[w(t)\, w(\tau)^T] = Q(t).\delta(t-\tau)$ where δ is the Dirac delta function.

By integrating equation 1.4 the time history of P can be obtained. The time history of the mean, $\bar{x}$, can be obtained by a modified form of equation 1.3.

$$\dot{\bar{x}} = F\bar{x} + \Gamma b \tag{1.5}$$

Thus the desired statistical information [$\bar{x}$ (t) and P (t)] can be obtained by integrating Equations (1.4) and (1.5).

Published studies of the covariance propagation method have indicated that it requires only approximately 1/10 to 1/15 of the computer time required for Monte Carlo simulations, (e.g., Reference 3). Covariance propagation also simplifies data handling and storage because it works directly with the statistical quantities that are desired, avoiding the computation of these

---

3. Gelb, A., and R. S. Warren, Direct Statistical Analysis of Nonlinear Systems: CADET, AIAA J., Vol. 11, No. 5, May 1973, p 689-694.

quantities as supplementary items after the numerous sample time histories have been run.

Quasilinearization: Because Equations 1.4 and 1.5 are linear some special adjustments must be made in order to apply covariance propagation to nonlinear systems such as the VSTOL launch and recovery system. Significant nonlinearities are built in to this system through the thrust limitations of the aircraft. Aerodynamic nonlinearities may also be important. To explain how nonlinearities can be handled within the framework of Equations 1.4 and 1.5 let us consider a specific example.

Figure 2 illustrates a nonlinear C_L versus α variation. This characteristic is approximated by a purely linear gain which is selected to give the best least-squares approximation to the output of the actual nonlinearity. This gain is known as the "describing function". For a given probability distribution of the input, (e.g., Gaussian, as shown in Figure 2), the describing function is determined by the mean and standard deviation of the input. This method of approximating nonlinearities is known as quasilinearization.

To apply the covariance propagation equations 1.4, 1.5 to a nonlinear system each nonlinearity is replaced by its describing function, which is computed for the mean and standard deviation of the input at the beginning of each computing interval. By updating these describing functions at each computing interval, good accuracy can be obtained even for complicated nonlinearities.

We shall refer to this technique as "nonlinear covariance propagation" (N.C.P.) although all the calculations performed within any computing interval are linear. The N.C.P. technique was originally developed for analyses of missile guidance and control systems (References 4, 5 and 6). The computer program described in these references (the CADET program) was not used as the basis for Vought's launch and recovery dynamics

---

4. Warren, R. S. and J. Siegel, SAM-D Performance Analyses Using CADET. Vols I and II. TASC TR 268-1,-2, Contract DAAH01-72-C-0826. Aug. 73.
5. J. H. Taylor, "Handbook for the Direct Statistical Analysis of Missile Guidance Systems via CADET," The Analytic Sciences Corp., TR 385-2, ONR Contract No. N00014-73-C-0213, May 1975.
6. J. H. Taylor and C. F. Price, "Direct Statistical Analysis of Missile Guidance Systems via CADET, Final Report," ONR Contract No. N00014-73-C-0213, March 1976.

A = SMALL MEAN,
LARGE VARIANCE

B = LARGE MEAN,
SMALL VARIANCE

LOCAL $\frac{dC_L}{d\alpha}$ IS THE
'DESCRIBING FUNCTION'

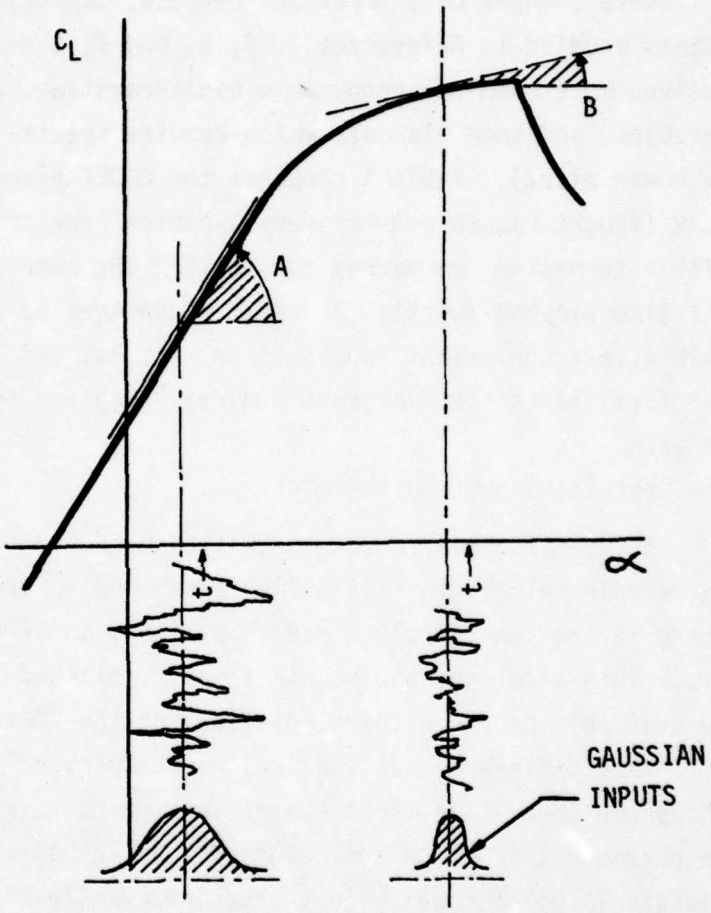


FIGURE 2 ILLUSTRATION OF QUASI-LINEARIZATION

program. Instead an alternative N.C.P. program 'COVAR' (Reference 7) was selected as being better suited for our technical requirements. The N.C.P. program presented in this report is specially written for modeling the VSTOL launch and recovery system and incorporates numerous changes from COVAR.

These changes were necessary because, compared with the missile guidance systems studied in References 4, 5, 6, and 7, the launch and recovery system involves more complex aerodynamic nonlinearities, a larger number of state variables, and some elements which require special modeling techniques (e.g., the human pilot). Table 1 compares the CADET program versus COVAR, and VOLAR (Vought Launch and Recovery Dynamics Program). CADET, COVAR, and VOLAR offer alternative approaches for solving the same problem, i.e. evaluation of a time varying function P. Main advantages of VOLAR, not indicated in Table 1, are convenient input/output features and a programming philosophy that facilitates the many varied models required for launch and recovery analysis.

1.5 Organization of this Report

This report is arranged so that each section leads step-by-step through two example calculations of VSTOL launch and recovery dynamics. Both examples relate to the same airplane and ship, i.e., an AV-8A landing on an LPD-class ship. This airplane-ship combination is selected because flight test data are available to check the predictions of the VOLAR program.

A key difference between the two examples relates to the human pilot models employed. The first example employs a relatively simple pilot model, the parameters of which are determined by verbal rules. This is called the "classical" pilot model. In the second example the pilot model parameters are determined automatically as the result of a mathematical optimization procedure. This model is known as the "optimal pilot" model. Both models are equivalent. The choice of model is a matter of user preference and convenience. The former model is computationally simple but demands user skill and experience to select valid pilot parameters. The optimal controller model avoids this restriction, but requires a considerable increase in computer storage and run time.

---

7. Abzug, M. J., User's Manual for FORTRAN COVAR Computer Programs, Aeronautical Consultant Associates, 14951 Camarosa Dr., Pacific Palisades, Ca. 90272, Rpt. ACA R-122. Jan. 1976.

TABLE 1. Comparison of Nonlinear Covariance Propagation Programs.

	CADET	COVAR	VOLAR	ADVANTAGES/ DISADVANTAGES
Treatment of analytic nonlinearities, such as sin θ	Gaussian describing functions (GDF)	Linearization around reference trajectory found using nonlinear equations	Same as COVAR	COVAR needs fewer GDF's, reducing complexity of program
Treatment of discontinuous nonlinearities, such as limiters and dead zones	GDF	Same	Same	Methods are the same
Mean solution	Propagated linearly, using GDF in $\dot{m} = Fm + Gw$	Propagated nonlinearly, using $\dot{m} = f(m) + Gw$	Propagated nonlinearly using $\dot{m} = f(m) + Gw$	COVAR and VOLAR provide more accurate mean solution; in COVAR mean solution is offline reducing program size
	↑ Coupled	| Input	↑ Interactive*	
Covariance solution	Propagated linearly, using GDF in $\dot{P}=FP+PF^T+GQG^T$	Propagated linearly, using GDF with means found in nonlinear solution and $\dot{P}=FP+PF^T+GQG^T$	Propagated linearly as in CADET	CADET and VOLAR have capability to provide more accurate covariances for large perturbations.

NOTE: m = mean vector
F = system state matrix
f = system nonlinear state equations
G = noise weighting matrix
P = covariance matrix
Q = white noise power spectral density matrix
w = white noise inputs

*VOLAR may be 'input' or 'coupled' to suit the individual requirement.

Section 2 of this report presents a general formulation of the aircraft equations of motion in a form compatible with Equation 1.1, known as "state-variable" form. For some launch and recovery situations the longitudinal and lateral aircraft degrees of freedom may be effectively coupled (e.g., for aircraft with large asymmetries such as helicopters, or aircraft with high turn rates or large mean sideslip angles). Hence Section 2 presents the fully coupled algebraic equations of motion in state variable form. The uncoupled equations are also presented.

Section 3 discusses the selection of AV-8A data and presents some general information on modeling stability augmenter systems, using the AV-8A as an example. Section 3 concludes with a summary of the AV-8A numerical data used in the subsequent example calculations.

Section 4 describes a model for the air wake of a LPD-class ship. This model is based upon wind tunnel measurements of a FF1052 frigate with appropriate scaling corrections applied.

Section 5 summarizes the classical pilot model. Section 6 describes how this model, plus the air wake and AV-8A models, is inputted to the VOLAR program. The resulting time histories of means and variances of key state variables computed by VOLAR are presented in Section 6. This first VOLAR example applies for an approach performed in a low sea state, for which ship motions are negligible.

The "optimal controller" pilot model is described in detail in Section 7. In Section 8 this model is applied to compute means and variances of the longitudinal degrees of freedom of an AV-8A performing an approach to an LPD-class ship, in a low sea state with 20 kts wind over deck.

Section 9 describes the ship motion model that Vought has developed from the Navy RAOH model. In Section 10, the example of Section 8 is generalized to include ship motion. This example assumes a moderate sea state with 35 kts wind over deck.

Section 11 summarizes the limited data currently available on ground effects, or (more properly) 'proximity' effects. Section 12 covers some miscellaneous topics relating to covariance propagation methods, with particular reference to interpretation of results in terms of probability of successful launch and recovery. In Section 13 the results of the example calculations of Sections 6, 8, and 10 are compared with flight test data.

Conclusions are given in Section 14. A User's Manual, program listing, and some specialized mathematical topics are presented in appendices.

2.0 AIRCRAFT DYNAMIC MODEL

AIRCRAFT EQUATIONS OF MOTION IN STATE-VARIABLE FORM

2.1 Introduction

The launch and recovery dynamics program, like other computational methods based on modern control theory, requires the system dynamic equations to be written in the form

$$I\dot{x} = Fx + Gw \tag{2.1}$$

where

x = the system output state vector

F = the system matrix

w = the input state vector

G = the input matrix

I = the identity matrix

The above form will be referred to here as the "state-variable form". It differs from the form in which airplane equations of motion are conventionally written. The most common form for airplane equations involves second derivatives of an output state vector x', thus

$$A \frac{d^2x'}{dt^2} + B \frac{dx'}{dt} + Cx' = Dw' \tag{2.2}$$

where

w' = control and gust input vector

By introducing additional state variables augmenting x' to x" this can be reduced to a first order equation of the form

$$M \frac{dx"}{dt} + Nx" = Ew' \tag{2.3}$$

In theory, reduction to the state-variable form is possible by substituting numerical values in equation 2.3 and subsequently premultiplying by M^{-1}, however, it is generally more convenient and more accurate to re-formulate the original literal equations in the algebraic form of equation 2.1 before substituting numerical values. This section describes the appropriate literal forms for the longitudinal and lateral

equations of motion, and discusses the reduction of cross-coupled lateral-plus-longitudinal equations of motion to state-variable forms.

2.2 Transformation of Lateral Equations to State-Variable Form

From Reference 8 the linearized equations describing small lateral perturbations from straight-line flight are:

$$\begin{bmatrix} s & -W_o & U_o & -g\cos\Theta_o & 0 \\ 0 & s & -\frac{I_{xz}}{I_x}s & 0 & 0 \\ 0 & -\frac{I_{xz}}{I_z}s & s & 0 & 0 \\ 0 & -1 & -\tan\theta_o & s & 0 \\ 0 & 0 & \frac{-1}{\cos\Theta_o} & 0 & s \end{bmatrix} \begin{bmatrix} v \\ p \\ r \\ \phi \\ \psi \end{bmatrix} = \begin{bmatrix} Y \\ L \\ N \\ 0 \\ 0 \end{bmatrix} \quad (2.4)$$

mY, I_xL, I_yN, are the applied aerodynamic forces and moments due to motion perturbations v, p, r and also due to control deflections. It is generally assumed that the aerodynamic forces and moments due to $\dot{v}$, $\dot{p}$, $\dot{r}$, and higher order derivatives are negligible. With this assumption, equation 2.4 can be reduced to the desired form through the following manipulations: multiply the third row by I_{xz}/I_x and add the result to the second row; multiply the second row by I_{xz}/I_z and add the result to the third row; multiply the fifth row by $\sin\Theta_o$ and add to the fourth row; finally, divide the second and third rows by $(1 - \frac{I_{xz}^2}{I_xI_z})$. These manipulations yield:

---

8. McRuer, D. T., I. L. Ashkenas, and F. D. Graham, Aircraft Dynamics and Automatic Control, Princeton University Press, Princeton, New Jersey, 1973.

$$\begin{bmatrix} s & -W_o & U_o & -g\cos\Theta_o & 0 \\ 0 & s & 0 & 0 & 0 \\ 0 & 0 & s & 0 & 0 \\ 0 & -1 & -\tan\Theta_o & s & 0 \\ 0 & 0 & \frac{-1}{\cos\Theta} & 0 & s \end{bmatrix} \begin{bmatrix} v \\ p \\ r \\ \phi \\ \psi \end{bmatrix} = \begin{bmatrix} Y \\ L' \\ N' \\ 0 \\ 0 \end{bmatrix} \qquad (2.5)$$

where L', N' are prime derivatives as defined in Reference 8:

$$L_i' = \frac{L_i + N_i \frac{I_{xz}}{I_x}}{1 - \frac{(I_{xz})^2}{I_x I_z}} \qquad N_i' = \frac{N_i + L_i \frac{I_{xz}}{I_z}}{1 - \frac{(I_{xz})^2}{I_x I_z}} \qquad (2.6)$$

With the addition of the kinematic relation for lateral displacement from the desired flight path, Δy, equation (2.5) can be written in the desired form

$$[I]\{\dot{x}\} = [F]\{x\} + [G]\{w\} \qquad (2.7)$$

$$\{x\}^T = \{v, p, r, \phi, \psi, \Delta y\}$$

$$[F] = \begin{bmatrix} Y_v & W_o+Y_p & -U_o+Y_r & g\cos\Theta_o & 0 & 0 \\ L_v' & L_p' & L_r' & 0 & 0 & 0 \\ N_v' & N_p' & N_r' & 0 & 0 & 0 \\ 0 & 1 & \tan\Theta_o & 0 & 0 & 0 \\ 0 & 0 & \frac{1}{\cos\Theta_o} & 0 & 0 & 0 \\ 1 & 0 & 0 & 0 & U_o\cos\theta_o + W_o\sin\theta_o & 0 \end{bmatrix} \qquad (2.8)$$

$$[G] = \begin{bmatrix} Y_{\delta A} & Y_{\delta R} & -Y_v & 0 & 0 & 0 \\ L_{\delta A}' & L_{\delta R}' & -L_v' & 0 & 0 & 0 \\ N_{\delta A}' & N_{\delta R}' & -N_v' & 0 & 0 & 0 \\ 0 & 0 & 0 & 0 & 0 & 0 \\ 0 & 0 & 0 & 0 & 0 & 0 \\ 0 & 0 & 0 & 0 & 0 & 0 \end{bmatrix} \tag{2.9}$$

$$\{w\}^T = \{\delta_A, \ \delta_R, \ v_g, \ 0, \ 0\} \tag{2.10}$$

This formulation excludes the aerodynamic forces due to lateral gust gradient terms, $\frac{\partial v_g}{\partial x}$, $\frac{\partial u_g}{\partial y}$; these are expected to be negligible for VSTOL aircraft with closely grouped engines at low speeds.

2.3 Longitudinal Equations in State-Variable Form

From reference 8 the linearized equations describing small perturbations from straight-line flight are:

$$\begin{bmatrix} s & 0 & g\cos\Theta_o & W_o \\ 0 & s & g\sin\Theta_o & -U_o \\ 0 & 0 & s & -1 \\ 0 & 0 & 0 & s \end{bmatrix} \begin{bmatrix} u \\ w \\ \theta \\ q \end{bmatrix} = \begin{bmatrix} X \\ Z \\ 0 \\ M \end{bmatrix} \tag{2.11}$$

where mX, mZ, I_yM are the applied aerodynamic forces and moments due to the controls and gust inputs, and to the motion perturbations. It is generally assumed that X, Z, and M are linearly dependent on u, w, q, and also on the time derivative of w, which is assumed to affect the aircraft response via derivatives $X_{\dot{w}}$, $Z_{\dot{w}}$, $M_{\dot{w}}$. Usually only $M_{\dot{w}}$ is retained, yielding

$$\begin{bmatrix} s & 0 & 0 & 0 \\ 0 & s & 0 & 0 \\ 0 & 0 & s & -1 \\ 0 & -M_{\dot{w}}s & 0 & s \end{bmatrix} \begin{bmatrix} u \\ w \\ \theta \\ q \end{bmatrix} = \begin{bmatrix} X - g\cos\Theta_o\,\theta - W_o q \\ Z - g\sin\Theta_o\,\theta + U_o q \\ 0 \\ \overline{M} \end{bmatrix} \tag{2.12}$$

where $\bar{M} = M - M_{\dot{w}} \dot{w} = M_q q + M_w w + M_u u$

To reduce equation (2.13) to the desired form multiply the second row by $M_{\dot{w}}$, and subtract the result from the fourth row. To this is adjoined kinematic equations for the horizontal and vertical position increments Δx, Δz. This yields an equation of the form of equation (2.1).

$$\dot{Ix} = Fx + Gw \tag{2.14}$$

where $\{x\}^T = \{u, v, \theta, q, \Delta x, \Delta z\}$

$$F = \begin{bmatrix} X_u & X_w & -g\cos\Theta_o & X_q - W_o & 0 & 0 \\ Z_u & Z_w & -g\sin\Theta_o & Z_q + U_o & 0 & 0 \\ 0 & 0 & 1 & 0 & 0 & 0 \\ M_u - Z_u M_{\dot{w}} & M_w - Z_w M_{\dot{w}} & 0 & M_q - (Z_q + U_o) M_{\dot{w}} & 0 & 0 \\ \cos\Theta_o & \sin\Theta_o & W_o\cos\Theta_o - U_o\sin\Theta_o & 0 & 0 & 0 \\ -\sin\Theta_o & \cos\Theta_o & -U_o\cos\Theta_o - W_o\sin\Theta_o & 0 & 0 & 0 \end{bmatrix} \tag{2.1}$$

$$G = \begin{bmatrix} X_{\delta_1} & X_{\delta_2} & X_{\delta_3} & -X_u & -X_w \\ Z_{\delta_1} & Z_{\delta_2} & Z_{\delta_3} & -Z_u & -Z_w \\ 0 & 0 & 0 & 0 & 0 \\ M_{\delta 1} - Z_{\delta 1} M_{\dot{w}} & M_{\delta 2} - Z_{\delta 2} M_{\dot{w}} & M_{\delta 3} - Z_{\delta 3} M_{\dot{w}} & -M_u + Z_u M_{\dot{w}} & -M_w + Z_w M_{\dot{w}} \\ 0 & 0 & 0 & 0 & 0 \\ 0 & 0 & 0 & 0 & 0 \end{bmatrix} \tag{2.15}$$

$$\{w\}^T = \{\delta_1, \delta_2, \delta_3, u_g, w_g, 0, 0\} \tag{2.16}$$

δ_1, δ_2, δ_3 represent the deflections of the appropriate longitudinal controls, e.g. stick, throttle vectoring nozzles, etc.

2.4 Transformation of Cross-Coupled Equations of Motion to State-Variable Form

The longitudinal and lateral equations of motion become coupled for aircraft performing small perturbations from curved flight paths and also for straight-line flight of aircraft with asymmetric aerodynamic and/or inertial characteristics, e.g. helicopters. The transformation to state-variable form of the standard coupled equations of motion (e.g., as given in Reference 8) is more complicated than for the uncoupled cases considered previously. The procedure described below requires that the aircraft x and y body axes shall be defined such that $I_{xy} = I_{yz} = 0$, but I_{xz} is in general non-zero. The assumption is made that all acceleration derivatives such as $M_{\dot{w}}$ can be neglected.

For compactness the equations will be presented here in terms of the uncoupled longitudinal and lateral equations already derived, with additional terms added as necessary.

The 12-component state vector $\{x\}$ is defined as

$$\{x\}^T = \{u, w, \Theta, q, \Delta x, \Delta z; v, p, r, \phi, \psi, \Delta y\} \tag{2.17}$$

The (n + 3) component input vector is defined as

$$\{w\}^T = \{u_g, w_g, \delta_1 \ \delta_2, \ldots \delta_p; v_g, \delta_{p+1} \cdots \delta_n\} \tag{2.18}$$

where u_g, v_g, and w_g are gust inertial velocities, δ_1, δ_2 ... δ_p represent longitudinal control deflections, and δ_{p+1}, δ_{p+2},... δ_n represent lateral control deflections.

For these state and control vectors, the equations of motion in the desired form are

$$I\dot{x} = Fx + Gw \tag{2.19}$$

where F and G are defined as described below.

DEFINITION OF THE F-MATRIX

The F-matrix is a 12 x 12 matrix with rows compatible with the x vector defined previously.

The order selected for the elements listed in Equation 2.17 facilitates decomposition of the F-matrix into the sub-matrices F_{11}, F_{12}, F_{21}, F_{22} as shown below, which for $P_o = R_o = Q_o$ and zero values of cross-coupling derivatives such as L_q, M_r, etc. yields the uncoupled lateral and longitudinal F-matrices previously discussed as F_{11}, F_{22}, with $F_{12} = F_{21} = 0$.

$$\begin{Bmatrix} \dot{x}_{LONG} \\ \dot{x}_{LAT} \end{Bmatrix} = \left[\begin{array}{c|c} F_{11} & F_{12} \\ \hline F_{21} & F_{22} \end{array}\right] \begin{Bmatrix} x_{LONG} \\ x_{LAT} \end{Bmatrix} + \left[\begin{array}{c|c} G_{11} & G_{12} \\ \hline G_{21} & G_{22} \end{array}\right] \begin{Bmatrix} W_{LONG} \\ W_{LAT} \end{Bmatrix}$$

The size of the F-matrix precludes single-page presentation. Therefore, to facilitate the visualization of physical effects the F-matrix is given in transposed form in Table 2, so that all the contributions to any particular given force or moment appear on a single page. For compactness the abbreviations s = sin, c = cos, t = tan are employed, and roll and yaw accelerations are denoted by L', L", N', N", as explained below. The G-matrix is given in Table 2.

DEFINITIONS OF L', N', L", N" TERMS

$$L_i' = \frac{L_i + N_i \frac{I_{xz}}{I_x}}{1 - \frac{(I_{xz})^2}{I_x I_z}} \qquad N_i' = \frac{N_i + L_i \frac{I_{xz}}{I_z}}{1 - \frac{(I_{xz})^2}{I_x I_z}}$$

where $i = u, w, v, p, q, r$

$$L_p'' = \left[L_p + \frac{I_{xz}}{I_x} \cdot Q_o + \left(N_p + \frac{I_x - I_y}{I_z} Q_o\right) \frac{I_{xz}}{I_x}\right] \Big/ \left[1 - \frac{(I_{xz})^2}{I_x I_z}\right]$$

$$L_q'' = \left[L_q + \frac{I_{xz}}{I_x} P_o + \frac{I_y - I_z}{I_x} R_o + \left(N_q + \frac{I_x - I_y}{I_z} P_o - \frac{I_{xz}}{I_z} R_o\right) \frac{I_{xz}}{I_x}\right] \Big/ \left[1 - \frac{(I_{xz})^2}{I_x I_z}\right]$$

$$L_r'' = \left[L_r + \frac{I_y - I_z}{I_x} Q_o + \left(N_r - \frac{I_{xz}}{I_z} Q_o\right) \frac{I_{xz}}{I_x}\right] \Big/ \left[1 - \frac{(I_{xz})^2}{I_x I_z}\right]$$

$$N_p'' = \left[N_p + \frac{I_x - I_y}{I_z} Q_o + \left(L_p + \frac{I_{xz}}{I_x} \cdot Q_o\right) \frac{I_{xz}}{I_z}\right] \Big/ \left[1 - \frac{(I_{xz})^2}{I_x I_z}\right]$$

$$N_q'' = \left[N_q + \frac{I_x - I_y}{I_z} P_o - \frac{I_{xz}}{I_z} R_o + \left(L_q + \frac{I_y - I_z}{I_x} \cdot R_o + \frac{I_{xz}}{I_x} P_o\right) \frac{I_{xz}}{I_z}\right] \Big/ \left[1 - \frac{(I_{xz})^2}{I_x I_z}\right]$$

$$N_r'' = \left[N_r - \frac{I_{xz}}{I_z} Q_o + \left(L_r + \frac{I_y - I_z}{I_x} \cdot Q_o\right) \frac{I_{xz}}{I_z}\right] \Big/ \left[1 - \frac{(I_{xz})^2}{I_x I_z}\right]$$

Note that for $P_o = Q_o = R_o = 0$, $L_p'' = L_p'$, $L_q'' = L_q'$, $L_r'' = L_r'$, $N_p'' = N_p'$, $N_q'' = N_q'$, $N_r'' = N_r'$.

TABLE 2. TRANSPOSED F-MATRIX

	Elements appearing in the equation for				
MULTIPLIES PERTURBATION	$\dot{u}$	$\dot{w}$	$\dot{\theta}$	$\dot{q}$	$\Delta\dot{x}$
u	X_u	Z_u+Q_o	0	M_u	$c\Theta_o c\psi_o$
w	X_w-Q_o	Z_w	0	M_w	$c\Phi_o s\Theta_o c\Psi_o+s\Phi_o s\Psi_o$
Θ	$-gc\Theta_o$	$-gs\Theta_o c\Phi_o$	0	0	$-U_o s\Theta_o c\Psi_o+V_o s\Phi_o c\Theta_o c\Psi_o+W_o c\Phi_o c\Theta_o c\Psi_o$
q	X_q-W_o	Z_q+U_o	1	M_q	0
Δx	0	0	0	0	0
Δz	0	0	0	0	0
v	X_v+R_o	Z_v-P_o	0	M_v	$s\Phi_o s\Theta_o c\Psi_o-c\Phi_o s\Psi_o$
p	X_p	$Z_p - V_o$	0	$M_p+\frac{I_z-I_x}{I_y} R_o-2\frac{I_{xz}}{I_y} P_o$	0
r	X_r+V_o	Z_r	0	$M_r+\frac{I_z-I_x}{I_y} P_o+2\frac{I_{xz}}{I_y} R_o$	0
ϕ	0	$-gc\Theta_o s\Phi_o$	0	0	$V_o(c\Phi_o s\Theta_o c\Psi_o+s\Phi_o s\Psi_o)+W_o(c\Phi_o s\Psi_o-s\Phi_o c\Psi_o s\Theta_o)$
ψ	0	0	0	0	$-U_o c\Theta_o s\psi_o-V_o(s\Phi_o s\Theta_o s\Psi_o+c\Phi_o c\Psi_o)-W_o(c\Phi_o s\Theta_o s\Psi_o-s\Phi_o c\Psi_o)$
Δy	0	0	0	0	0

TABLE 2. TRANSPOSED F-MATRIX (CONTINUED)

MULTIPLIES PERTURBATION	Elements appearing in the equation for $\Delta\dot{z}$	$\dot{v}$	$\dot{p}$	$\dot{r}$	$\dot{\phi}$
u	$-s\Theta_o$	Y_u-R_o	L_u'	N_u'	0
w	$c\Phi_o c\Theta_o$	Y_w+P_o	L_w'	N_w'	0
θ	$-U_o c\Theta_o-V_o s\Phi_o s\Theta_o-W_o c\Phi_o s\Theta_o$	$-gs\Theta_o s\Phi_o$	0	0	$Q_o s\Phi_o(c\Theta_o)^{-2}+R_o c\Phi_o(c\Theta_o)^{-2}$
q	0	Y_q	L_q''	N_q''	$s\Phi_o t\Theta_o$
Δx	0	0	0	0	0
Δz	0	0	0	0	0
v	$s\Phi_o c\Theta_o$	Y_v	L_v'	N_v'	0
p	0	Y_p+W_o	L_p''	N_p''	1
r	0	Y_r-U_o	L_r''	N_r''	$c\Phi_o t\Theta_o$
ϕ	$V_o c\Phi_o c\Theta_o-W_o s\Phi_o c\Theta_o$	$gc\Theta_o c\Phi_o$	0	0	$Q_o c\Phi_o t\Theta_o-R_o s\Phi_o t\Theta_o$
ψ	0	0	0	0	0
Δy	0	0	0	0	0

TABLE 2. TRANSPOSED F-MATRIX (CONCLUDED)

MULTIPLIES PERTURBATION	Elements appearing in the equation for $\dot{\psi}$	Elements appearing in the equation for $\Delta\dot{y}$
u	0	$c\Theta_o s\psi_o$
w	0	$c\Phi_o s\Theta_o s\Psi_o - s\Phi_o c\Psi_o$
Θ	$(c\Theta_o)^{-1}(Q_o s\Phi_o t\Theta_o + Rc\Phi_o t\Theta_o)$	$-U_o s\Theta_o s\Psi_o + V_o s\Phi_o c\Theta_o s\Psi_o + W_o c\Phi_o c\Theta_o s\Psi_o$
q	$(c\Theta_o)^{-1} s\Phi_o$	0
Δx	0	0
Δz	0	0
v	0	$s\Phi_o s\Theta_o s\Psi_o + c\Phi_o c\Psi_o$
p	0	0
r	$(c\Theta_o)^{-1} c\Phi_o$	0
ϕ	$(c\Theta_o)^{-1}(Q_o c\Phi_o - R_o s\Phi_o)$	$V_o(c\Phi_o s\Theta_o s\Psi_o - s\Phi_o c\Psi_o) - W_o(s\Phi_o s\Theta_o s\Psi_o + c\Phi_o c\Psi_o)$
ψ	0	$U_o c\Theta_o c\Psi_o + V_o(s\Phi_o s\Theta_o c\Psi_o - c\Phi_o s\psi_o) + W_o(c\Phi_o s\Theta_o c\Psi_o + s\Phi_o s\Psi_o)$
Δy	0	0

TABLE 3. G-MATRIX

ELEMENTS IN EQUATION FOR	Multiplies perturbation							
	u_g	w_g	δ_E	δ_T	θ_j	v_g	δ_A	δ_R
$\dot{u}$	$-X_u$	$-X_w$	X_{δ_E}	X_{δ_T}	X_{θ_j}	$-X_v$	X_{δ_A}	X_{δ_R}
$\dot{w}$	$-Z_u$	$-Z_w$	Z_{δ_E}	Z_{δ_T}	Z_{θ_j}	$-Z_v$	Z_{δ_A}	Z_{δ_R}
$\dot{\theta}$	0	0	0	0	0	0	0	0
$\dot{q}$	$-M_u$	$-M_w$	M_{δ_E}	M_{δ_T}	M_{θ_j}	$-M_v$	M_{δ_A}	M_{δ_R}
$\Delta\dot{x}$	0	0	0	0	0	0	0	0
$\Delta\dot{z}$	0	0	0	0	0	0	0	0
$\dot{v}$	$-Y_u$	$-Y_w$	Y_{δ_E}	Y_{δ_T}	Y_{θ_j}	$-Y_v$	Y_{δ_A}	Y_{δ_R}
$\dot{p}$	$-L_u'$	$-L_w'$	L_{δ_E}	L_{δ_T}	L_{θ_j}	$-L_v$	L_{δ_A}'	L_{δ_R}'
$\dot{r}$	$-N_u'$	$-N_w'$	N_{δ_E}	N_{δ_T}	N_{θ_j}	$-N_v'$	N_{δ_A}'	N_{δ_R}'

3.0 AIRCRAFT DATA AND STABILITY AUGMENTER SYSTEM MODEL

3.1 Introduction

It is desirable to demonstrate the validity of the nonlinear covariance propagation technique by comparing the results that it yields versus data from actual flight operations. This requires mathematical models of the ship motion, the airwake and the atmospheric conditions prevailing during the flight tests, plus a model of the airframe and control system dynamics. The data currently available do not permit one-to-one matching of all these factors. For example, published quantitative flight data on the AV-8 aircraft are extremely limited, and not compatible with the available ship motion and airwake models. Thus dynamic interface charts are available for the LPD (Reference 9) and LPH class ships (Reference 10), but satisfactory airwake models based on wind tunnel data are only available for the FF-1052 and DD-963 ships (References 11 and 12 respectively). It is therefore not advisable to focus narrowly on a super-accurate model of the airframe while tolerating gross uncertainties in other system elements. This is particularly true for simulations which replace the human pilot by a mathematical model. The human pilot may require modeling of secondary dynamic effects (such as stall and buffet frequency characteristics) in order to reassure him of the overall fidelity of the simulation, but such detail is unnecessary if a pilot model is employed. These considerations influence the selection of aircraft data from the sources listed below.

References

9. Anon., AV-8A Shipboard Suitability Trials. Naval Air Test Center, Patuxent River, Md., Report No. FT-65R-73, 17 Oct. 1973.

10. Hutchins, D. E., Review of U. S. Navy VSTOL Handling Qualities Requirements, Proc. Navy/NASA VSTOL Flying Qualities Workshop, April 1977, Naval Postgraduate School, Monterey, Ca., published Aug. 1977.

11. Fortenbaugh, R. L., A Math Model for the Airwake of a DE-1052 Class Ship, Vought Corporation, Report 2-53300/7R-3397, May 1977.

12. Fortenbaugh, R. L., Application of the Vought Small Ship Airwake Model for Starboard Approaches to DD-963 Class Ships, Vought Corporation, Report 2-55830/8AVO-153 (to be published in final report under Contract N62269-78-C-0129).

AV-8 aircraft models of sufficient detail for correlation have been published in References 13, 14, and 15. All these models are based on McAir data. The model of Reference 13 was developed for the AV-8A and includes numerous nonlinearities which are represented by tables of the appropriate dependent variable for given values of one or at most two independent variables. Graphs of these tables are included in Reference 13, the tabulated values of the independent variables being joined by straight lines. Reference 14 presents the basic McAir aerodynamic data on the AV-8A and AV-8B and Reference 15 presents AV-8B models used for the X-22A in-flight simulator. Data on the AV-8A stability augmenter system (S.A.S.) is given in Reference 14. S.A.S. was employed during the flight tests described in References 9 and 10. After comparing the available data sources, Reference 15 was selected as the most suitable for our use, based on its demonstrated accuracy, and its simplicity compared to the alternative models. The model represents the AV-8B rather than the AV-8A, but for the flight conditions of interest here, the differences are minor, as noted in Reference 14, and can be corrected as indicated in the following subsection.

3.2 AV-8A and AV-8B Models

Reference 15 lists aerodynamic data for two AV-8B approach profiles, one for a 30 degree approach from 105 knots, the other for a 5 degree approach from 65 knots and also gives "single-model" data which approximate the aircraft characteristics for both profiles. Table 4 lists these "single-model data", which are used in the present simulation. Although some nonlinear effects have been neglected, these derivatives are shown in Reference 15 to give good agreement with the results of the McAir fully nonlinear simulation.

---

13. Nave, R. L., Progress Toward a Computerized VSTOL/Small Platform Landing Dynamics Investigation Model, NADC Report 77024-30, Naval Air Dev. Ctr., Warminster, Pa., 1977.

14. Anon., AV-8B Simulator Evaluation, VSTOL Performance, McDonnell Douglas Corp. Rept. MDC-A3922, Contract N00019-75-C-0487, March 1976.

15. Lebacqz, J. V., Summary Documentation of AV-8A Model Development and X-22A Simulation of AV-8B, Calspan Corp., Buffalo, N. Y. X-22A TM No. 98, W/A P63-054, July 1977.

TABLE 4(a). "SINGLE-MODEL" AV-8B LONGITUDINAL MODEL

V_o(KT)	0	30	50	65	80	105
X_u	-.044	-.044	-.044	-.044	-.044	-.044
Z_u	0.0	-.023	-.054	-.092	-.101	-.105
M_u	0.0	-.0009	-.0020	-.0026	-.0008	0.0
X_w	0.0	0.0	+.0035	+.010	+.0175	+.035
Z_w	-.018	-.125	-.195	-.240	-.300	-.390
M_w	+.0042	+.0047	+.0040	+.0021	-.0015	-.0070
X_q	0	+.03	+.05	+.052	+.085	.11
Z_q	-.05	-.29	-.40	-.47	-.61	-.79
M_q	-.056	-.118	-.160	-.191	-.224	-.280
$X_{\delta ES}$†	-.161	-.151	-.145	-.139	-.134	-.126
$Z_{\delta ES}$†	-.350	-.340	-.335	-.330	-.295	-.205
$M_{\delta ES}$†	.230	.235	.237	.240	.241	.243
$X_{\delta T}$*	.34	.30	.262	.225	.180	.140
$Z_{\delta T}$*	-2.55	-2.46	-2.37	-2.26	-2.10	-1.75
$M_{\delta T}$*	-0.036	-0.036	-0.036	-0.036	-0.036	-0.036
$X_{\delta T}$**	-	-	-	.66	-	.60
$Z_{\delta T}$**	-	-	-	-2.11	-	-1.41
$X_{\Theta j}$*	-.555	-.546	-.530	-.510	-.476	-.400
$Z_{\Theta j}$*	-.066	-.061	-.050	-.028	-.023	-.040
$M_{\Theta j}$*	0	0	0	0	0	0
$X_{\Theta j}$**	-	-	-	-.456	-	-.380
$Z_{\Theta j}$**	-	-	-	-.066	-	-.055

*Θ_j = 81 degrees **For trimmed condition
† Units of δES are not defined in Reference 15

TABLE 4(b): "SINGLE-MODEL" AV-8B LATERAL-DIRECTIONAL MODEL

V_o	0	30	50	65	80	105
Y_v	-.034	-.063	-.088	-.104	-.120	-.138
L_v'	-.0020	-.0144	-.0197	-.0204	-.0184	-.0104
N_v'	-.0036	-.0021	-.0010	0.0	+.0014	.0047
Y_p	0	0	0	0	0	0
L_p'	-.13	-.42	-.62	-.79	-1.0	-1.38
N_p'	-.005	-.032	-.053	-.072	-.091	-.126
Y_r	-.225	-.24	-.24	-.235	-.235	-.215
L_r'	.015	.15	.24	.31	.375	.49
N_r'	-.042	-.088	-.12	-.142	-.164	-.203
$Y_{\delta as}$ †	0	-.006	-.015	-.026	-.039	-.065
$L_{\delta as}'$ †	0.5	0.5	0.5	0.5	0.5	0.5
$N_{\delta as}'$ †	.030	.030	.031	.033	.035	.040
$Y_{\delta RP}$ †	-.68	-.67	-.70	-.75	-.80	-.90
$L_{\delta RP}'$ †	-.060	-.065	-.075	-.080	-.095	-.13
$N_{\delta RP}'$ †	.225	.235	.243	.248	.255	.265

† Units of δas and δRP are not defined in Reference 15.

In the present simulation, nonlinearities are introduced to model the limits on maximum roll and yaw acceleration capabilities. Reference 15 notes the N_v' derivative as being very nonlinear at certain speeds. The N' versus v variation can be modeled as an odd function of v comprised of linear segments with break points at -12, -8, 8, and 12 degrees (see Figure 3). This was not required because N_v' was linear over the speed range simulated here.

AV-8A maximum control power capabilities are obtained from Reference 14 as:

$$L_{MAX} = 0.45 \text{ rad/sec}^2, \; M_{MAX} = 0.25 \text{ rad/sec}^2, \; N_{MAX} = 0.125 \text{ rad/sec}^2$$

Due to the bleed system the maximum T/W ratio depends on the utilization of the above control moments. The appropriate T/W describing function could be programmed to reflect this dependence, but this does not appear to be necessary for purposes of demonstrating correlation with the particular flight data of interest here. A mean value of T/W = 1.3 was used, appropriate to an installed static thrust of 21,500 pounds out of ground effect.

Reference 14 discusses the differences in stability and control characteristics of the AV-8A and AV-8B. For the low speeds of interest here (<65 kt) the effects of increased span and area of the AV-8B are apparently secondary, compared to the improvement in roll control of the AV-8B due to realignment of the roll puffers to reduce adverse yaw. This could be simulated by adjusting the ratio of $N_{\delta AS}'$ to $L_{\delta AS}'$, if desired. A second difference involves ground effects, which Reference 14 notes are improved on the AV-8B due to the fuselage strakes. The numerical simulation examples presented in this report are mainly out of ground effect, so the AV-8B representation is adequate. Finally, the AV-8B is claimed to have improved inlet stall characteristics due to the use of two rows of blow-in doors near the inlet lips. From References 14, 15, and 16 it appears that this change does not affect L_v' except at large sideslip angles, since the L_v' data supplied in these references are essentially linear for moderate sideslip angles.

---

16. Lacy, T. R., MIL-F-83300; View from an Aircraft Designer, Proc. Navy/NASA VSTOL Flying Qualities Workshop, April 1977, Naval Postgraduate School, Monterey, California, Published August 1977.

FLIGHT CONDITION 'L' OF REF. 15 (65 KTS., α = 8.0 DEG., Θ_j = 69.9 DEG.)

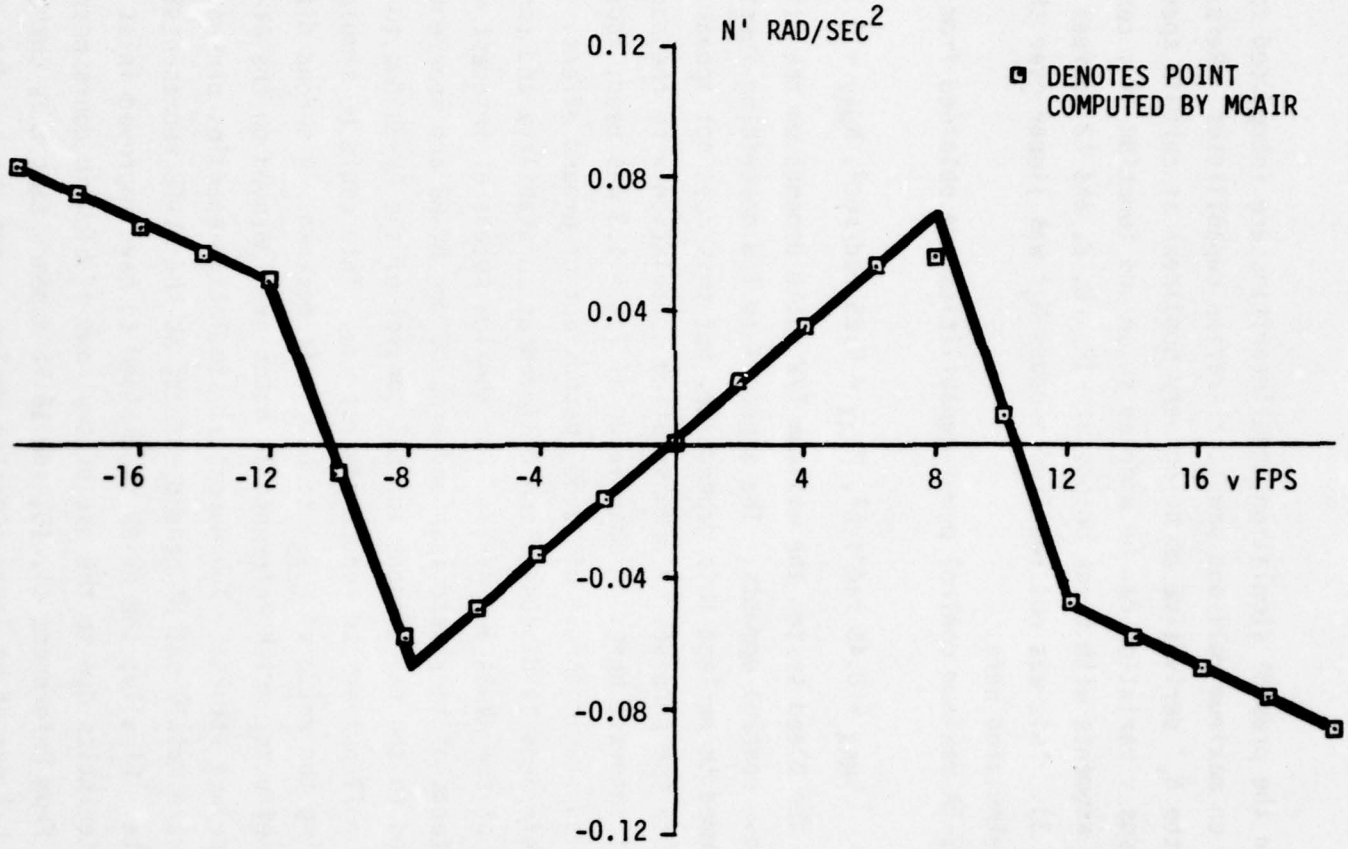


FIG. 3. NONLINEAR VARIATION OF AV-8B YAW ACCELERATION (N') VERSUS SIDESLIP VELOCITY

3.3 Representation of Stability Augmenter Systems

The representation of stability augmenter systems for the Launch and Recovery Dynamics Program and for covariance propagation methods in general is complicated by the need to also represent the human pilot. The output of the human pilot model must be summed with the output of the S.A.S. in order to compute the total forces and moments applied to the aircraft by the controls. Complications arise because the authority limits on the S.A.S. are generally set such that the forces and moments produced as a result of S.A.S. commands are considerably less than the maximum values of the forces and moments that can be produced in response to pilot commands.

Figure 4 (page 32) illustrates these considerations. A fly-by-wire system is selected for simplicity because only one set of actuators need be considered, (We assume that pilot commands and S.A.S. commands generate electrical signals which are summed and input to these actuators). The principles discussed below apply to other types of flight control systems, but their implementation changes for systems where some (but not all) of the commanded control deflections are fed through some or all of the actuators. The describing functions shown on Figure 4 are computed as follows.

The maximum values of the forces and moments that can be generated by the flight control system determine the lower describing function block shown on Figure 4. For VSTOL aircraft this block typically represents four 'saturation' describing functions, one each for yaw, pitch, and roll and maximum thrust. The upper describing function block represents the saturation describing functions that define the limits on the maximum values of the S.A.S. commands. For covariance propagation it is necessary to sum the output of the pilot model (u_{pilot}) with the linearized output of the S.A.S. describing function (u_s). The mean, $\bar{u}_T$, and variance, σ_{u_T}, of the summed signal, u_T, determine the effective gain of the lower describing function in Figure 4.

3.4 AV-8A Autopilot

Later in this report the Launch and Recovery Dynamics Program is employed to compute the behavior of the AV-8A approaching and landing on a small

ship of the LPD class. The program's predictions are correlated with flight test results for the AV-8A landing on the U.S.S. 'Raleigh'. These flight test data were obtained on early AV-8A's which were fitted with a roll S.A.S. of very limited authority and had no pitch or yaw stability augmentation. On subsequent AV-8A's the S.A.S. was upgraded to a level similar to that of the AV-8B S.A.S. described in Reference 14 except that no roll-yaw interconnect was fitted. A brief summary of this S.A.S. is given below. This summary facilitates the extrapolation of the results given in this report to later versions of the AV-8A and also to the AV-8B.

Block diagrams of the AV-8A S.A.S. are given in Reference 14. These may be expressed in the form of Figure 4 with the following substitutions.

TABLE 5. AV-8A&B S.A.S. DYNAMICS

STATE VARIABLE	S.A.S. COMPENSATION	GAIN	ACTUATOR TIME CONSTANT (SEC)
r	$\frac{Ks}{1 + 3.11\ s}$	$K = 0.669\ \frac{\text{deg}\ \delta_R}{\text{deg/sec}}$	0.0175
a_y	$\frac{K\ (1 + 0.25\ s)}{1 + 0.125\ s}$	$K = 0.83\ \frac{\text{deg}\ \delta_R}{\text{ft/sec}^2}$	0.0175
p	$\frac{K\ (1 + 0.781\ s)}{1 + 0.129\ s}$	$K = 0.346\ \frac{\text{deg}\ \delta_A}{\text{deg/sec}}$	0.04
q	$\frac{K\ (1 + 0.189\ s)}{1 + 0.741\ s}$	$K = 0.495\ \frac{\text{deg}\ \delta_E}{\text{deg/sec}}$	0.01755 (front reaction control system) 0.0833 (aft reaction control system plus stabilizer)

TABLE 6. AV-8A&B S.A.S. CONTROL AUTHORITY

CONTROL	S.A.S. AUTHORITY LIMITS	MAX SAS CONTROL MOMENT / MAX AVAILABLE CONTROL MOMENT AT HOVER
δ_E	± 1.5 Deg. Stabiliator	0.266
δ_A	± 2.0 Deg. Ailerons	0.123
δ_R	± 5.0 Deg. Rudder	0.50

For details of the roll-yaw interconnect system which is fitted to the AV-8B only see Ref. 14. The very low authority of the roll S.A.S. should be noted.

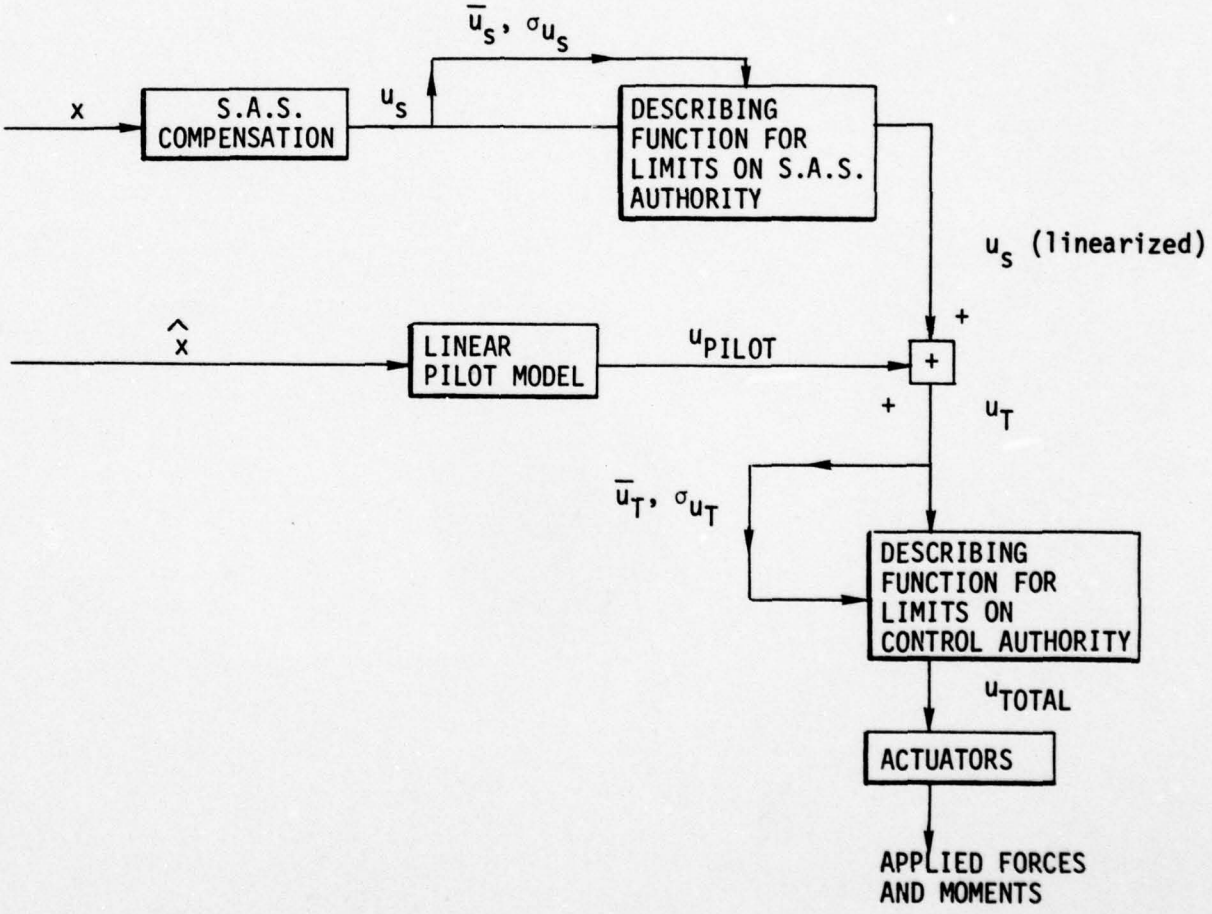


Figure 4. Simplified Representation of S.A.S. for Fly-By-Wire System

4.0 ATMOSPHERIC MODEL

4.1 Introduction

The Vought launch and recovery dynamics program is compatible with many different models of the atmospheric environment. The simplest type of model applies when the airplane is completely outside the ship airwake. For this case the atmospheric model comprises steady wind (including wind shear), and turbulence. For critical phases of VSTOL operations the airplane is either within or near the physical airwake; this necessitates a more complicated model, such as that presented below. This model is, however, not restricted to the space within the physical airwake, since it blends into a general low altitude atmospheric model as the airwake boundaries are crossed.

The ship airwake model is derived from wind tunnel measurements on a model of an FF 1052 frigate. It was previously presented in Reference 11, so only a brief description is given here. The model gives airwake properties as functions of the airplane position with respect to the ship, for six wind over deck conditions. These six conditions are presented in Table 7. VOLAR interpolates between these six conditions to provide ship airwake information, at any point in space, for a wind over deck orientation between 30 degrees and 50 degrees to port, with a magnitude between 20 knots and 50 knots.

The major departure from Reference 11 occurs in the bookkeeping of the airwake and ambient winds. VOLAR allows the user to select no airwake at all or to model an airplane flying in and/or out of the airwake. Hence, VOLAR bookkeeping is different from that of Reference 11. In VOLAR, subroutine AIRWAKE returns the incremental disturbance velocities due to the ship's presence, not the total airwake velocities (which include the ambient wind) given by Reference 11. In other words, the ambient wind is subtracted from the airwake and accounted for separately.

VOLAR can also represent Dryden type turbulence alone or in addition to the ship airwake turbulence.* In the work reported here, Dryden turbulence was used in conjunction with the ship airwake to model random atmospheric disturbances to the airframe.

---

*VOLAR is not restricted to Dryden type turbulence. Any turbulence that can be represented by white noise fed through a physically realizable filter with a finite number of poles and zeros can be modeled by VOLAR.

Table 7. Wind-Over-Deck Conditions for Airwake Model

V_{WOD} ~ KTS	ψ_s ~ DEGREES
20	-30
20	-50
35	-30
35	-50
45	-30
45	-50

ψ_s is the wind over deck direction with respect to the ship heading, positive if wind over deck is coming into the starboard side.

4.2 Summation of Airwake Components

This section outlines the development of the aircraft airspeed, V_A, from the aircraft body axis inertial velocities and the various atmospheric wind and/or turbulence models.

4.2.1 Ship Airwake Model

A schematic diagram depicting the ship airwake model is presented in Figure 5. This flow chart shows the inputs, summarizes the manipulations, and shows the outputs of the ship airwake calculations in VOLAR.

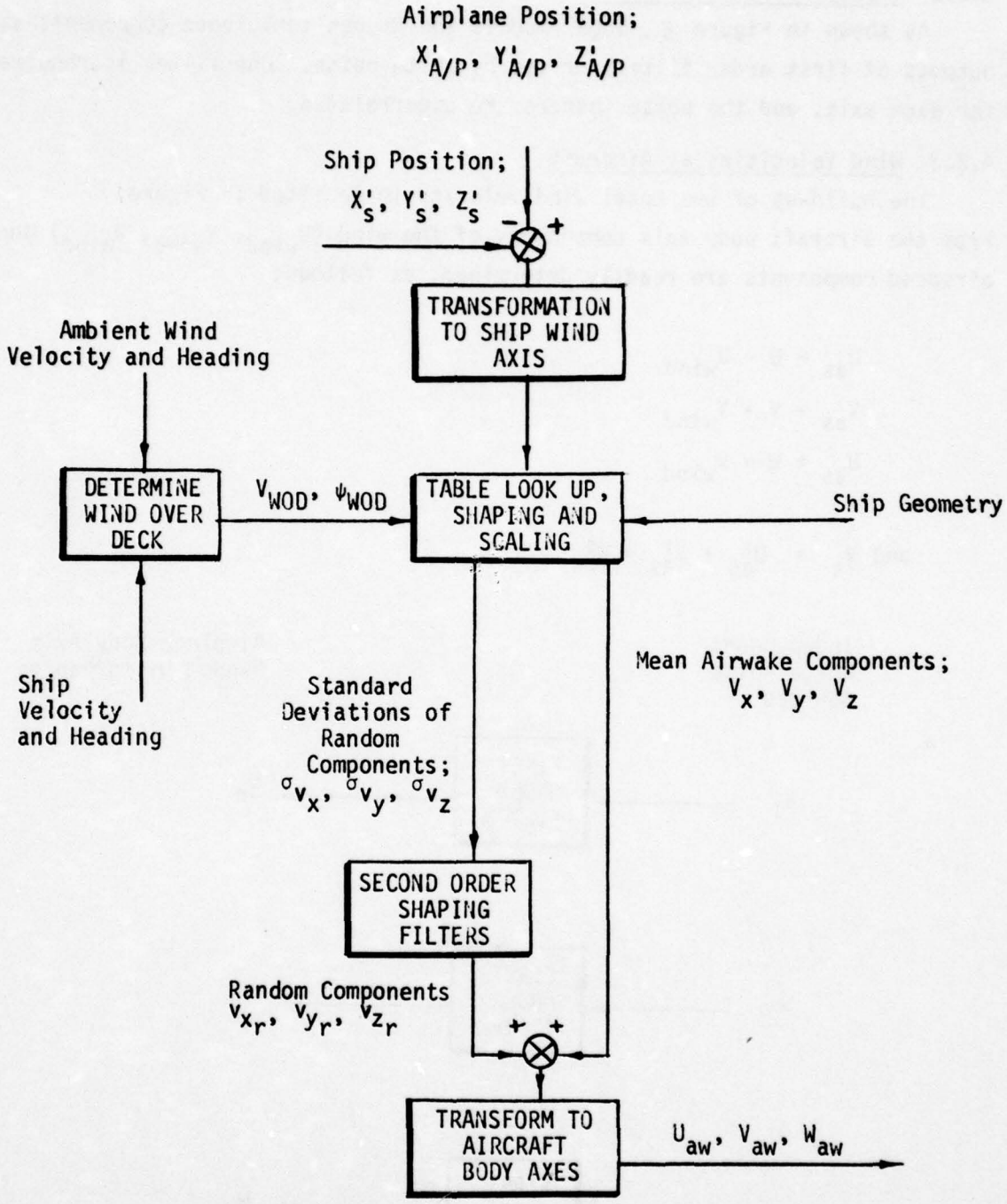


Figure 5. Airwake Model Flow Chart

4.2.2 Dryden Turbulence Model

As shown in Figure 6, VOLAR models the Dryden turbulence components as outputs of first order filters driven by white noise. One filter is required for each axis, and the noise sources are uncorrelated.

4.2.3 Wind Velocities at Aircraft

The build-up of the total wind velocity is depicted in Figure 7. From the aircraft body axis components of the wind (U_{wind}, V_{wind}, W_{wind}) the airspeed components are readily determined, as follows:

$$U_{as} = U - U_{wind}$$

$$V_{as} = V - V_{wind}$$

$$W_{as} = W = W_{wind}$$

$$\text{and } V_A = U_{as}^2 + V_{as}^2 + W_{as}^2$$

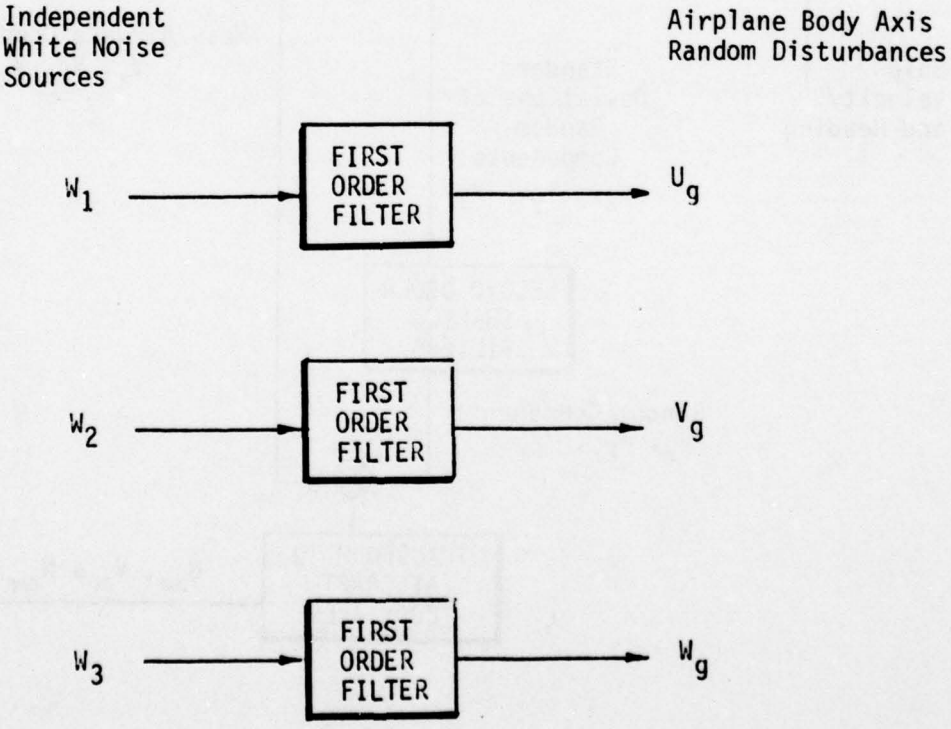


FIGURE 6. TURBULENCE SIMULATION

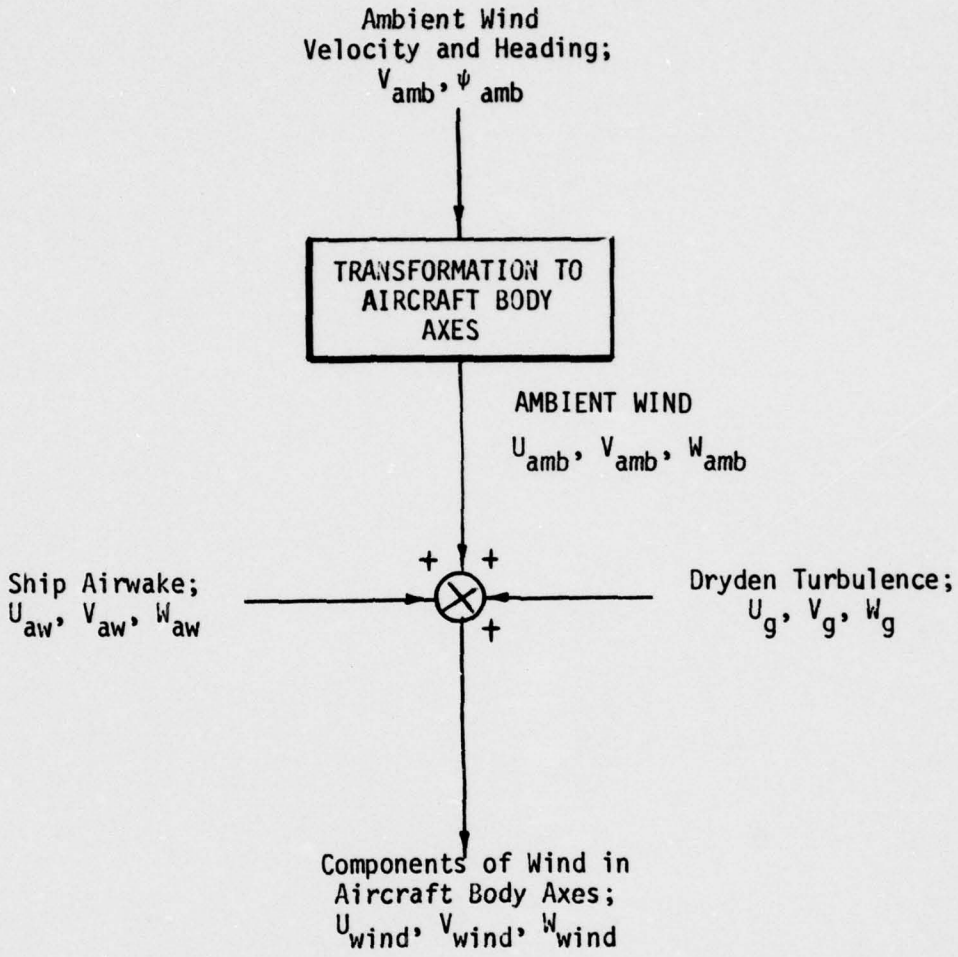


Figure 7. Summation of Airwake Components

5.0 CLASSICAL PILOT MODEL

5.1 Types of Pilot Model

The human pilot is an essential element of the VSTOL launch and recovery system and his dynamics should be modeled as accurately as any other major element of the system. Two approaches to modeling the human pilot are currently in widespread use. These will be designated the "classical" model and the "optimal pilot" model respectively. The dynamic models that result from these two modeling methods are equivalent (if both models are accurate).

The rationale for choosing one pilot model over the other will become clear after reading this section and section 7. These sections describe both models.

5.2 Example of Classical Pilot Model

Since the classical pilot model for closed-loop control has been documented extensively in Reference 17 and elsewhere only a highly condensed description will be given here. The model essentially consists of blocks with describing functions of the form

$$\frac{\text{Output}}{\text{Input}} = K_p \, e^{-\tau s} \cdot \frac{(T_L s + 1)}{(T_N s + 1)}$$

where

K_p = pilot gain, τ = time delay, T_L = lead time constant,
T_N = neuromuscular time constant

Additional leads and lags may be introduced as necessary. These leads and lags and the pilot gain are adjusted to meet certain "verbal adjustment rules" given in Reference 17. These rules are unfortunately not stated in forms suitable for computer mechanization. Therefore use of the classical pilot model requires judgement and experience, i.e., it is something of an "art". This comment also applies to the choice of loop structure into which the

---

17. McRuer, D. T., and H. R. Jex, A Review of Quasi-Linear Pilot Models, Trans. I.E.E.E, Vol. HFE-8, No. 3, September 1967.

pilot describing function blocks are inserted for multiloop control situations. Further adjustments are required to correct the pilot model for variations in system dynamics caused by changes in flight condition. For lateral control of the AV-8A at low speeds and hover the variations are sufficiently small that a constant loop structure and fixed gains and time constants may be used, as shown in Figure 8. The numerical values shown in Figure 8 are selected to match the classical pilot model verbal adjustment rules.

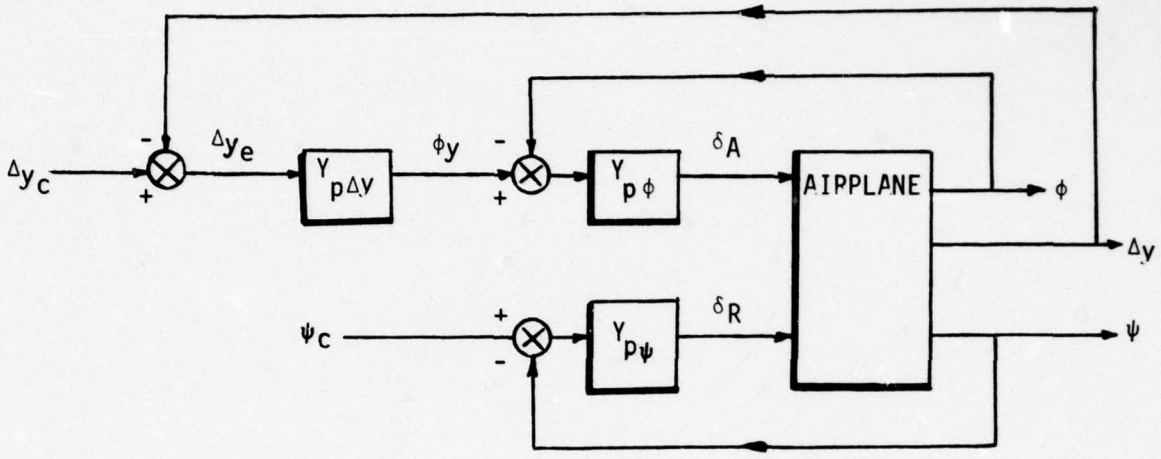
Details of classical pilot models for other VSTOL control situations (e.g., longitudinal control) are given in References 18, 19 and 20.

---

18. Craig, S. J., and A. Campbell, "Analysis of VTOL Handling Qualities Requirements" Part I: "Longitudinal Hover and Transition," AFFDL-TR-67-179, 1968.

19. Craig, S. J., A. Campbell, and R. H. Klein, "Analysis of VTOL Handling Qualities Requirements, Part II: Lateral-Directional Hover and Transition," AFFDL-TR-67-179, Part II, 1970.

20. Craig, S. J., I. L. Ashkenas, and R. K. Heffley, "Pilot Background and Vehicle Parameters Governing Control Techniques in STOL Approach Situations," FAA RD 72-69, June 1972.



$$Y_{p\phi} = -112.0 \frac{(s + 0.10)(s - 10.0)}{(s + 10.0)(s + 10.0)} \quad \frac{\text{units of } \delta_A}{\text{rad. } \phi}$$

$$Y_{p\Delta y} = 0.010 \quad \frac{\text{rad. } \phi}{\text{ft. } \Delta_y}$$

$$Y_{p\psi} = -58.6 \frac{(s + 1.0)(s - 10.0)}{(s + 10.0)(s + 10.0)} \quad \frac{\text{units of } \delta_R}{\text{rad. } \psi}$$

Figure 8. Lateral Pilot Model for AV-8A Hover and Low-Speed

6.0 EXAMPLE APPROACH FOR AV-8A WITH CLASSICAL PILOT MODEL

6.1 Introduction

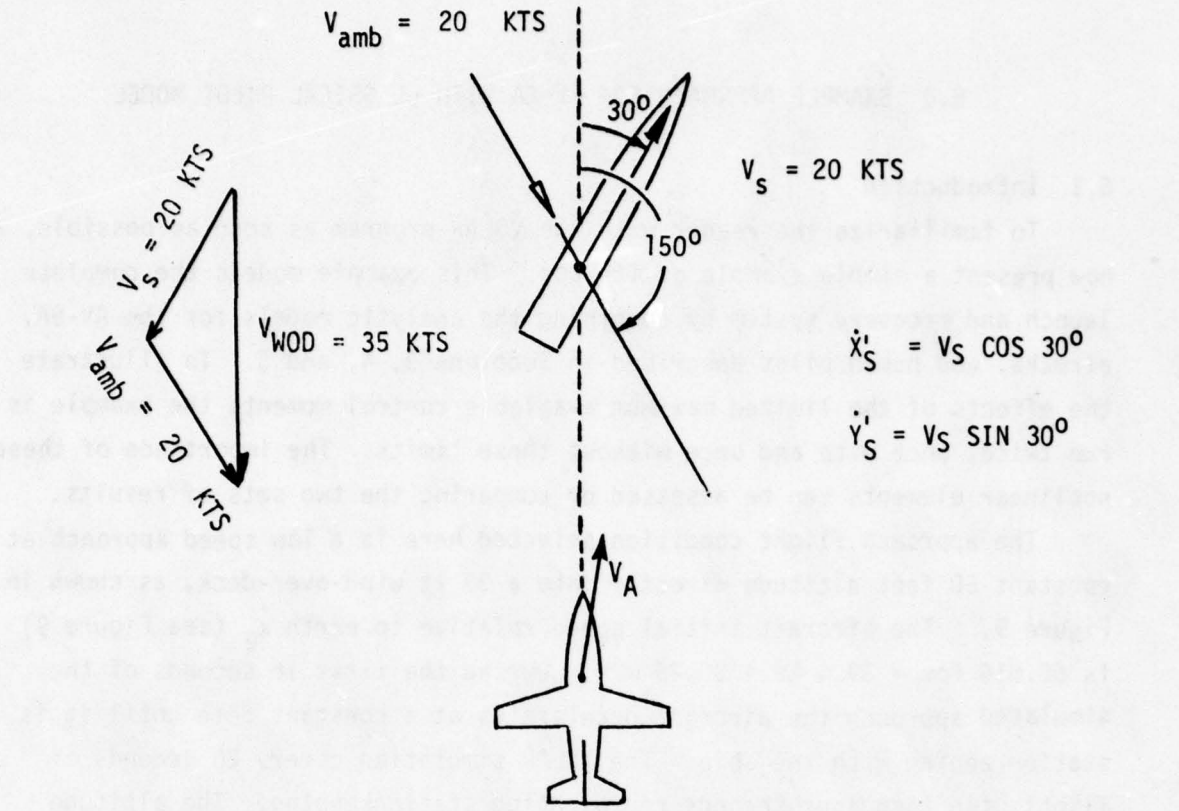
To familiarize the reader with the VOLAR program as soon as possible, we now present a simple example of its use. This example models the complete launch and recovery system by combining the analytic models for the AV-8A, airwake, and human pilot described in Sections 3, 4, and 5. To illustrate the effects of the limited maximum available control moments the example is run twice, once with and once without these limits. The importance of these nonlinear elements can be assessed by comparing the two sets of results.

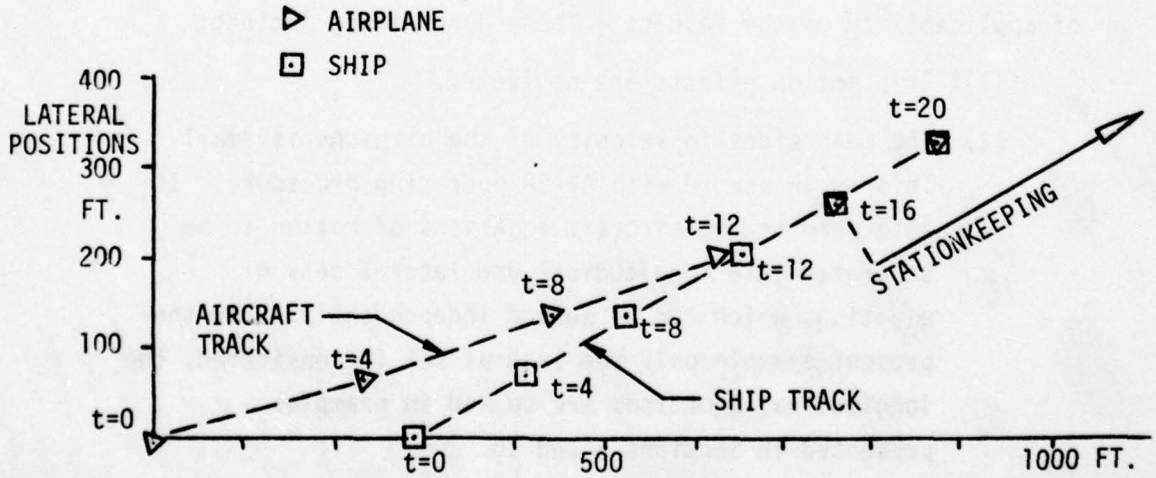
The approach flight condition selected here is a low speed approach at constant 50 feet altitude directly into a 35 kt wind-over-deck, as shown in Figure 9. The aircraft initial speed relative to earth $\dot{x}_e$ (see Figure 9) is 66.516 fps = 39.4 kt = 20.28 m/s. During the first 16 seconds of the simulated approach the aircraft decelerates at a constant rate until it is stationkeeping with the ship. The VOLAR simulation covers 20 seconds of flight, the last four seconds representing stationkeeping. The altitude (50 ft) is constant throughout; the final descent stage of the approach is not simulated in this example, although it is simulated in examples presented later in this report. A number of assumptions are made for this particular example which simplify the calculations, at the cost of restricting the range of applicability of the results. These assumptions include:

(1) Ship motion effects are neglected.

(2) The mean sideslip velocity of the airplane is small. This is in accord with AV-8A operating procedure. It also permits the aircraft equations of motion to be separated into longitudinal and lateral sets of equations which can be solved independently. For the present example only the lateral set is considered, the longitudinal equations are solved in examples presented in Sections 8 and 10.

The aircraft inertial flight path is curved. This follows from Figure 9, because the aircraft's component of inertial velocity parallel to the x_e-axis decreases with time, but the ship inertial lateral





LONGITUDINAL POSITIONS OF AIRPLANE AND SHIP IN INERTIAL AXES $X'_{A/P}$ AND X'_S

FIG. 9 COMMANDED LATERAL APPROACH PROFILE

velocity is constant = 20 cos 30^0 = 17.3 kts. Figure 9 also shows the inertial tracks of the ship and the airplane. The aircraft mean bank angle therefore has an initial bias, maintained during the transition to stationkeeping, since direct sideforce control is not available.

6.2 Discussion of Results

Figures 10(a), (b) and (c) show the principal results of the VOLAR runs. The dashed lines refer to limited (saturating) roll and yaw controls. The maximum values of the AV-8A roll and yaw control moments are given in Section 3. The solid lines represent results obtained with these saturation limits arbitrarily removed, i.e. a completely linear aircraft model.

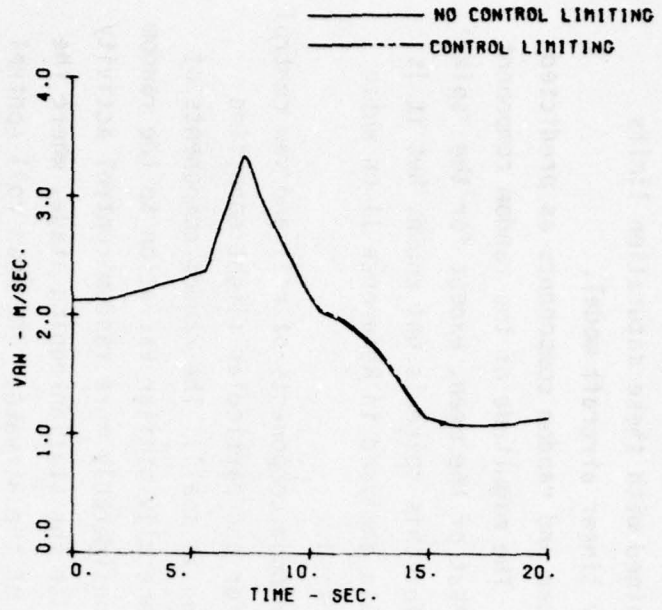
Figure 10(a) shows the airwake mean and random components as predicted by the airwake model of Reference 11. The magnitude of the random component follows a generally similar trend to that of the mean, except for the 'spike' at t = 7 secs.* The physical reason for this spike is not known, but it is distinctly shown by the wind tunnel data analysed in Reference 11 on which the airwake model of Reference 12 is based.

Figure 10(b) shows the mean and random components of roll and yaw control time histories. It is apparent that for the particular flight condition studied, the effect of control limiting is small. The random components of the control time histories follow a generally similar variation to the random airwake components. Hence there is considerably more random control activity at the beginning of the approach than at the stationkeeping stage, where the airplane is flying above the boundary of the airwake. The mean roll control deflection displays a spike at t = 7 secs demonstrating the pilot's reaction to the spike in the mean airwake.

Figure 10(c) shows the time histories of bank angle and lateral position error. The latter quantity is the deviation of the ground track from the commanded track. The mean lateral position error is small (< 1.2m) but the random component is larger (σ = 2.7m), especially at the beginning of the

---

*On Figure 10(a) the mean and random components are designated V_{AW} and V_{AY} respectively. For the case considered here these terms are equivalent. The commanded flight path requires the airplane to fly parallel to the W.O.D. direction, hence, the wind side component referred to ship wind axes (V_{AY}) equals aircraft sidegust component (V_{AW}).



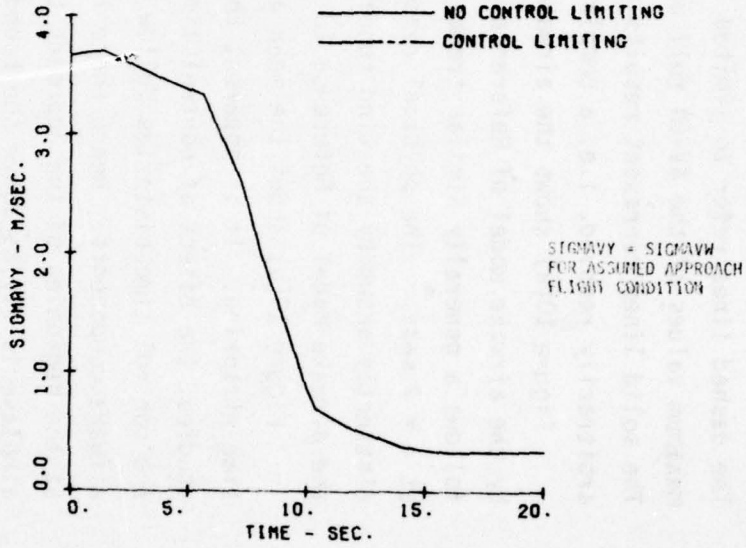


FIGURE 10(a). AV-8A APPROACH WITH CLASSICAL PILOT MODEL. MEAN AND RANDOM AIRWAKE SIDE VELOCITY COMPONENTS

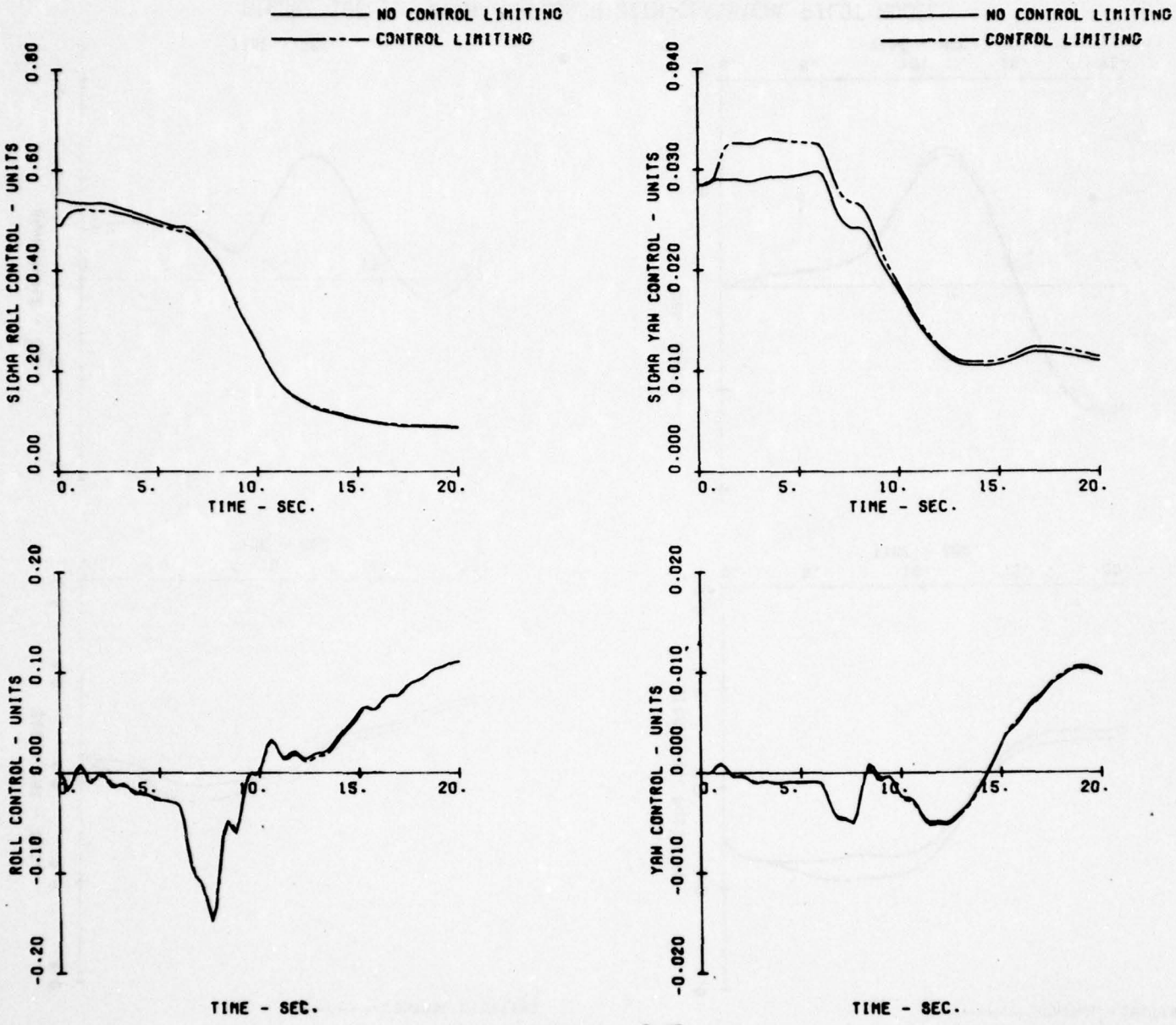


FIGURE 10(b). AV-8A APPROACH WITH CLASSICAL PILOT MODEL.
MEAN AND RANDOM CONTROL DEFLECTIONS

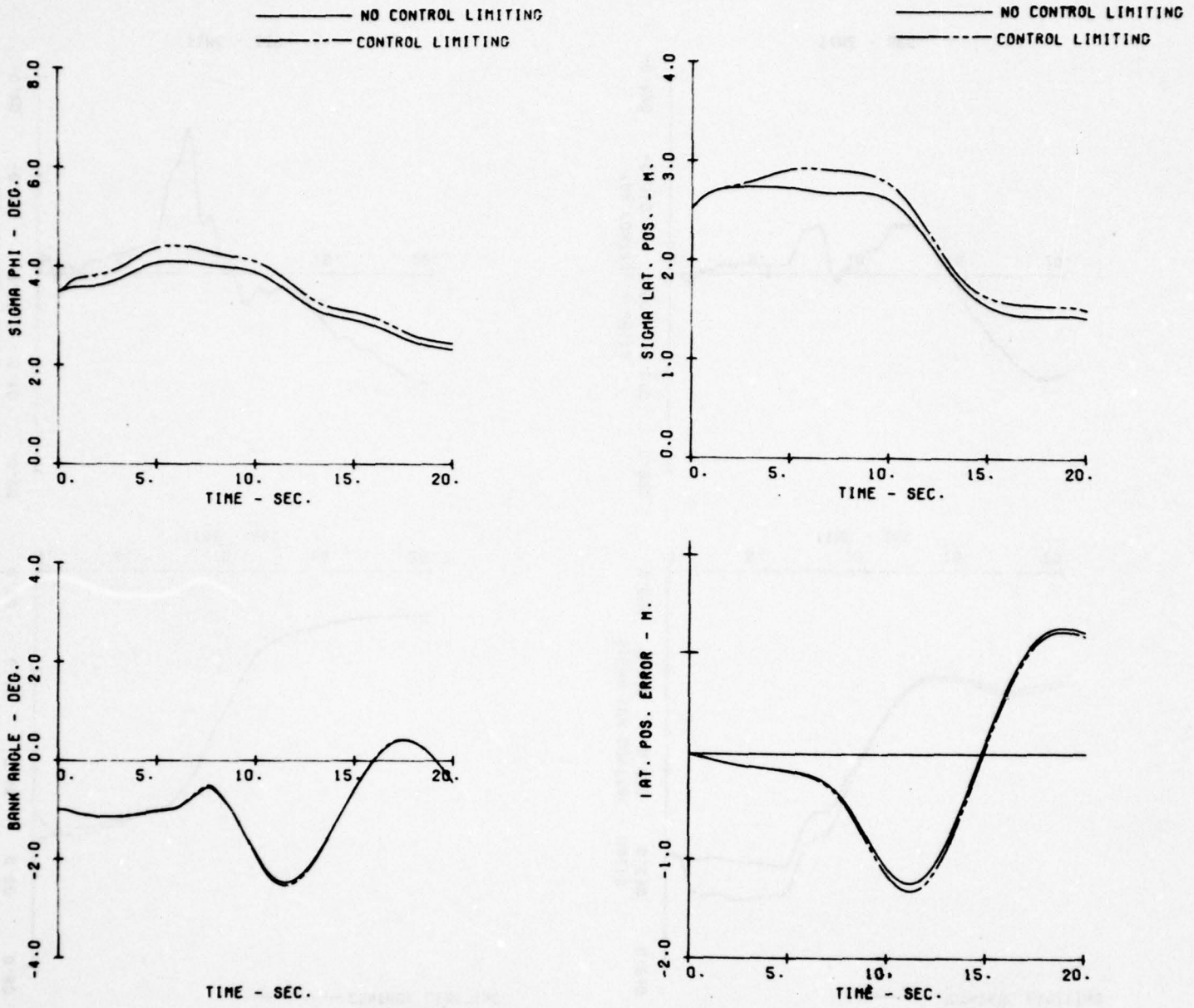


FIGURE 10(c). AV-8A APPROACH WITH CLASSICAL PILOT MODEL. MEAN AND RANDOM COMPONENTS OF BANK ANGLE AND LATERAL POSITION ERROR

approach. In practice, the 20 kt ambient wind / 35 kt W.O.D. condition would be associated with appreciable ship motion which would increase the error. Therefore the random lateral position error is disturbing, indicating that the AV-8A lateral characteristics may be unsatisfactory. Note that the bank angle time histories show a similar ratio of mean to random components, after subtracting the initial bias required to follow the curved ground track.

7.0 OPTIMAL PILOT MODEL

7.1 Background

A disadvantage of the classical pilot model described in Section 5 is that the criteria used to select the pilot gains are based on verbal adjustment rules which are essentially subjective. To remove this disadvantage Anderson (Reference 21)* and Dillow (Reference 22) replaced the verbal adjustment rules by mathematical optimization criteria. In the Anderson/Dillow approach (known as "Paper Pilot") classical loop structures are retained but the pilot gains and time constants are found as the result of minimizing a performance index. For example, for the longitudinal hover task (with no coupling into height control) the performance index is a linear combination of r.m.s. pitch rate, r.m.s. longitudinal hover error, and pilot lead time constant.

Paper Pilot type models have been developed for cruise and hover control of longitudinal and lateral motions. Each of these four cases requires a different performance index and a different loop structure. It was originally proposed to use the Paper Pilot series of computer programs developed by Anderson and Dillow (References 22, 23, 24)* as subroutines in VOLAR. Separate Paper Pilot programs exist for longitudinal hover, lateral hover, longitudinal cruise and lateral cruise. A subsequent publication by Dillow (Reference 25)* replaces these separate programs by a unified model, which is shown to give good agreement with measured data from simulator tests, (both fixed-base and moving-base). Dillow's model is shown in Figure 11. It models the pilot by a Kalman filter in series with an optimal controller. The optimal controller minimizes a performance index, J, of the following form:

$$J = \Sigma_{i=1}^{m} W_{y_i} \sigma_{y_i}^2 + R \dot{\delta}^2$$

where

y_i = the ith perceived state variable

$\dot{\delta}$ = rate of control deflection

W_y, R are weighting functions

Some differences between this index and the performance index used in previous pilot models should be noted, since these differences appear to be the reason

*References are listed on page 50.

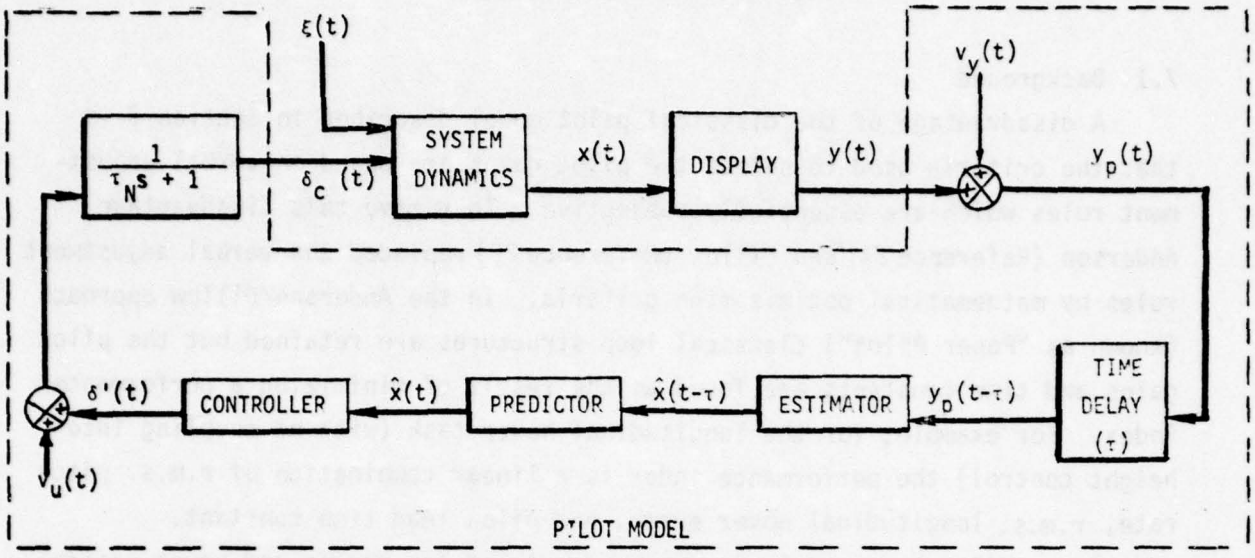


Figure 11. Block Diagram of the Optimal Pilot Model

References

21. Anderson, R. O. A New Approach to the Specification and Evaluation of Flying Qualities, AFFDL-TR-69-120, Wright-Patterson Air Force Base, Ohio: Air Force Flight Dynamics Laboratory, June 1970.

22. Dillow, J. D. The "Paper Pilot" - A Digital Computer Program to Predict Pilot Rating for the Hover Task, AFFDL-TR-70-40, Wright-Patterson Air Force Base, Ohio: Air Force Flight Dynamics Laboratory, March 1971.

23. Anderson, R. O., A. J. Conners, and J. D. Dillow, Paper Pilot Ponders Pitch, AFFDL-TM-70-1, Wright-Patterson Air Force Base, Ohio: Air Force Flight Dynamics Laboratory, November 1970 (Revised January 1971).

24. Nolting, D. L., Predicting Lateral Hover Flying Qualities with Paper Pilot, AFIT Thesis GA/MA-73A-2, Wright-Patterson Air Force Base, Ohio: Air Force Institute of Technology, December 1973.

25. Dillow, J. D., and D. G. Picha, Application of the Optimal Pilot Model to the Analysis of Aircraft Handling Qualities, AFIT-TR-75-4, Air Force Institute of Technology, Air University, Wright-Patterson Air Force Base, Ohio: 1975.

for the success of Dillow's model. For example, this index does not include all state variables, only those perceived by the pilot. Note also that control deflection does not appear in the index; instead control rate is employed. As explained below Dillow's new model appears to be better suited to our purposes than are the original paper pilot models.

This model requires some generalization to the multi-control task of V/STOL Launch and Recovery and the effect of airplane flight mode (cruise, transition, or hover) on the weighting functions demands careful study. Nevertheless the model offers the following advantages:

(1) A single general form of model is employed for all flight conditions (as opposed to the different model forms employed for "Cruise Paper Pilot", Reference 23, and "Hover Paper Pilot", Reference 22).

(2) The effects of visual landing aid and LSO cues can be incorporated in the performance index by increasing the number of perceived variables, m, in Equation 7.1 and by altering the weighting functions. This simplifies modeling the LSO and visual landing aids.

(3) One general formulation is employed irrespective of the number of degrees of freedom that the pilot is controlling.

On the other hand, some disadvantages of the optimal controller model must be noted.

(1) Relatively little multi-axis data has been analyzed to yield the appropriate performance indices.

(2) An estimate must be made (or implied) regarding the relative time spent controlling each axis, for situations where the axes are dynamically uncoupled, e.g., longitudinal and lateral control. Only a small data base exists for such estimates.

(3) As will be explained, minimization of the performance index is made more complicated because the model assumes that the covariance matrices describing measurement and neuromuscular noise are functions of the numerical value of the performance index.

(4) The model introduces a large number of additional states because of the estimator and predictor dynamics. This is a significant disadvantage for covariance propagation programs such as VOLAP because the run time of such programs tends to vary as the square of the number of state variables. (For Monte Carlo simulation programs run time tends to be linearly proportional to the number of state variables.)

7.2 The Model

This section reviews the evolution of the optimal pilot model from the form of Figure 11 to the form employed in VOLAP. The evolution was necessary to balance the completeness, accuracy, and efficiency of the pilot model versus these aspects of the other element models (ship, airwake, etc.). A general discussion is presented first, followed by equations representing the optimal pilot model used in VOLAP.

7.2.1 Simplification of Optimal Pilot Model

The model presented in Figure 11 will be referred to here as the "complete model". This form of the optimal pilot model has been validated in References 25, 26, 27, and elsewhere.

---

26. Baron, S., D. L. Kleinman, D. C. Miller, W. H. Levinson, and J. I. Elkind, Application of Optimal Control Theory to the Prediction of Human Performance in a Complex Task, AFFDL-TR-69-81, 1970.

27. Stengel, R. F., J. R. Broussard, P. W. Barry, and J. H. Taylor, Modern Methods of Aircraft Stability and Control Analysis, Report ONR-CR215-237-2, 1977.

Because VOLAR is presently programmed only for continuous systems, the pure time delay of Figure 11 was replaced by a first order Padé approximation. This removes the discrete element from the system and replaces it with a continuous one. In the continuous system all variables are defined at time t. (For the system of Figure 11 to be optimal, the controller must operate on $\hat{x}(t)$. However the estimator is providing estimates that are shifted back in time τ seconds because of the pure time delay on the measurements. The predictor is required to furnish (predict) $\hat{x}(t)$ to the controller using $\hat{x}(t-\tau)$ as its input.) These changes are reflected in the model shown in Figure 12. This figure shows the optimal controller pilot model that we initially employed for the longitudinal task. At the time of its use, this pilot model was part of a system model requiring 48 state variables, of which 30 were attributed to the pilot model.

Computer run time is approximately proportional to the square of the number of state variables. This indicates that a simpler pilot model would reduce costs. It is desirable therefore to keep the number of state variables low. Besides these considerations of economy, the complete pilot model appears unnecessarily refined for the present study when compared to the state-of-the art ship motion and airwake models employed.

Eliminating the Padé approximation substantially reduces the number of state variables associated with the pilot model. There is ample justification in the literature to support this simplification. For instance, Reference 28 uses the optimal pilot without the Padé approximation and in Reference 29 the authors present a strong case that the complete model is overparameterized, i.e. unnecessarily complicated. It was decided to drop the Padé approximation to take advantage of the run time savings and bring the pilot model more in line with the size and complexity of the other models in the overall system. The optimal pilot model used in VOLAR is shown in Figure 13 Note that in Figure 13 the block depicting the neuromuscular lag

---

28. Karmarkar, J. S., and J. A. Sorensen, Information and Display Requirements for Independent Landing Monitors, NASA CR-2687, 1976.

29. Phatak, A., H. Weinert, I. Segall, and C. N. Day, Identification of a Modified Optimal Control Model for the Human Operator, Automatica, Vol. 12, 1976.

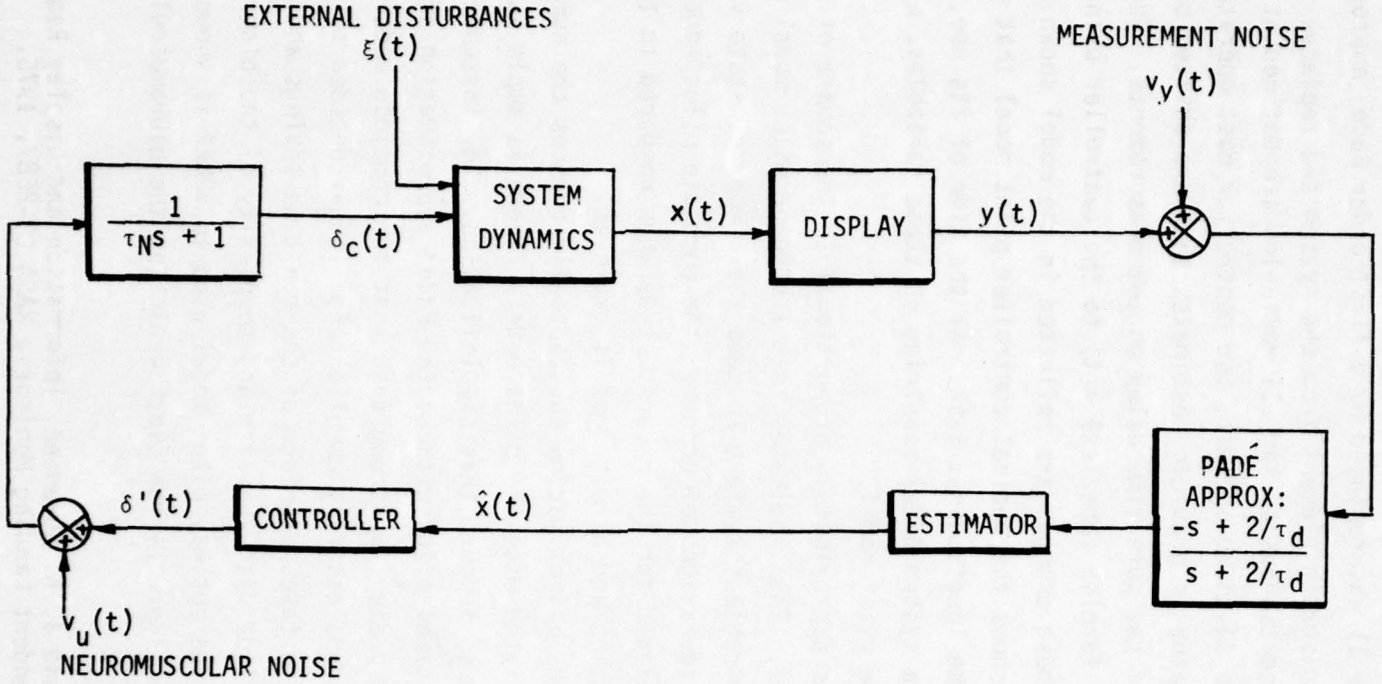


Figure 12. Block Diagram of Optimal Pilot Model with Padé Approximation

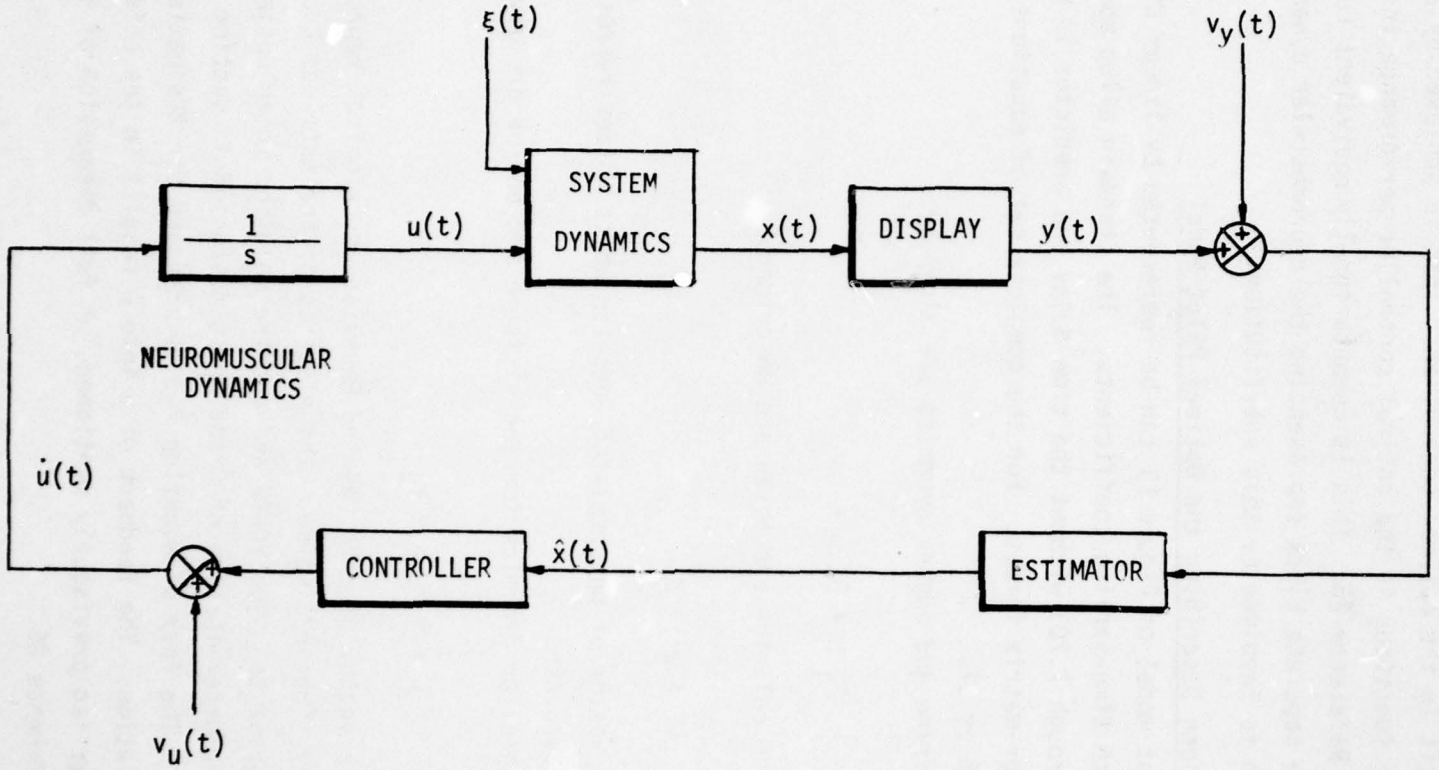


Figure 13. Block Diagram of Optimal Pilot Model Employed in VOLAR Program

does not appear explicitly. An effective neuromuscular lag is still present but is implicit in the optimal controller. This is achieved by altering the weighting functions in the optimal controller performance index, as explained in Reference 26. This is computationally equivalent to retaining the separate block representing the neuromuscular dynamics. No approximation is involved by this substitution.

7.2.2 Equations Describing the Optimal Pilot Model

The pilot model of Figure 13 can be represented by linear differential equations with time-varying coefficients. The standard pilot model, (Equations 7.1 through 7.20) without the time delay and predictor is presented here in vector-matrix format. For the complete set of equations, refer to References 26 or 27.

The airframe and engine dynamics are given by:

$$\dot{x} = F_1 x + G_1 u + \Gamma w' \tag{7.1}$$

The noise coloring processes are described by:

$$\dot{w}' = A w' + B w \tag{7.2}$$

where w is a vector of uncorrelated Gaussian white noises representing external disturbances.

The controller dynamics for the airframe and engine are given by:

$$\dot{u} = C \hat{x} + R_L \hat{u} + v_u \tag{7.3}$$

where v_u is a vector of uncorrelated Gaussian white noises representing pilot neuromuscular ("motor") noise. The elements of the matrices C and R_L must be determined prior to using VOLAR and are the solution to an optimal regulator problem. The determination of C and R_L is discussed in section 7.2.3 of this report. The form of equation 7.3 is standard for the optimal pilot model formulation. The feedback of u into $\dot{u}$ results in the effective neuromuscular lag previsously mentioned. A full discussion of this can be found in Reference 26.

The vector y represents the measurements, i.e. the quantities perceived by the pilot. The first derivatives of pilot perceived quantities are also included in y (References 25 and 26).

$$y = \begin{bmatrix} D & 0 & 0 \end{bmatrix} \begin{bmatrix} x \\ w' \\ u \end{bmatrix} + v_y \tag{7.4}$$

The quantity v_y is the vector of measurement noises. These are Gaussian, uncorrelated, and white.

The estimator dynamics* are described by:

$$\frac{d}{dt} \begin{bmatrix} \hat{x} \\ \hat{w}' \\ \hat{u} \end{bmatrix} = \begin{bmatrix} F_1 & \Gamma & G_1 \\ 0 & A & 0 \\ C & 0 & R_L \end{bmatrix} \begin{bmatrix} \hat{x} \\ \hat{w}' \\ \hat{u} \end{bmatrix} + K \left\{ y - \begin{bmatrix} D & 0 & 0 \end{bmatrix} \begin{bmatrix} \hat{x} \\ \hat{w}' \\ \hat{u} \end{bmatrix} \right\} \tag{7.5}$$

where the matrix K is given by:

$$K = P_E \begin{bmatrix} D^T \\ 0 \\ 0 \end{bmatrix} V_y^{-1} \tag{7.6}$$

where:

$$V_y = E\left\{ v_y \, v_y^T \right\} \tag{7.7}$$

The value of P_E (the estimator covariance matrix) is obtained from:

$$\dot{P}_E = F_E P_E + P_E F_E^T + Q_E - P_E \begin{bmatrix} D^T \\ 0 \\ 0 \end{bmatrix} V_y^{-1} \begin{bmatrix} D & 0 & 0 \end{bmatrix} P_E \tag{7.8}$$

where:

$$P_E = E\left\{ \begin{bmatrix} (x - \hat{x}) \\ (w' - \hat{w}') \\ (u - \hat{u}) \end{bmatrix} \begin{bmatrix} (x - \hat{x}) \\ (w' - \hat{w}') \\ (u - \hat{u}) \end{bmatrix}^T \right\} \tag{7.9}$$

and

$$F_E = \begin{bmatrix} F_1 & \Gamma & G_1 \\ 0 & A & 0 \\ 0 & 0 & 0 \end{bmatrix} \tag{7.10}$$

---

*A good general discussion of estimators is given in Reference 30.

$$Q_E = \begin{bmatrix} 0 & 0 & 0 \\ 0 & BWB^T & 0 \\ 0 & 0 & 0 \end{bmatrix} \tag{7.11}$$

$$W = E\left\{ w\, w^T \right\} \tag{7.12}$$

The covariance matrix for the estimated states is obtained from:

$$\dot{P}_{\hat{x}} = P_{\hat{x}}\, F_{\hat{x}}^T + F_{\hat{x}}\, P_{\hat{x}} + P_E \begin{bmatrix} D^T \\ 0 \\ 0 \end{bmatrix} V_y^{-1} \begin{bmatrix} D & 0 & 0 \end{bmatrix} P_E \tag{7.13}$$

where:

$$P_{\hat{x}} = E\left\{ \begin{bmatrix} \hat{x} \\ \hat{w}' \\ \hat{u} \end{bmatrix} \begin{bmatrix} \hat{x} \\ \hat{w}' \\ \hat{u} \end{bmatrix}^T \right\} \tag{7.14}$$

and

$$F_{\hat{x}} = \begin{bmatrix} F_1 & \Gamma & G_1 \\ 0 & A & 0 \\ C & 0 & R_L \end{bmatrix} \tag{7.15}$$

The measurement noise covariance matrix:

$$V_y = E\left\{ v_y\, v_y^T \right\}$$

and the neuromuscular noise covariance matrix:

$$V_u = E\left\{ v_u\, v_u^T \right\}$$

are functions of the covariance matrix P_x:

$$P_x = E\left\{ \begin{bmatrix} x \\ w' \\ u \end{bmatrix} \begin{bmatrix} x \\ w' \\ u \end{bmatrix}^T \right\} \tag{7.16}$$

where P_x is given by:

$$P_x = P_{\hat{x}} + P_E \tag{7.17}$$

and V_y is:

$$V_y = \rho_y \text{ diag } \left([D\ 0\ 0]\ P_x \begin{bmatrix} D^T \\ 0 \\ 0 \end{bmatrix} \right) \tag{7.18}$$

Noting that the lower right hand corner of P_x contains a submatrix P_{xu}, where:

$$P_{x_u} = E\left\{[u\ u^T]\right\} \tag{7.19}$$

we can write:

$$V_u = \rho_u \text{ diag } (P_{x_u}) \tag{7.20}$$

The choice of ρ_u, ρ_y requires some comment. Intuitively one would expect V_u and V_y to be constant. However Reference 26 suggests that V_u and V_y are proportional to P_x; i.e. ρ_u and ρ_y are constants. More experimental data are required to settle this point. For the present it seems advisable to follow the approach of Reference 26, for which supporting data exist.

7.2.3 Calculation of C and R_L

The elements of C and R_L in equation 7.3 are the feedback gains of the optimal controller. They are determined by solving an optimal regulator problem. In the equations below the vector u contains aircraft controllers (elevator, throttle, etc.) and u_c is a vector of commanded inputs.

Given the system

$$\begin{bmatrix} \dot{x} \\ w' \\ \dot{u} \end{bmatrix} = \begin{bmatrix} F_1 & \Gamma & G_1 \\ 0 & A & 0 \\ 0 & 0 & 0 \end{bmatrix} \begin{bmatrix} x \\ w' \\ u \end{bmatrix} + \begin{bmatrix} 0 \\ 0 \\ I \end{bmatrix} \{u_c\} \tag{7.21}$$

and performance criterion

$$J = \lim_{t \to \infty} \int_0^t \left\{ \left\{ \begin{bmatrix} x \\ w' \\ u \end{bmatrix}^T Q_c \begin{bmatrix} x \\ w' \\ u \end{bmatrix} + u_c^T R_c u_c \right\} dt \right. \tag{7.22}$$

determine the control strategy u_c^* that minimizes the cost function, J. Note that this formulation is similar to the classical optimal regulator problem with one exception. Here the conrol vector u has been adjoined to x and w'. Observe that $\dot{u} = Iu_c$ in equation 7.21 (I is the identity matrix); therefore 'control rate' is commanded, instead of 'control displacement'. Consequently there is a weighting matrix, R_c, on control rate in the cost function.

The solution to the optimal regulator problem is given in Reference 30, as follows:

The optimal control law is

$$u_c^* = \left[\begin{array}{c|c} C & R_L \end{array}\right] \begin{bmatrix} x \\ w' \\ \hline u \end{bmatrix} \tag{7.23}$$

where

$$\left[\begin{array}{c|c} C & R_L \end{array}\right] = -R_c^{-1} \left[\begin{array}{c|c} 0 & I \end{array}\right] P_c \tag{7.24}$$

and P_c is the steady state solution (i.e. $\dot{P}_c = 0$) of the matrix Riccati equation given below.

$$\dot{P}_c = P_c \begin{bmatrix} F_1 & \Gamma & G_1 \\ 0 & A & 0 \\ 0 & 0 & 0 \end{bmatrix} + \begin{bmatrix} F_1 & \Gamma & G_1 \\ 0 & A & 0 \\ 0 & 0 & 0 \end{bmatrix}^T P_c + Q_c - P_c \begin{bmatrix} 0 & 0 & 0 \\ 0 & 0 & 0 \\ 0 & 0 & R_c^{-1} \end{bmatrix} P_c \tag{7.25}$$

Because of the principle of separability the optimal estimator problem and the optimal controller problem can be worked independently. Thus one can conveniently solve for C and R_L apart from VOLAR. The resulting values of C and R_L become inputs to VOLAR.

7.2.4 The Collected Equations

The coupling between the estimator dynamics and the system dynamics is described by equation 7.3

$$\dot{u} = C\hat{x} + R_L\hat{u} + v_u \tag{7.3}$$

---

30. Bryson, A. E., and Y. C. Ho, Applied Optimal Control, Blairdell, Waltham, Mass., 1964.

This equation implies that the estimator equations must be adjoined to the basic system equations in order to characterize the complete pilot-plus-airframe system. Hence if the system dimensionality is of order n, the pilot-plus-airframe system is approximately 2n.

The overall system can be represented as:

$$\frac{d}{dt}\begin{bmatrix} x \\ w' \\ u \\ \hat{x} \\ \hat{w}' \\ \hat{u} \end{bmatrix} = [F]\begin{bmatrix} x \\ w' \\ u \\ \hat{x} \\ \hat{w}' \\ \hat{u} \end{bmatrix} + [G]\begin{bmatrix} w \\ v_y \\ v_u \end{bmatrix} \qquad (7.26)$$

Figures 14 and 15 show how F and G (respectively) breakdown into their sub-matrix components. Note that for simplicity and clarity the matrices K and C have also been partitioned.

The sub-matrix breakdown in Figure 14 and 15 is completely general; i.e., it is valid for any size matrix. The actual dimensions on each of the sub-matrices are problem-dependent. Regardless of how the F matrix is partitioned it must contain the basic system dynamics and the controller and estimator dynamics representing the human pilot.

This section has presented the equations describing the present "optimal pilot" model. Section 8 presents an example demonstrating the application of the optimal pilot model. Programming details for using the VOLAR option for the model are given in Appendix A. The decision whether to use the optimal pilot model or the classical pilot model may hinge upon the relative run times required by the VOLAR program for each mode. Comparing the "classical pilot" example of Section 6 with the "optimal pilot" example of Section 8 yields the following relative run times for a 20 second time history:

	Dimensionality (order of F)	Run Time CPU Secs	Relative Run Time
Classical	17	54.4	1.0
Optimal	39	355.9	6.5

For comparison, a 200-run Monte Carlo simulation of the classical pilot example requires 800 CPU seconds; thus, VOLAR requires only 7 percent of the computer time required for Monte Carlo analysis.

$$
F = \begin{bmatrix}
F_1 & \Gamma & G_1 & 0 & 0 & 0 \\
0 & A & 0 & 0 & 0 & 0 \\
0 & 0 & 0 & C_x & C_w & R_L \\
K_x D & 0 & 0 & (F_1 - K_x D) & \Gamma & G_1 \\
K_w D & 0 & 0 & (-K_w D) & A & 0 \\
K_u D & 0 & 0 & (C_x - K_u D) & C_w & R_L
\end{bmatrix}
$$

where $K = \begin{bmatrix} K_x \\ \hdashline K_w \\ \hdashline K_u \end{bmatrix}$ and $C = \left[\begin{array}{c:c} C_x & C_w \end{array}\right]$

Figure 14 Elements of the Generalized F-Matrix

$$
G = \begin{bmatrix}
0 & 0 & 0 \\
B & 0 & 0 \\
0 & 0 & I \\
0 & K_x & 0 \\
0 & K_w & 0 \\
0 & K_u & 0
\end{bmatrix}
$$

I = Identity Matrix

Figure 15 Elements of the Generalized G-Matrix

7.3 Modifications for Multi Axis Control

Degradation in pilot control of one axis due to an increased workload in another axis effects are readily included in the optimal pilot model. These effects are modeled as an increase in the noise to signal ratio ρ_{y_i}. Thus

$$\rho_{y_i} = \rho_y \cdot \frac{1}{f_c} \cdot \frac{1}{f_s} \cdot \frac{1}{f_i}$$

where

ρ_y = Noise to signal ratio associated with "full attention" (Equation 7.18)

f_c = Fraction of attention devoted to the control task as a whole

f_s = Fraction of attention devoted to subtasks; e.g., longitudinal control

f_i = Fraction of attention devoted to the i^{th} perceived variable and its first derivative in subtask s; e.g., control of pitch attitude in the longitudinal subtask

7.4 Visual Landing Aids

Visual landing aids and Landing Signal Officer (LSO) functions can be easily represented by appropriate augmentation of the pilot perceived variables, y, in Equation 7.4. Pilot perceived variables are selected to fit the task. These may include on board indicators as well as ship based landing aids. Additional perceived state variables, such as the LSO's signals are adjoined to y thereby increasing its dimensionality. If the LSO function is to emphasize certain state variables which are already included in the vector of pilot perceived variables then the noises on those variables must be adjusted according to the time spent viewing each of the sources. A discussion on the treatment of scanning behavior can be found in Reference 26.

8.0 AV-8A LONGITUDINAL APPROACH IN A LOW SEA STATE

8.1 Task Description

The simulated task is a constant altitude decelerating approach to a stationkeeping position 50 ft. (15.2 m) above the deck, followed by a 6 sec. descent to the deck. The aircraft is an AV-8A flown by the optimal pilot model. The external disturbances modeled are Dryden type atmospheric turbulence and the ship's airwake. Sea State 2 is assumed; this gives only small ship motions, which are considered to be negligible for this example. (Ship motions are modeled in a subsequent example which assumes a higher Sea State.)

Figures 16 and 17 illustrate the desired approach flight path. During the initial phase the airplane decelerates at a constant 2.33 fps^2 and is directed to the ship by commanding its inertial position. The ambient wind speed is 10.5 knots, and the ship is steaming at 15 knots. As shown in Figure 16, the wind and ship directions are such that the W.O.D. speed is 20 knots. The commanded flight path requires the aircraft to be headed into the W.O.D., hence the commanded sideslip angle is zero. It is therefore assumed that longitudinal and lateral motions are decoupled, and only longitudinal motions are simulated in this example.

8.2 Model Components

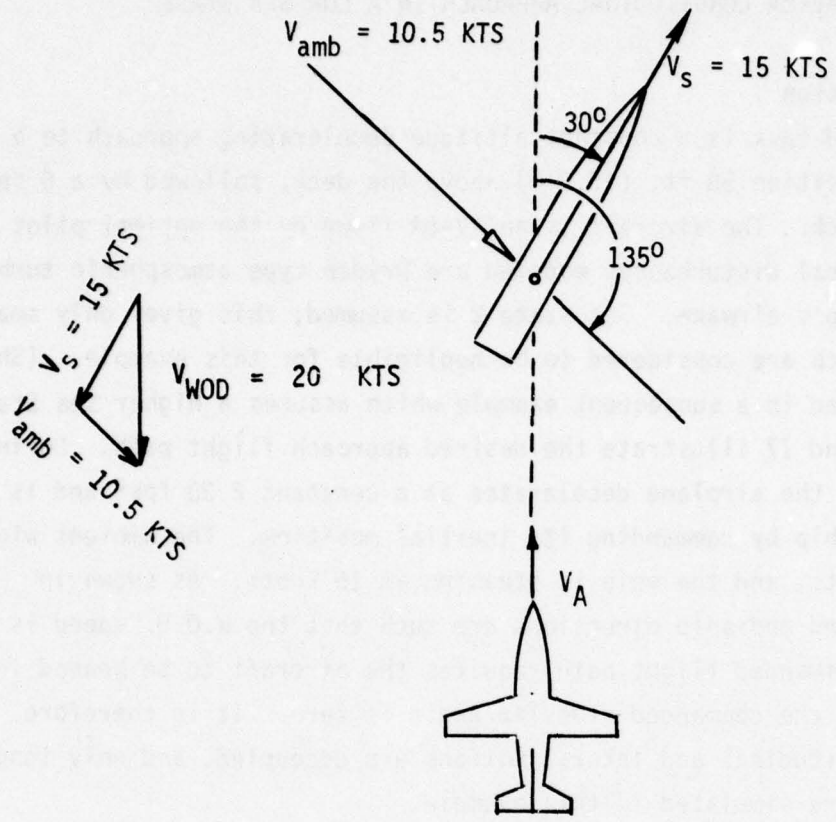
8.2.1 Airplane

The AV-8A airplane is modeled by the longitudinal equations of motion discussed in Section 2. The dynamics of the powerplant are modeled as a first order lag with a time constant of 0.2 seconds.

The airspeed of the AV-8A at the initiation of the approach segment simulated here is 24.6 knots (17.81 m/sec) and the terminal airspeed equals the W.O.D. speed. AV-8A flight data (Reference 35) indicate that the pilot flies this segment of the approach employing only two longitudinal controls, i.e. thrust magnitude and pitching moment. The third available control, nozzle angle, is set at a fixed trim setting. Our simulation follows the full-scale example, but core space is reserved for nozzle angle in the VOLAR program, so it can readily be included as a control variable if desired.

8.2.2 Atmosphere

The atmospheric model is discussed in Section 4. Dryden turbulence



COMMANDED $X'_{A/P} = 59.207t - 1.165t^2$, $t < 16$; $= X'_S$, $t \geq 16$

$Z'_{A/P}$ = -50 FT

$\gamma = 0^o$, $\theta = 8^o$

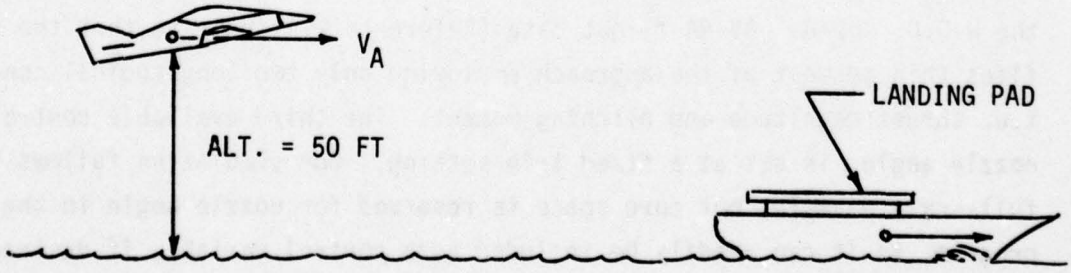


Figure 16 Schematic of AV-8A Landing Task

PROFILE EQUATIONS:

$$\text{Commanded } X'_{A/P} = 59.207\,t - 1.165\,t^2,\ t < 16$$
$$= X'_S,\ t > 16$$
$$\text{Commanded } Z'_{A/P} = -50$$

for $X'_{A/P}$, $Z'_{A/P}$ in feet.

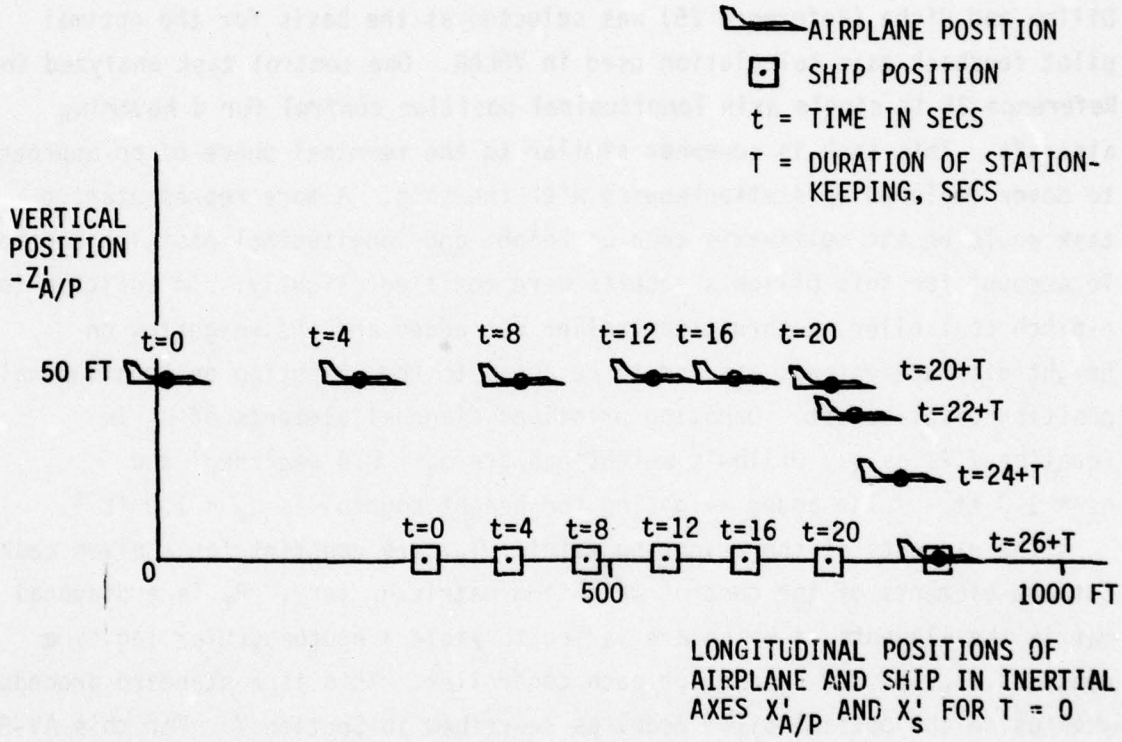


Figure 17 Commanded Longitudinal Approach Profile

r.m.s. values for u_g and w_g were 1 ft/sec. The ship airwake was, of course, varied as a function of aircraft position with respect to the ship.

8.2.3 Optimal Pilot Model

A description of equations representing the optimal pilot are presented in Section 7. The feedback gains of the optimal controller are required as input to VOLAR. These are computed separately. This is a corresponding task to the root locus, frequency, and/or time history analyses that are performed 'off line' when using the classical pilot model. The work of Dillow and Picha (Reference 25) was selected as the basis for the optimal pilot feedback gain calculation used in VOLAR. One control task analyzed in Reference 25 is single axis longitudinal position control for a hovering aircraft. This task is somewhat similar to the terminal phase of an approach to hover followed by stationkeeping with the ship. A more representative task would be the multi-axis case of height and longitudinal position control. To account for this Dillow's results were modified slightly. In addition to a pitch controller, a thrust controller was added and the weighting on height displacement was assumed to be equal to the weighting on longitudinal position displacement. Denoting principal diagonal elements of Q_c in Equation 7.22 as q_i. Dillow's weightings are $q_q = 0.4$ sec^2/deg^2 and $q_x = 1.0$ ft^{-2}. The added weighting for height control is $q_z = 1.0$ ft^{-2}.

The elements of the weighting matrix, Q_c, are constant for a given task, but the elements of the control weighting matrix R_c vary. R_c is a diagonal matrix the elements of which are varied to yield a neuromuscular lag time constant, τ_N, of 0.2 second for each controller. This is a standard procedure when using the optimal pilot model as described in Section 7. For this AV-8A simulation, at 20 knots airspeed the values of the main diagonal elements of R_c were $r_{\delta_e} = 0.0489$ and $r_{\delta_T} = 0.00603$.

The numerical solutions for the feedback gains were obtained using a computer program from Reference 31. This program was selected for its availability; however, any program that will solve the matrix Riccati equation (Equation 7.25) may be used.

---

31. Melsa, James L., and Stephen K. Jones, Computer Programs for Computational Assistance in the Study of Linear Control Theory, McGraw-Hill, Inc., 1973.

Following the determination of the optimal controller feedback gains the user must address the estimator. Here, as before, the work of Dillow and Picha served as a guide. The values of ρ_y and ρ_u (Equations 7.18 and 7.20) were taken from Dillow and are 0.01π and 0.003π respectively. The pilot was assumed to perceive the variables $X'_{A/P}$, $Z'_{A/P}$, and θ. Standard optimal pilot model practice (References 25 and 26) places the pilot perceived variables and their first derivatives in the measurement vector y (Equation 7.4). This practice was followed here with the additional assumption that the pilot perceives the displays (measurements) simultaneously. In more detailed analyses (References 25 and 26) the pilot is assumed to divide his time between the various displays. This results in some degradation in pilot performance. This effect could be modeled by VOLAR if desired, but would result in a pilot model which is over-sophisticated relative to the models currently used for the other elements of the Launch and Recovery system.

A similar simplification was made concerning multi-axis control. The standard optimal pilot model apportions the time spent controlling each axis. In other words, while the pilot may be 'flying' all axes, he mentally gives more priority to one axis over another; which further degrades his performance. Currently the optimal pilot in VOLAR does not include this additional penalty. He is assumed to apply his full attention simultaneously to all the axes that he is controlling. This assumption is justified by: (1) the degree of sophistication of the other element models as discussed above and, (2) the lack of experimental data on multi-axis task control apportionment. Multi-axis control apportionment could be included as outlined in Section 7.3 as more experimental data become available.

8.2.4 Ship Motion

The sea conditions for this example produce negligible ship disturbances; i.e. there are no random ship motions. The only ship motion is the mean motion along the X earth axis; $\dot{X}'_S = V_{SHIP} \cos(\psi_{SHIP})$. (The Y earth axis motion is not relevant in this longitudinal-only simulation.)

8.3 Simulation of Two-Stage Approaches

Current practice for the AV-8A performing an approach and landing to a small ship involves a two-stage approach. The first stage consists of a decelerating transition from some initial speed and altitude to a 'stationkeeping' flight condition where the aircraft maintains a constant position relative

to the ship. (This position is near the ship but may be outside the airwake.) The second stage of the approach comprises the final descent and touchdown. This stage may not commence until an appreciable time after the stationkeeping mode has been established, since the pilot may have to wait for deck clearance, or a lull in ship motion. The duration of the stationkeeping interval is therefore highly variable.

For the present simulation the stationkeeping interval was not explicitly represented, although each of the above stages was simulated. It was therefore necessary to do two runs, one for each stage, and to re-initialize the state variables at the commencement of the second stage. This re-initialization procedure involves re-setting the covariance matrix P in Equation 1.4. It would be unrealistic to reset P equal to zero because at the commencement of the second stage the aircraft has been stationkeeping for an unspecified period in the presence of atmospheric turbulence, and other noise sources. P was therefore obtained by solving the matrix Riccati equation for an abritrarily chosen time t = 5 secs, assuming P = 0 at t = 0. No problems were encountered with this technique for the cases studied here since P converged rapidly to a steady-state value. However, for such initialization runs it is desirable to employ a higher order integration algorithm than for the rest of the simulation. Smaller time increments should also be employed. Detailed comments on this point are given in Appendix A. This re-initialization is unnecessary for simulations of STOL approaches, VTOL launches, and other continuously defined maneuvers, including VTOL landings that are performed without a 'break'. For such simulations P is initialized only once, to provide the proper initial conditions for the beginning of the interval that is being simulated.

8.4 Results

Figures 18(a) through 18(i) show the results of the simulation of AV-8A longitudinal approach characteristics. The commanded flight profile is as shown in Figure 17 and the optimal pilot model is employed. The ship motion is negligible for the assumed Sea State 2 condition. The figures will be discussed below in three groups, as follows:

Figures 18(a) and (b) - Airwake Characteristics

Figures 18(c) and (d) - Control Deflections Generated by Optimal Pilot

Figures 18(e) thru (i)- Aircraft Response

Each figure shows the time history of (i) the mean and (ii) the standard deviation (σ) of the appropriate quantity. The left side of each figure illustrates the decelerating constant altitude stage of the approach, the right side illustrates the descent stage (the left and right sides of the figures are separated to indicate that the second stage follows the first after a stationkeeping stage of indeterminate duration). For the present, only the dashed lines on the figures should be studied. The solid lines represent a Sea State 5 case for which ship motion is significant. This case is discussed in Section 10, and compared with the Sea State 2 case.

Airwake Characteristics - Figures 18(a) and (b) show the airwake horizontal and vertical velocity components. These components are scaled directly from FF-1052 wind tunnel data as described in Reference 11. Note that the mean and standard deviation of the horizontal component becomes most intense at the beginning and end of the approach. A similar trend is noted for the standard deviation of the vertical component σ_{v_z}, indicating that at the stationkeeping location the turbulence level is low. On the other hand a considerable upwash exists at this location ($W_{AW} \simeq -4.0$ m/s).

Control Applied by Optimal Pilot - Figure 18(c) shows the time histories of the mean and standard deviation of the pitch attitude control, $\sigma\delta_E$. The doublet applied by optimal pilot to mean $\sigma\delta_E$ at t = 15 secs is required to null the airplane speed relative to the ship. This rapid control movement is a mean activity only, and is not matched by a corresponding increase in random stick motions. On the contrary, the latter are most pronounced at the initiation and at the completion of the recovery. As shown in Figure 18(d) the throttle time histories show similar characteristics to the pitch control motions.

The time integrals of the variances of the random control deflections are known to be correlated with pilot opinion, as shown in References 21, 22, and 25. On this basis one would expect the pilot opinion to be worse at the beginning and at the end of the recovery, when the airplane is immersed in the highest turbulence levels.

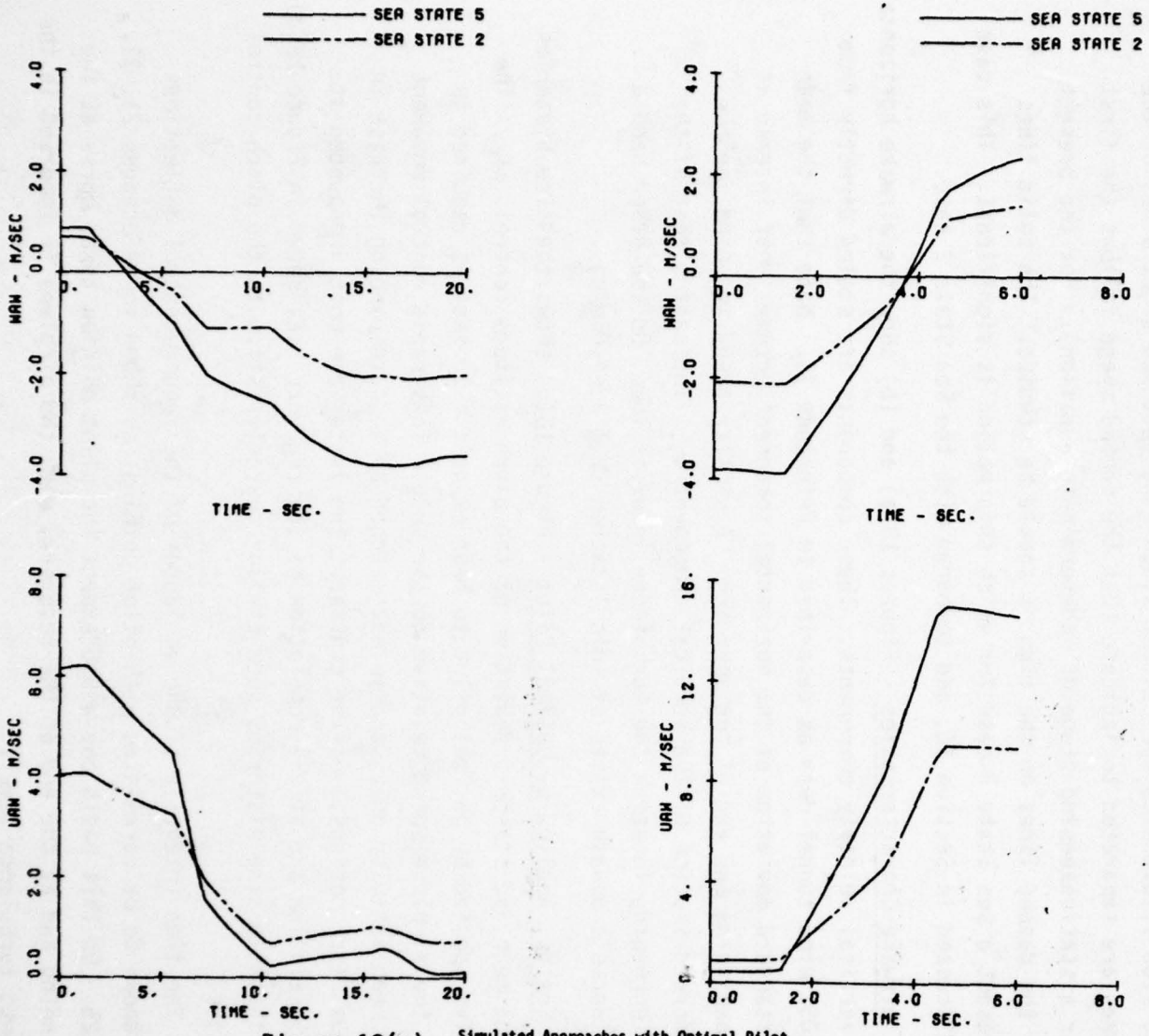


Figure 18(a) Simulated Approaches with Optimal Pilot Mean Wind Components

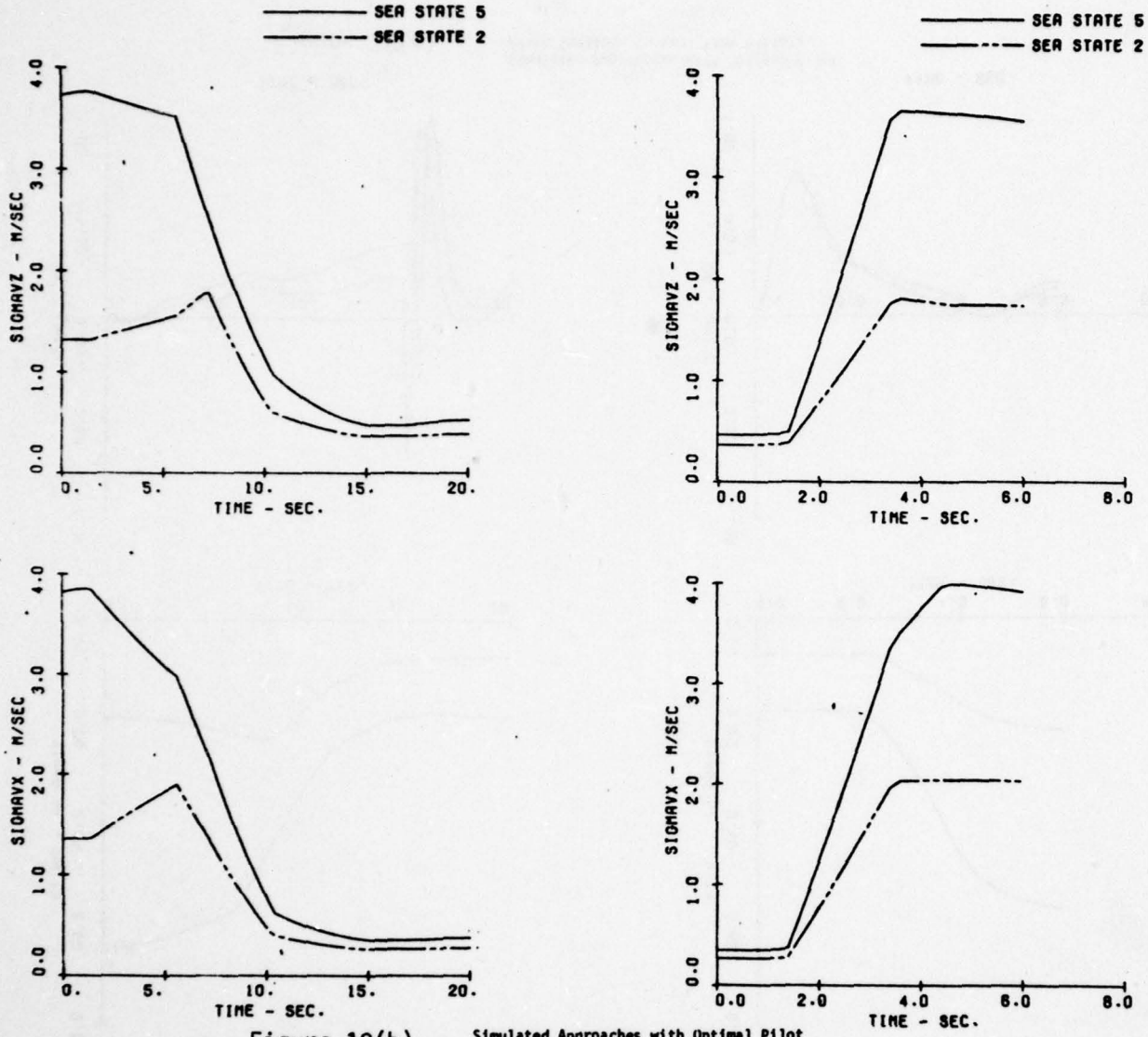


Figure 18(b) Simulated Approaches with Optimal Pilot Random Wind Components

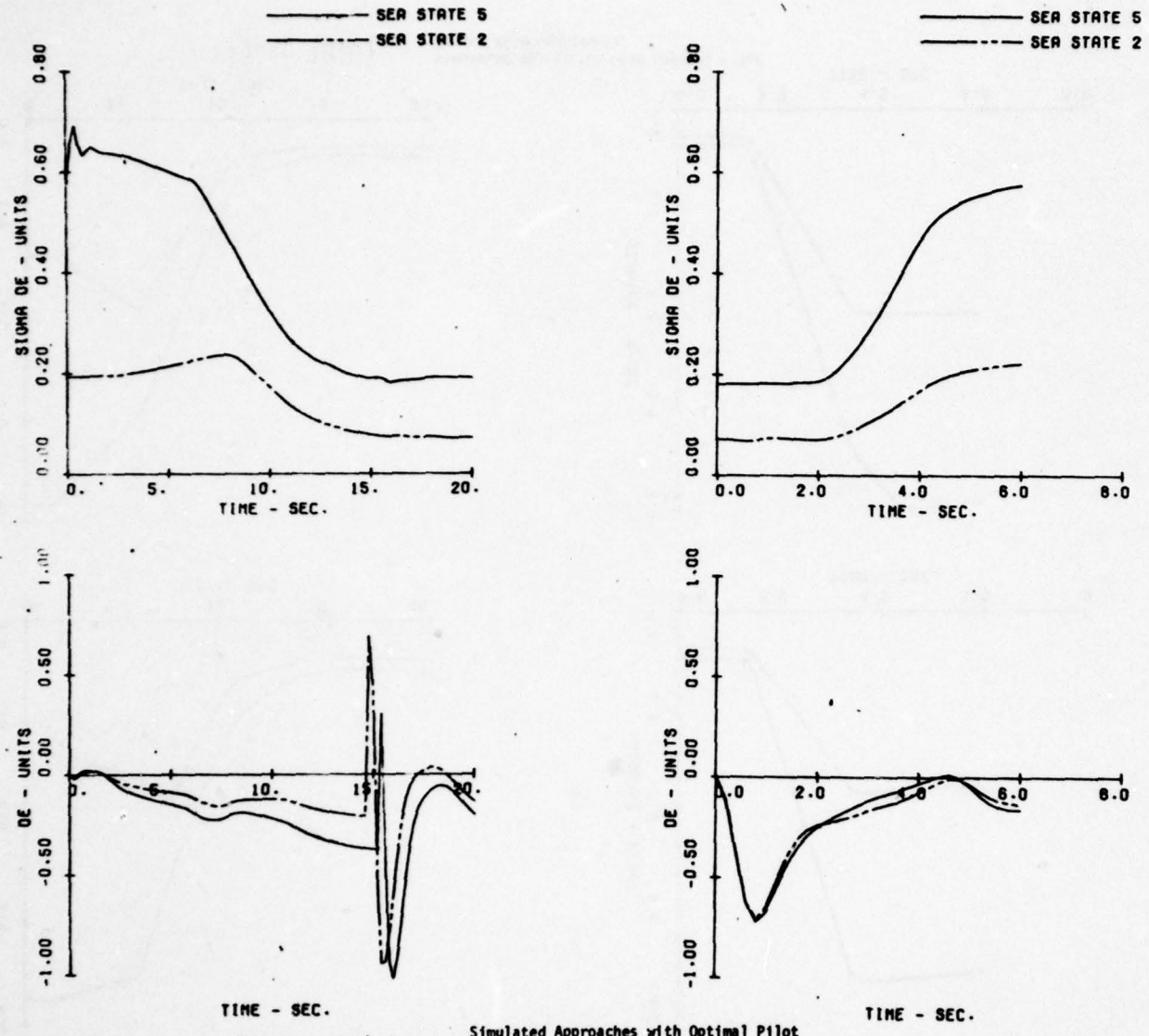


Figure 18(c) Simulated Approaches with Optimal Pilot Pitch Attitude Control Time History

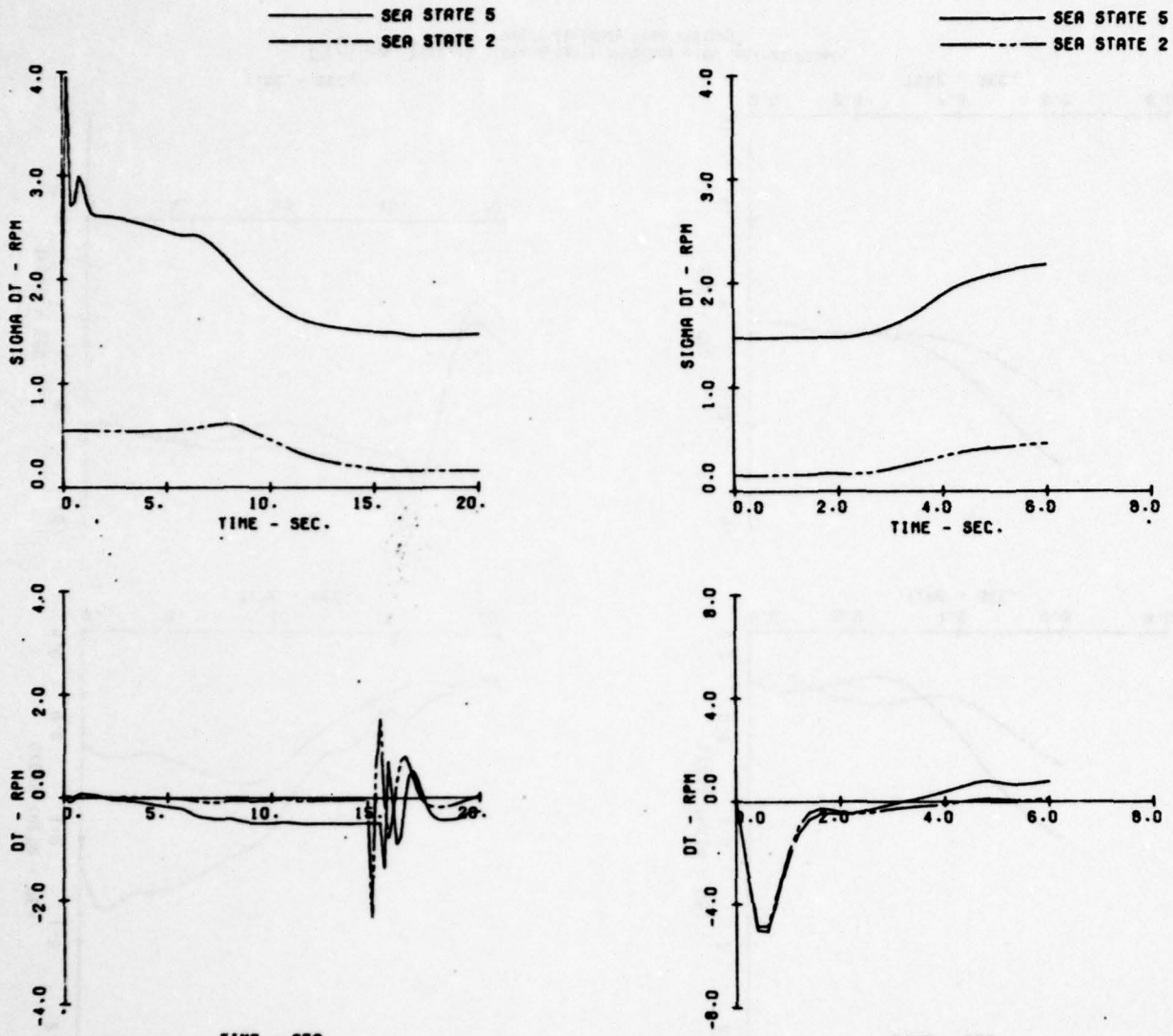


Figure 18(d) Simulated Approaches with Optimal Pilot Thrust Magnitude Control Time History

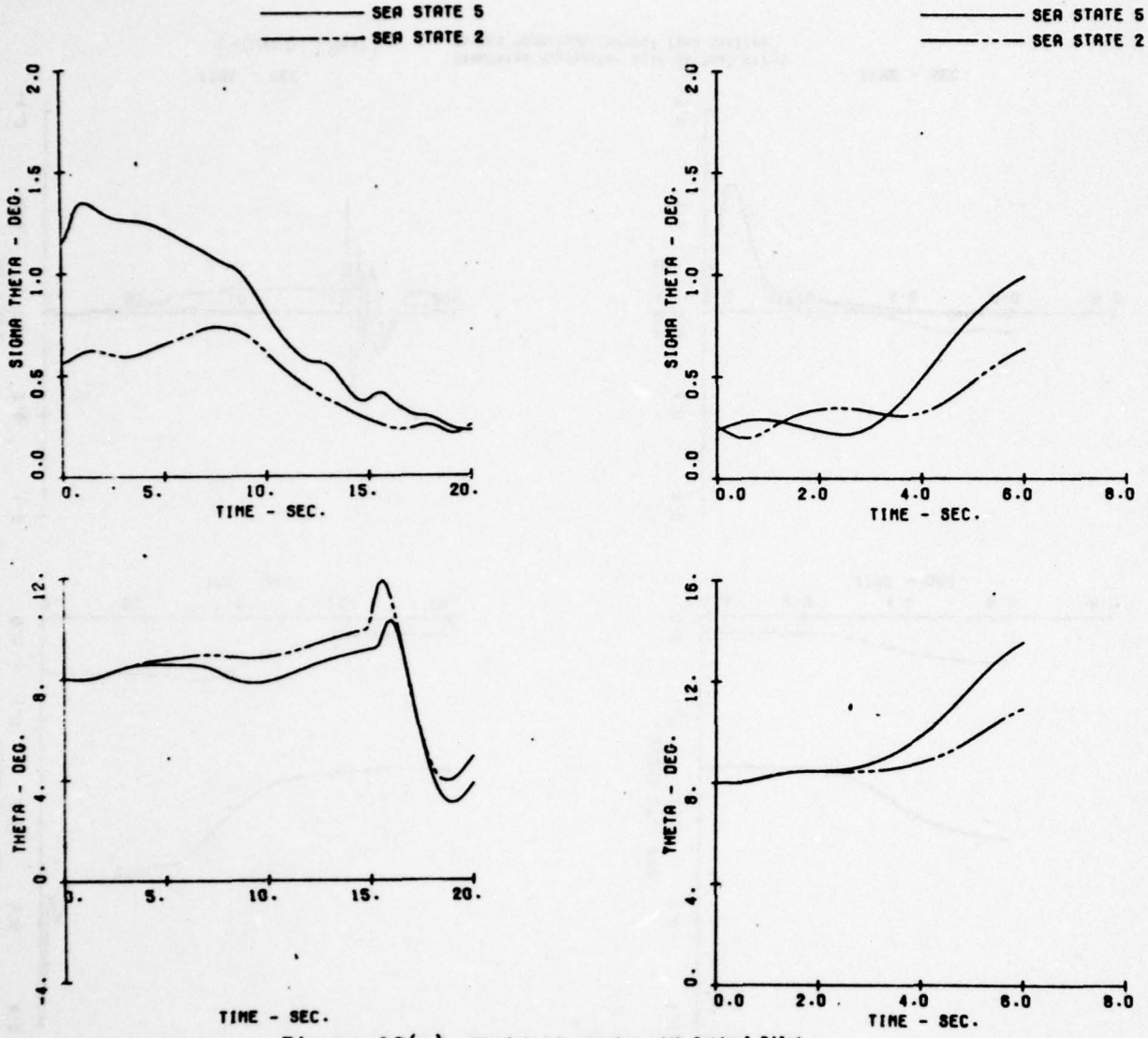
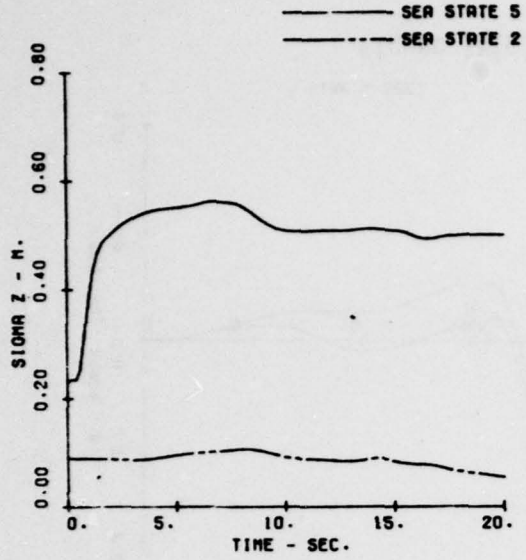
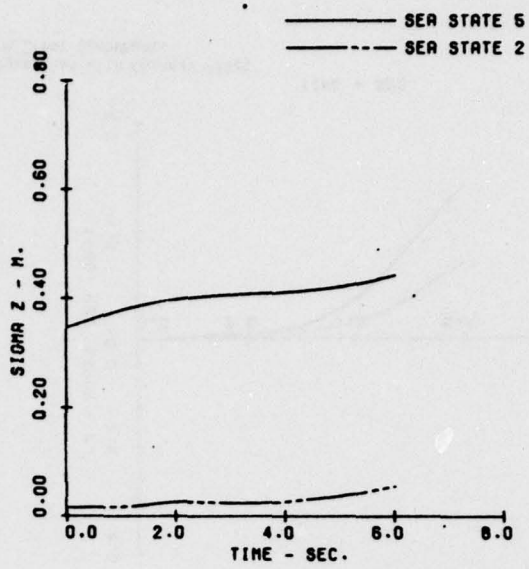
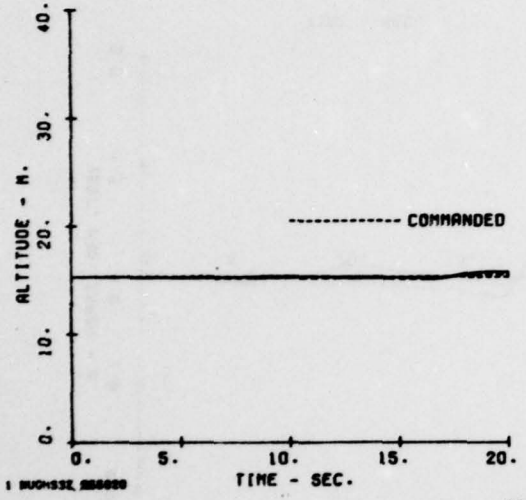


Figure 18(e) Simulated Approaches with Optimal Pilot Pitch Attitude Time History







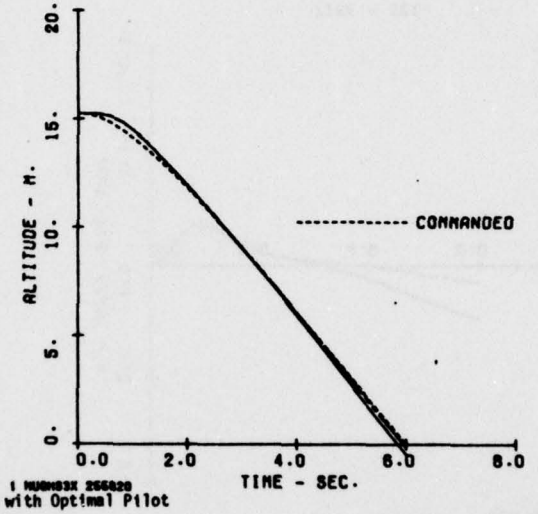


Figure 18(f) Simulated Approaches with Optimal Pilot Altitude Time History

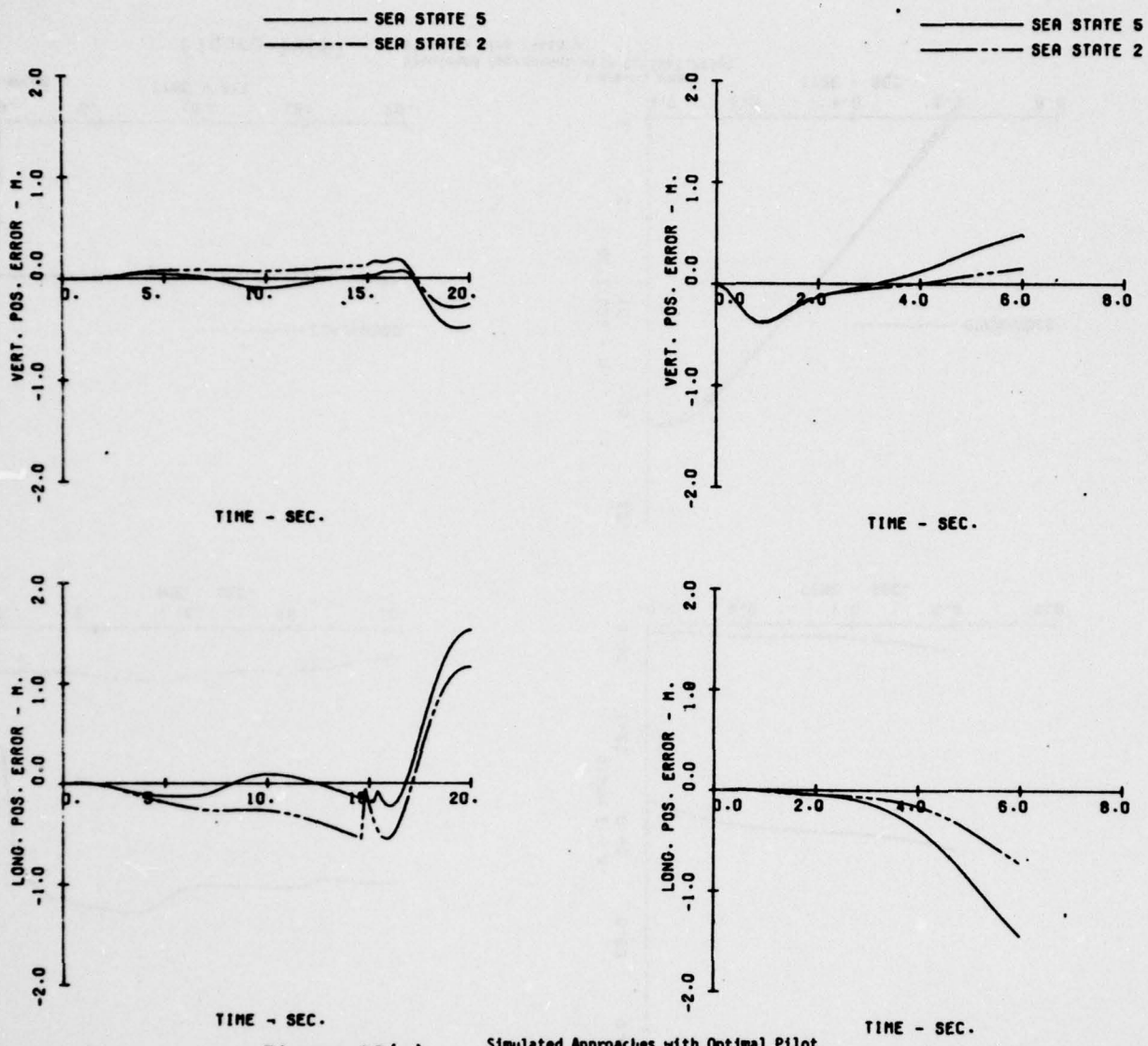
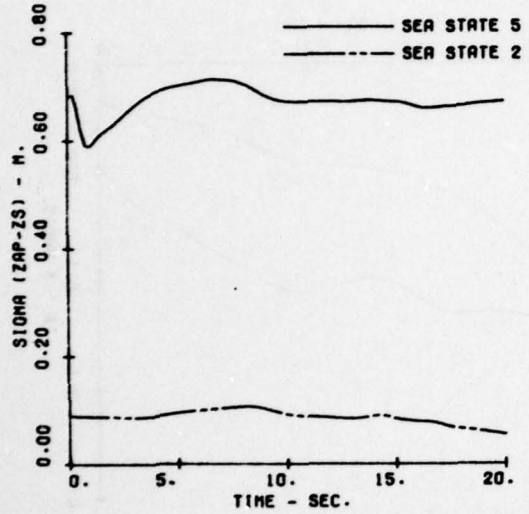


Figure 18(g) Simulated Approaches with Optimal Pilot
Mean Position Error Components

AV-8A APPROACHES A DD-963
FLOWN BY OPTIMAL PILOT



AV-8A APPROACHES A DD-963

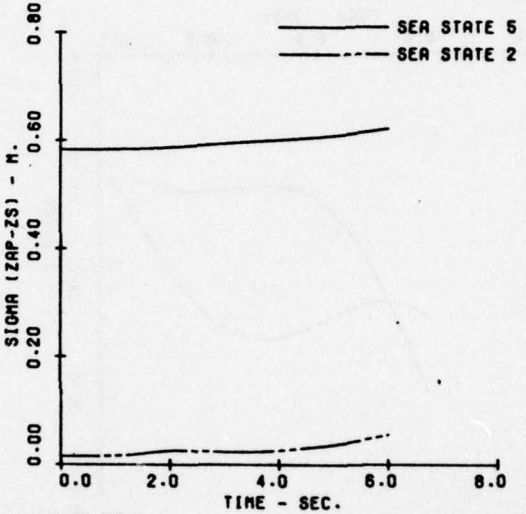


Figure 18(h) Simulated Approaches with Optimal Pilot
Time History of Airplane Height Relative to

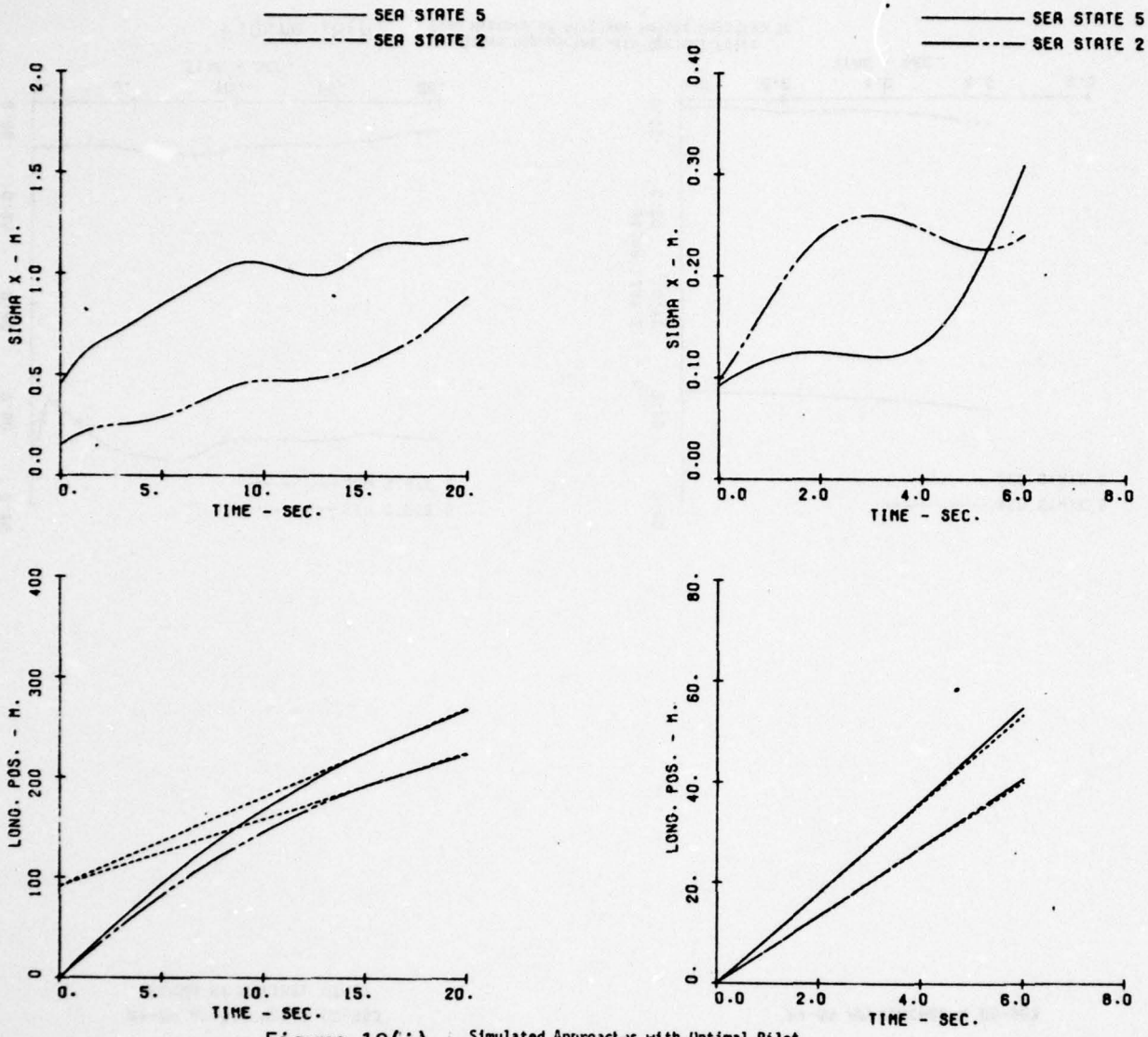


Figure 18(i) Simulated Approaches with Uptimal Pilot Random Components of Position Error

Aircraft Response - The appropriate pitch attitude time histories are shown on Figure 18(e). As one would expect, σ_θ varies with time in a generally similar manner to the standard deviation of the horizontal airwake velocity component. The maximum magnitude of σ_θ is approximately 0.6 degrees. indicating that for this sea state the pilot is controlling the aircraft within close tolerances. Figure 18(e) indicates relatively large variations in mean θ of approximately 4^0. These correspond to the pull-up maneuvers required to terminate each stage of the approach. These large terminal pitch angles could be trimmed out by collective nozzle deflection, but as explained previously this trimming control was fixed for the present simulation.

Figure 18(f) shows actual and commanded altitude time histories. The mean height error is very small, and the standard deviation is less than 0.2m for this case with negligible ship motion. An enlarged plot of the mean height error is given on Figure 18(g), together with the mean longitudinal position error. The latter quantity is approximately 0.8m at touchdown, with a corresponding standard deviation of approximately 0.25m as shown in Figure 18(h). As shown by the near-coincidence of the lower graphs on Figure 18(h) the commanded and actual positions are extremely close for the final part of the approach.

Correlation of the above results with flight data is discussed in Section 13. On the basis of the results presented here the recovery at 20 kts W.O.D. with the wind direction specified in Figure 16 appears to be a maneuver which is well within the capabilities of the pilot and the aircraft.

9.0 SHIP MOTION MODEL

9.1 Introduction

The examples of VSTOL recoveries presented in previous sections have been for low sea states, where ship motion is negligible. This section describes how ship motion effects are modeled by VOLAR, and section 10 presents a numerical example for a Sea State 5 condition for which ship motion is important.

Three steps are required to include ship motion in the state-variable equations which express the basic covariance propagation relationship of VOLAR.

(1) An accurate mathematical model must be found for ship response to specified sea states.

(2) The model must be approximated by a model which is in state-variable form and which does not unduly increase the dimensionality of the state-variable equations for the complete system.

(3) The approximate model must be adjoined to the equations previously formulated for the case of negligible ship motion.

The above steps are described in Sections 9.2, 9.3, and 9.4 respectively.

9.2 The RAOH Ship Motion Model

The RAOH ship motion model is described in Reference 32. It predicts ship motion spectral characteristics at any given frequency ω rad/sec by multiplying wave spectra by operators known as "PAO"s (response amplitude operators). For the example of Section 10 it was assumed that the wave spectra could be determined from the Bretschneider formula (Reference 32),

---

32. Brown, R. G., and F. A. Camaratta, Navairengcen Ship Motion Computer Program, Naval Air Engineering Center, Lakehurst, New Jersey, Report NAEC-MISC-903-8, 1977.

which is a function of the significant wave height (H_s) and the modal period (T_o). These parameters are related to the wind and ship velocity vectors as indicated in Table 8 (taken from Reference 33).

For the present application the RAO's were taken from data supplied by NSRDC for a DD-963 ship.

9.3 Approximation of the RAOH Ship Motion Spectra

The approximations described below were developed by P. L. Fortenbaugh in Reference 33. The following description is condensed from Reference 33, which should be consulted for more detailed descriptions of modelling procedures for ship-wave interactions.

The numerical data for the ship motion spectra calculated by RAO's given in Reference 32 were approximated by equations of the following general form.

$$G_i\ (j\omega_e) = \frac{K_i\ j\omega_e}{\left(1 - \frac{\omega_e^2}{\omega_{n_i}^2}\right) + 2\zeta_i \frac{j\omega_e}{\omega_{n_i}}} \qquad (9.1)$$

where i = the motion variable = x, y, z, θ_s, ϕ_s, ψ_s

K_i = Filter gain

ω_{n_i} = The equivalent natural frequency of the spectrum

ζ_i = The equivalent damping ratio of the spectrum

ω_e is the wave encounter frequency

The form of $G_i\ (j\omega_e)$ was determined by examination of the spectra developed for the conditions in Table 8. For the most part these spectra assumed the shape shown in Figure 19 which is reasonably represented by the squared magnitude of $G_i\ (j\omega_e)$. It is expected that this is an adequate representation

33. Fortenbaugh, R. L., Application of the NAEC Ship Motion Simulation Program for Starboard Approaches to DD-963 Class Ships, Enclosure to Vought Report 2-55830/8AVO-153, 1978.

Table 8 Candidate Ship Speed-Wave Direction-Wave Spectrum Parameters-Wind Over Deck Combinations

COMBIN-ATION	SEA STATE	V_s	μ	ψ_{WIND}	ψ_{WOD}	V_{WIND}	V_{WOD}	H_s	T_o
1	6	25	120	-60	-30	25.00	43.30	18	15.13
2	5	25	120	-60	-30	25.00	43.30	12	13.50
3	5	20	120	-60	-30	20.00	34.64	12	13.50
4	5	10	135	-45	-30	19.32	27.32	12	13.07
5	5	25	180	0	0	20→24	45→49	12	12.07
6	5	5	180	0	0	20→24	25→29	12	11.51
7	4	25	105	-75	-30	17.68	34.15	6.9	10.6
8	3	25	105	-75	-30	17.68	34.15	4.6	8.8
9	3	20	105	-75	-30	14.14	27.32	4.6	8.8
10	3	25	90	-90	-30	14.43	28.87	4.6	8.8
11	3	15	120	-60	-30	15.00	25.98	4.6	8.8
12	3	25	180	0	0	14→18	39→43	4.6	8.8
13	3	5	180	0	0	14→18	19→23	4.6	8.8

V_s - Ship Speed (kt)

μ - Wave Direction (deg)

ψ_{WIND} - Ambient Wind Direction (deg)

ψ_{WOD} - Wind Over Deck Direction (deg)

V_{WIND} - Ambient Wind Speed (kt)

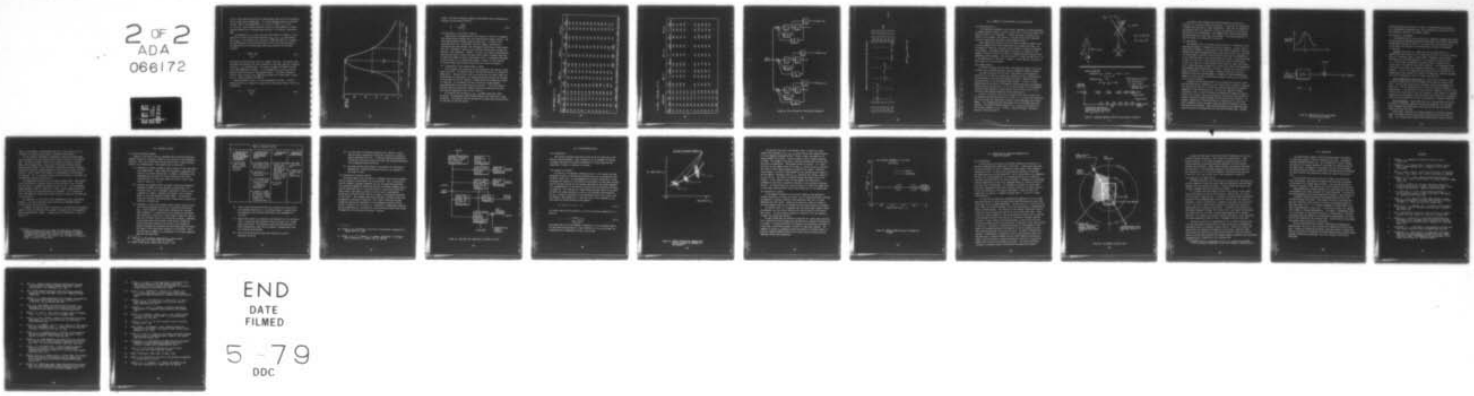
V_{WOD} - Wind Over Deck Speed (kt)

H_s - Significant Wave Weight (ft)

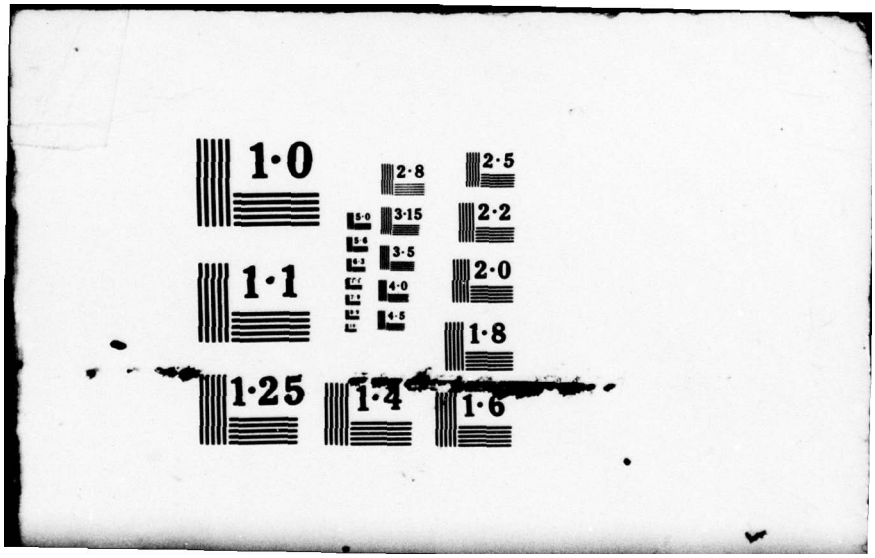
T_o - Modal Period (sec)

AD-A066 172 VOUGHT CORP DALLAS TEX F/G 1/2
VOLAR: A DIGITAL COMPUTER PROGRAM FOR SIMULATING VSTOL AIRCRAFT--ETC(U)
DEC 78 J WOLKOVITCH, B B BRASSELL N62269-77-R-0389
UNCLASSIFIED 2-32000/8R-41672-VOL-1 NADC-77123-30-VOL-1 NL

2 OF 2
ADA
066172



END
DATE
FILMED
5-79
DDC


1·0
1·1
1·25
1·4
1·6
1·8
2·0
2·2
2·5
2·8
3·15
3·5
4·0

for all single mode (having one well defined peak) spectra which are generally found in head, bow, and beam seas. It is not expected to apply to multimode spectra. (One of the combinations - V_s = 5 kt, $\mu = 180^o$, H_s = 4.6 ft, T_o = 8.8 sec - had a bimodal spectrum in heave) or where moderate to severe spectrum warping due to frequency mapping occurs in following or quartering seas.

To eastablish K_i, ω_{n_i}, and ζ_i for each ship degree of freedom for each condition in Table 8, the three frequencies ($\omega_{e_{max}}$, ω_{HI}, ω_{LO}) and maximum gain ($K_{i_{max}}$ in its normal units) indicated in Figure 19 were first recorded. The two frequencies at the 50 percent peak level of the spectrum establish the damping ratio of the equivalent spectrum according to the following relation:

$$\zeta_i = \frac{(\omega_{HI} - \omega_{LO})}{2\omega_{n_i}} \tag{9.2}$$

The choice of the 50 percent level was somewhat arbitrary: the spectral data indicated that generally more than 50 percent of the total power was contained in the $\omega_{HI} - \omega_{LO}$ frequency band. The natural frequency and damping of each filter was determined as follows. It was assumed that ω_{HI} and ω_{LO} are the same for both the equivalent and measured spectra. The natural frequency for this case is given by $\omega_{n_i} = \sqrt{\omega_{HI}\ \omega_{LO}}$ and Equation 9.2 again used to calculate ζ_i. Table 9 presents the results.

Having obtained ω_{n_i} and ζ_i, K_i was determined as follows. It can be shown that the r.m.s. output of $G_i\ (j\omega_e)$ with a white noise input of unit r.m.s. is given by:

$$\sigma_i^2 = \frac{K_i^2\ \omega_{n_i}^3}{2\zeta_i} \tag{9.3}$$

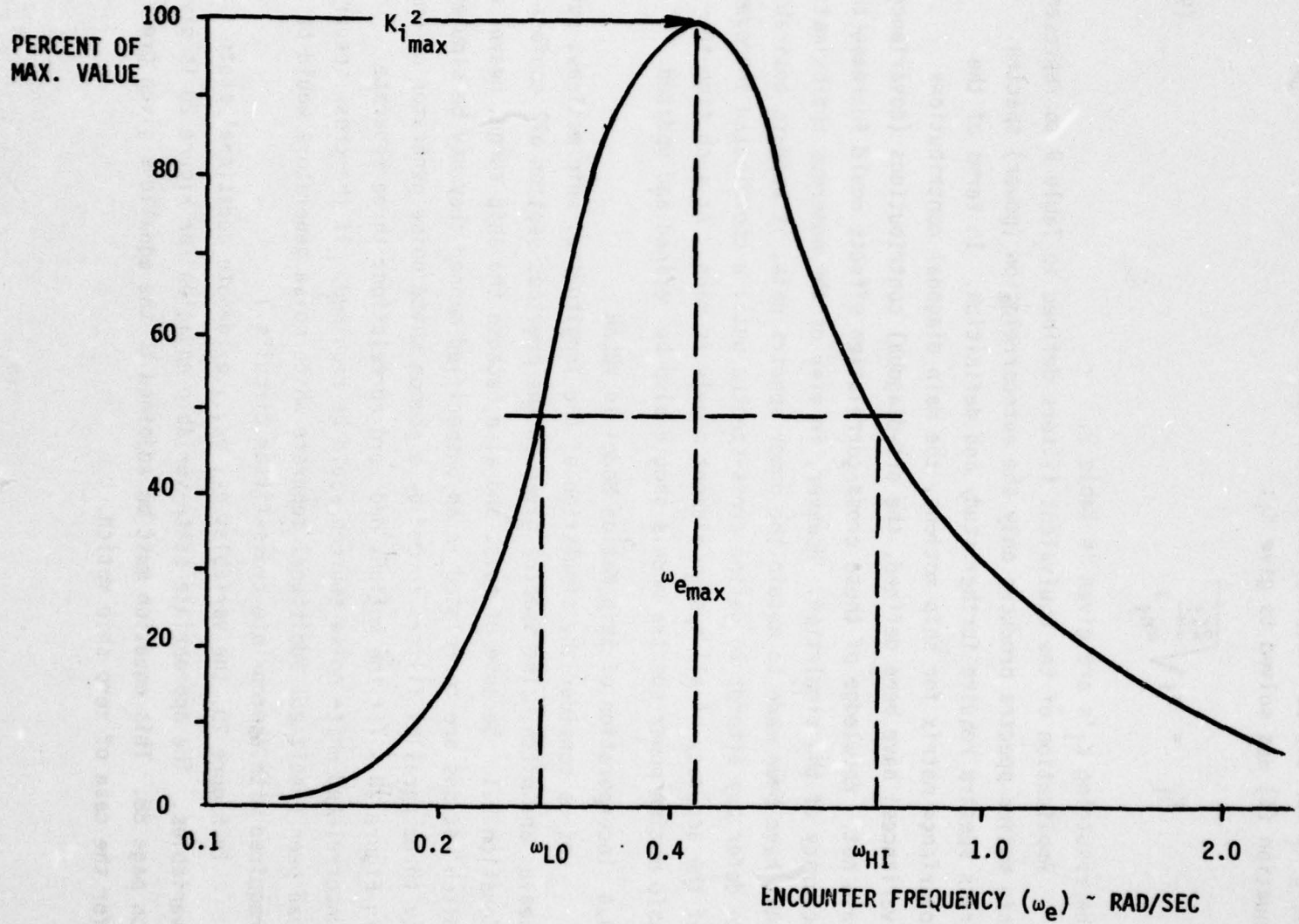


Figure 19. Typical Ship Motion Response Spectrum

Using σ_i for the 32 frequency component approximation data of Reference 32, Equation (4) was solved to give K_i:

$$K_i = \sigma_i \sqrt{\frac{2\zeta_i}{\omega_{n_i}^3}} \tag{9.4}$$

The resulting K_i's are given in Table 9.

Application of the equivalent filters defined in Table 9 to represent ship motion spectra produces only the autocorrelation (power) spectra. The cross spectra require further study and definition. In terms of the covariance matrix for ship motions, the main diagonal contributions (variances) have been defined, the off-diagonal contributions (covariances) have not. Knowledge of these cross-correlation effects would increase the accuracy of the simulation. However, in view of the numerous approximations that have been made to obtain the power spectra data, it appears desirable to defer any attempt to define cross-spectra until a coordinated improvement of the accuracy of all system element models is made. At such time the ship motion power spectra models should also be refined and updated.

9.4 Incorporation of Ship Motion Model in VOLAR

Let us consider the simulation of the longitudinal ship motions, surge, heave, and pitch. The spectra given in the previous section all conform to Equation 9.1. Because of this, and also because the ship surge, heave, and pitch motions are correlated in an unspecified manner they may be simulated by three parallel filters forced by a common white noise generator as shown in Figure 20. (If the motions had zero correlation, three separate uncorrelated white noise sources would be required. If the cross spectra had been specified, additional separate white noise generators would be required with appropriate cross-filter circuits.)

In Figure 20, the variables e_1, e_2,...e_6 denote additional state variables. The appropriate state-variable equation for Figure 20 is given on page 88. This equation must be adjoined to the equations given previously for the case of zero ship motion.

Table 9 Equivalent Ship Motion Response Parameters

a) LONGITUDINAL (AT C.G.)

COMBINATION				SURGE (X)			HEAVE (Z)			PITCH (θ_s)		
V_s (kts)	μ (deg)	H_s (ft)	T_o (sec)	K_x (ft/ft)	ζ_x	ωn_x (rad/sec)	K_z (ft/ft)	ζ_z	ωn_z (rad/sec)	K_θ (deg/ft)	ζ_θ	ωn_θ (rad/sec)
25	120	18.0	15.13	1.593	.280	.512	9.895	.433	.592	1.461	.421	.744
25	120	12.0	13.50	.791	.256	.580	5.060	.446	.717	.892	.361	.797
20	120	12.0	13.50	.930	.285	.563	5.483	.443	.654	1.000	.364	.762
10	135	12.0	13.07	1.407	.265	.533	4.137	.270	.557	1.312	.319	.693
25	180	12.0	12.07	.469	.250	.736	2.349	.275	.879	.742	.245	.905
5	180	12.0	11.51	1.228	.198	.548	2.166	.198	.548	1.140	.216	.638
25	105	6.9	10.60	.202	.279	.678	2.278	.368	.812	.322	.300	.866
25	105	4.6	8.80	.0771	.241	.824	.981	.251	.936	.169	.220	.942
20	105	4.6	8.80	.0884	.249	.804	1.013	.257	.909	.209	.223	.865
25	90	4.6	8.80	.0489	.244	.679	1.422	.310	.759	.082	.316	.916
15	120	4.6	8.80	.117	.217	.793	.742	.234	.909	.245	.205	.936
25	180	4.6	8.80	.0378	.183	.932	.251	.122	1.062	.104	.155	1.071
5	180	4.6	8.80	.144	.155	.670	.320 (.335)*	.190 (.253)*	.693 (.738)*	.213	.157	.731

NOTE: *BIMODAL RESPONSE - DATA CORRESPOND TO PEAK WIDTH SELECTED TO FIT TOTAL PESPONSE WITH ONE PEAK

b) LATERAL - DIRECTIONAL (AT C.G.)

COMBINATION				SWAY (Y)			ROLL (ϕ_s)			YAW (χ_s)		
V_s (kts)	μ (deg)	H_s (ft)	T_o (sec)	K_y (ft/ft)	ζ_y	ωn_y (rad/sec)	K_ϕ (deg/ft)	ζ_ϕ	ωn_ϕ (rad/sec)	K_ψ (deg/ft)	ζ_ψ	ωn_ψ (rad/sec)
25	120	18.0	15.13	4.980	.251	.473	4.566	.203	.553	.680	.289	.601
25	120	12.0	13.50	2.393	.267	.545	2.602	.188	.589	.452	.385	.677
20	120	12.0	13.50	2.689	.258	.521	2.933	.159	.594	.501	.301	.630
10	135	12.0	13.07	1.792	.181	.491	3.836	.148	.567	.527	.169	.540
25	180	12.0	12.07	-	-	-	-	-	-	-	-	-
5	180	12.0	11.51	-	-	-	-	-	-	-	-	-
25	105	6.9	10.60	1.261	.305	.662	1.393	.210	.634	.205	.422	.814
25	105	4.6	8.80	.413	.211	.800	.617	.315	.812	.0898	.329	1.009
20	105	4.6	8.80	.461	.235	.793	.737	.306	.782	.102	.319	.965
25	90	4.6	8.80	.951	.244	.679	.835	.155	.622	.0432	.714	.634
15	120	4.6	8.80	.239	.193	.774	.612	.257	.798	.0983	.245	.919
25	180	4.6	8.80	-	-	-	-	-	-	-	-	-
5	180	4.6	8.80	-	-	-	-	-	-	-	-	-

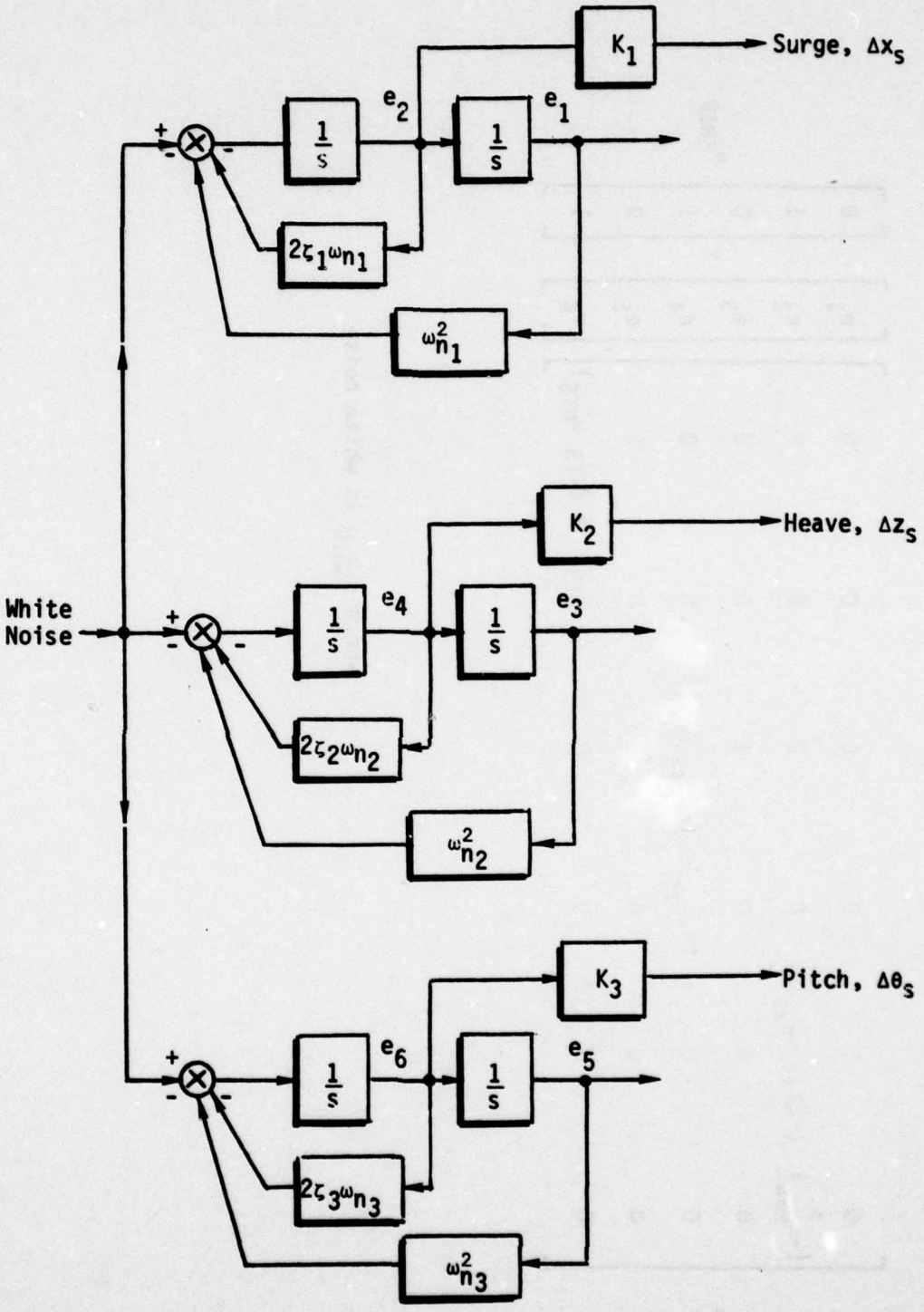


Figure 20 Block Diagram for Ship Motion Simulation

Equation for Simulation of Correlated 3 DOF Ship Motion

$$\begin{bmatrix} \dot{e}_1 \\ \dot{e}_2 \\ \dot{e}_3 \\ \dot{e}_4 \\ \dot{e}_5 \\ \dot{e}_6 \end{bmatrix} = \begin{bmatrix} 0 & 1 & 0 & 0 & 0 & 0 \\ (-\omega_{n_{xs}}^2) & (-2\zeta_{xs}\ \omega_{n_{xs}}) & 0 & 0 & 0 & 0 \\ 0 & 0 & 0 & 1 & 0 & 0 \\ 0 & 0 & (-\omega_{n_{zs}}^2) & (-2\zeta_{zs}\ \omega_{n_{zs}}) & 0 & 0 \\ 0 & 0 & 0 & 0 & 0 & 1 \\ 0 & 0 & 0 & 0 & (-\omega_{n_{TS}}^2) & (-2\zeta_{TS}\ \omega_{n_{TS}}) \end{bmatrix} \begin{bmatrix} e_1 \\ e_2 \\ e_3 \\ e_4 \\ e_5 \\ e_6 \end{bmatrix} + \begin{bmatrix} 0 \\ 1 \\ 0 \\ 1 \\ 0 \\ 1 \end{bmatrix} n_{SHIP} \qquad -(9.5)$$

where n_{SHIP} is white noise

10.0 EXAMPLE OF AV-8A RECOVERY IN A HIGH SEA-STATE

10.1 Task Description

The simulation presented in this section represents an AV-8A performing an approach maneuver which is similar to that given in Section 8 except that the ship motion is not negligible. A higher Sea State is selected; Sea State 5 is now assumed. Ship motion is included in the VOLAR simulation using the formulations described in the preceding section.

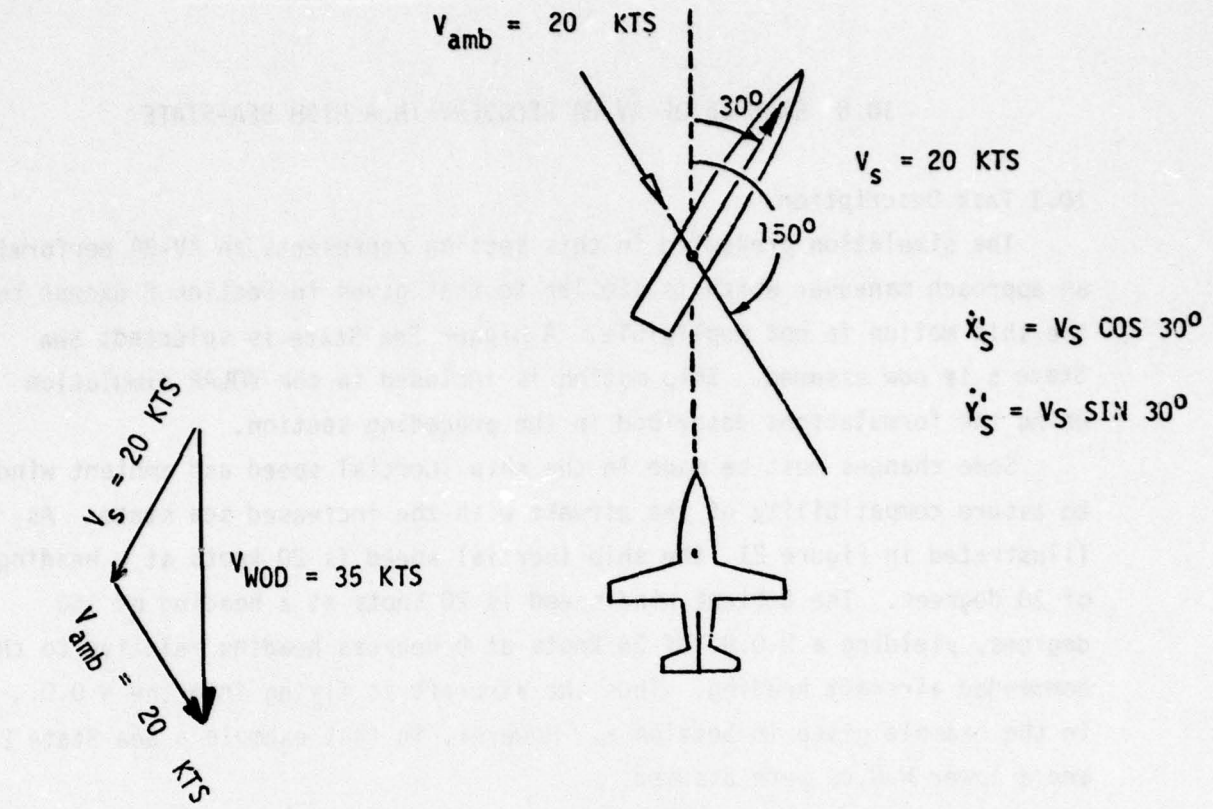
Some changes must be made in the ship inertial speed and ambient wind to assure compatibility of the airwake with the increased sea state. As illustrated in Figure 21 the ship inertial speed is 20 knots at a heading of 30 degrees. The ambient wind speed is 20 knots at a heading of 150 degrees, yielding a W.O.D. of 35 knots at 0 degrees heading relative to the commanded aircraft heading. Thus the aircraft is flying into the W.O.D., as in the example given in Section 8. However, in that example a Sea State 2 and a lower W.O.D. were assumed.

10.2 Element Models

The AV-8A airframe, control system, and powerplant models are the same as those used in previous sections, but are extended to higher airspeeds.

The rate-of-closure with the ship is the same as in the example of Section 8, but the inertial speeds and airspeeds have been changed because of differences in ship speed and ambient wind speed. Keeping rate-of-closure constant in the two examples seems logical. A pilot in a VTOL approach may not be aware of wind speed or ground speed but he can perceive rate-of-closure with the ship. He can fly the airplane with this parameter fixed and accept whatever airspeed results since a VTOL aircraft is not limited to some minimum airspeed by stall characteristics.

For this simulation, the initial airspeed is 44.7 knots (23 m/s) and the terminal airspeed equals the W.O.D. speed. As in the previous simulation, the pilot employs two longitudinal controls; thrust magnitude and pitching moment. It is assumed that the nozzle angle is not re-trimmed during the approach. The Dryden turbulence spectra r.m.s. values are the same as in the previous example $u_g = w_g = 1$ ft/sec. The ship airwake is different because of the higher W.O.D.



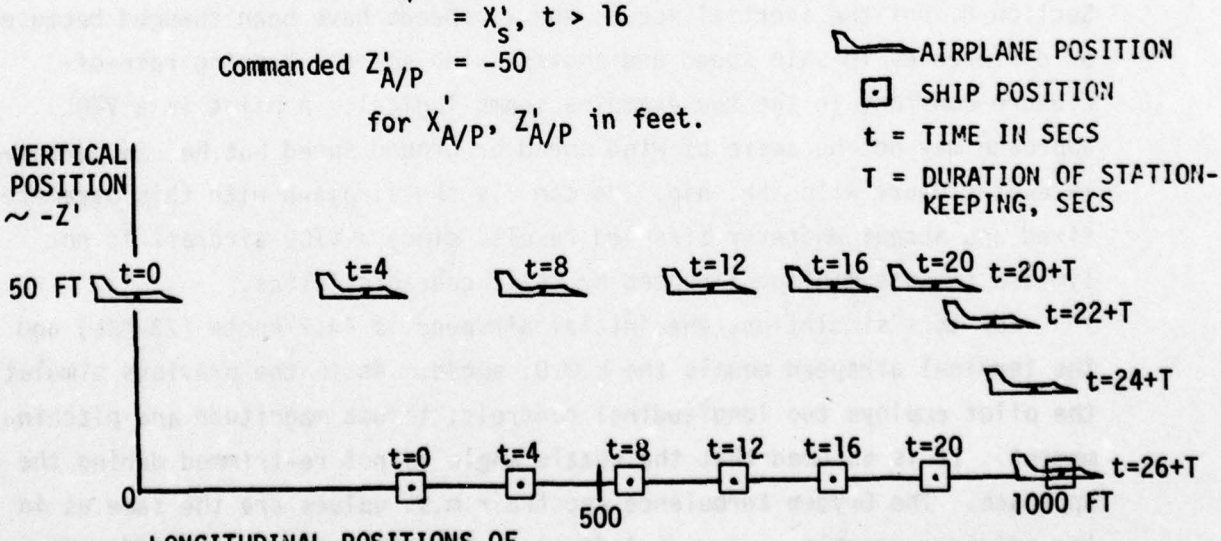
PROFILE EQUATIONS:

Commanded $X'_{A/P} = 66.516\ t - 1.165\ t^2$, $t < 16$

$= X'_S$, $t > 16$

Commanded $Z'_{A/P} = -50$

for $X'_{A/P}$, $Z'_{A/P}$ in feet.



LONGITUDINAL POSITIONS OF AIRPLANE AND SHIP IN INERTIAL AXES, $X'_{A/P}$ AND X'_S FOR T = 0.

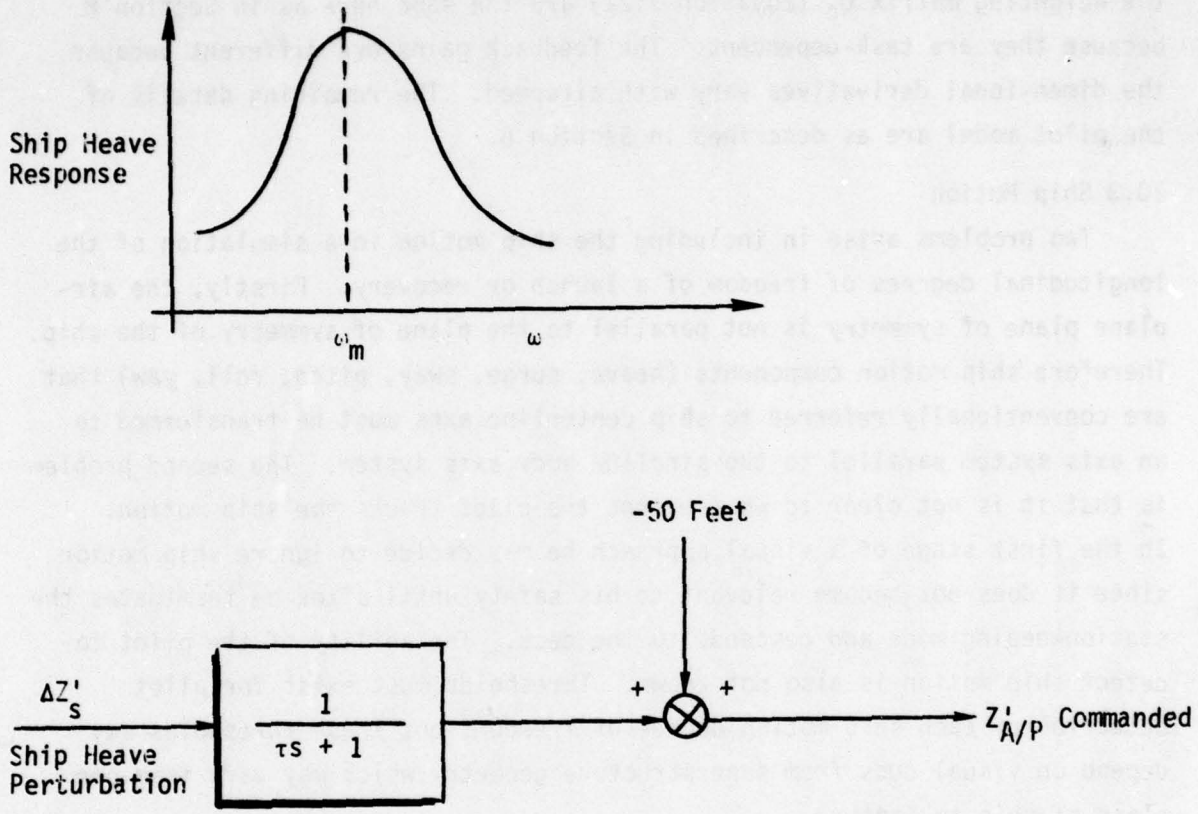
Figure 21 Commanded Approach Profile for Sea-State 5 Condition

The optimal pilot feedback gains were determined as discussed in Section 8 for two points along the trajectory. The values for intermediate airspeeds were obtained by linear interpolation. Note that the elements of the weighting matrix Q_c (Equation 7.22) are the same here as in Section 8 because they are task-dependent. The feedback gains are different because the dimensional derivatives vary with airspeed. The remaining details of the pilot model are as described in Section 8.

10.3 Ship Motion

Two problems arise in including the ship motion in a simulation of the longitudinal degrees of freedom of a launch or recovery. Firstly, the airplane plane of symmetry is not parallel to the plane of symmetry of the ship. Therefore ship motion components (heave, surge, sway, pitch, roll, yaw) that are conventionally referred to ship centerline axes must be transformed to an axis system parallel to the airplane body axis system. The second problem is that it is not clear to what extent the pilot tracks the ship motion. In the first stage of a visual approach he may decide to ignore ship motion since it does not become relevant to his safety until after he terminates the stationkeeping mode and descends to the deck. The ability of the pilot to detect ship motion is also not known. Thresholds must exist for pilot detection of each ship motion degree of freedom, but these thresholds may depend on visual cues from superstructure geometry which may vary from one class of ship to another.

To demonstrate the VOLAR program it was assumed that the pilot tracks the ship heave motion, smoothed by a first-order filter as shown in Figure 22 This implies that the pilot is primarily concerned about the low frequency components of the ship heave motion. The only ship degree of freedom simulated is heave. Some of the other ship degrees of freedom are known to be small (e.g. surge), and the cross-spectral (covariance) data required to properly simulate the phasing between ship motions were not available. For example, computation of the heave motion of a general point on the ship's axis of symmetry requires the heave spectrum, the pitch spectrum, and the pitch-heave cross-spectrum. When such cross-spectral data become available they can readily be incorporated within the existing VOLAR input. Without



where $\tau = \frac{1}{\omega_m}$

Figure 22 Modified Pilot Altitude Command due to Ship Heave Motion

such cross-spectral data there is no point in performing the ship/airplane axis transformation mentioned above. By considering only heave ship motion this problem is avoided in the present example.

10.4 Results of the Example

The VOLAR results are given on Figure 18, (page 69), together with results for the case with negligible ship motion (Sea State 2). The latter results have already been discussed in Section 8. As before, the stationkeeping stage is not shown; only approach to stationkeeping and descent are presented in Figure 18.

Airwake (Figures 18c, d) - Referring first to Figure 18(b) it is apparent that the increase in W.O.D. speed from 20 knots to 35 knots increases the r.m.s. turbulence levels in the airwake. Although a similar general trend exists for the mean components it is interesting to note that for $7 < t < 20$ secs the u-component of the mean airwake is smaller for the 35 knot W.O.D. case than for the 20 knot condition. This phenomenon exists in the basic wind tunnel data analysed in Reference 11. No explanation is apparent. In view of the reasonable-looking nature of the remainder of the airwake data it was decided not to adjust this apparently anomalous characteristic to fit preconceived ideas of airwake characteristics.

Control Deflections (Figures 18c, d) - These figures indicate a large increase in random control activity between the 20 knot and 35 knot W.O.D. cases. The one-sigma random throttle movements increase approximately by a factor of 6. The corresponding factor for the pitch control movements is approximately 3. The difference in these factors is expected. The difficulty of the pilot's height control task has increased not only because of increased turbulence but also because of the ship heave motion, whereas his longitudinal control task has become more difficult only because of increased turbulence.

Aircraft Response - Figure 18(e) shows the pitch attitude time history. The mean θ is increased compared to the 20 knot condition. The high mean pitch altitudes shown result partly from the fact that the thrust nozzle vector control was not used.

Figure 18(f) illustrates the random component of the height response. There is a marked increase in this quantity associated with the higher sea state. This increase occurs despite the increased thrust control activity

shown on Figure 18(d), indicating that the pilot is more active but less successful in controlling the inertial altitude of the airplane.

As the instant of touchdown is approached, inertial altitude becomes less significant than the altitude of the airplane relative to the heaving deck. The mean and random values of this quantity are shown in Figures 18(g) and (h) respectively. Figure 18(g) illustrates the mean vertical position error,* which is less than 0.5m for both the sea states simulated. Figure 18(h) shows the random component of the airplane altitude relative to the ship. The 1σ value of this quantity is approximately 0.6m throughout the recovery. This is a marked increase above the Sea State 2 case where the corresponding value was less than 0.1m.

The longitudinal position error is shown on Figure 18(g). Some degradation in performance is evident relative to the Sea State 2 case; the mean position error at touchdown increases from 0.5m to 1.5m. The corresponding random component, shown on Figure 18(i), shows a similar degradation during the first stage of the approach but not at touchdown. This is apparently due to the anomalous airwake model characteristics discussed at the beginning of this section.

The lower part of Figure 18(i) shows commanded and actual longitudinal position. This shows that the aircraft acquires the commanded approach profile without any oscillations.

In summary, the example results presented here indicate that the predicted behavior of the aircraft-ship-pilot system is consistent with the assumptions made for modeling each element. A comparison with flight tests is given in Section 13.

---

*The mean vertical position error shown on Figure 18(g) is the mean difference between the airplane inertial altitude and the commanded altitude, which as explained in Section 10.3, includes a filtered component of ship motion. This filter is not included in the quantity $\sigma(Z_{AP} - Z_S)$ shown in Figure 18(h).

11.0 PROXIMITY EFFECTS

11.1 List of Proximity Effects

Table 10 lists several distinct phenomena which cause the forces and moments acting on an airplane to depend on the proximity of the airplane to the ship. Only very limited data are available on most of these proximity effects, as indicated below. (The numbers refer to Table 10.)

1.A Reference 14 presents extensive look-up tables for STOL-type power-off ground effect. These tables were apparently computed on the basis of an infinite ground plane. As shown in Reference 34 this assumption may be invalid for aircraft operating from ships, particularly so for small ships where the ratio of span to deck width is large (i.e. > 0.5).

2.A Fountain and suckdown effects are highly configuration-dependent. Reference 13 models the AV-8A dominant suckdown effect as a 6 percent thrust loss at touchdown, decreasing to zero at a deck clearance of 7 meters. Reference 14 presents a fairly complex model for the AV-8B fountain/suckdown effect. The AV-8A and AV-8B have different fountain/suckdown characteristics because the AV-8B has a fountain box.

2.B Reingestion is the process whereby exhaust gases diffuse and then re-circulate around the aircraft due to convection and relative wind. The AV-8A NATOPS flight manual (Reference 35) indicates that reingestion is a potentially serious problem for protracted VSTOL operations in which the airplane remains within the same air mass for sufficient time for re-circulation to develop. Reference 35 also notes that a more rapidly acting type of reingestion occurs during STOL operations due to part of the forward jet exhausts impinging on the ground plane and being deflected forward just ahead of the intake where the gases are reingested. Apart from qualitative comments (e.g. Reference 35) no AV-8A reingestion data have been published.

---

34. Levey, H. C., The "Ground" Interference of a Carrier Deck, J. Roy. Aero. Soc., April 1957, pp. 276-281.

35. NATOPS Flight Manual, NAVAIR Rept 01-AV8A-1, 1976.

TABLE 10 PROXIMITY EFFECTS

1. "Ground Effects" on aerodynamic forces and moments of the power-off configuration	2. "Ground Effects" associated with lifting engine thrust	3. Landing gear reactions	4. Restraining system forces
1A. Ground plane alters induced angle of attack of lifting surfaces.	2A. Fountain effects and suckdown alter mean forces acting on the airplane. 2B. Reingestion effects are slowly time-varying. 2C. The random forces are also affected since the aircraft is immersed in self-generated turbulence. 2D. Changes in these effects are induced by irregular ground planes (e.g., "edge of deck", or "sculptured deck").	3A. These include brake forces, landing gear reactions, and oleo damping. The latter modify the ship motions transmitted to the airplane. 3B. Ski-jump effects.	4A. Haul-down and securing gear. 4B. Launch and arrester gear where appropriate.

2C. AV-8A flight experience (Reference 35) indicates that the aircraft self-generated turbulence is a significant factor in ground effect. No quantitative data have been published on this phenomenon for the AV-8A.

2D. Edge-of-deck effects are expected to be important for VTOL configurations in conditions where fountain effects are large (e.g., AV-8B rather than AV-8A). No quantitative data have been published for VSTOL configurations other than helicopters, although model tests are currently being planned.

3A. Data on AV-8A and AV-8B landing gear reactions are given in References 13 and 14.

3B. The "ski-jump" STO technique (Reference 34) involves a curved deck which acts through the landing gear reactions to produce an upward acceleration for STO. If data are supplied regarding the landing gear reactions and the deck shape, the applied acceleration can be computed without difficulty.

4A. Haul-down and securing systems for helicopters are described in Reference 36. No data have been published on such systems for the AV-8A or AV-8B.

11.2 Simulation of Proximity Effects

The above summary shows that there is inadequate data on many proximity effects to permit accurate models to be constructed. This is particularly true for random or unsteady components such as self-generated turbulence. For covariance propagation simulations the mean and random components may be equally significant and it is not justifiable to simulate one without the other without experimental evidence to justify such an approximation. Accordingly, proximity effects were not included in the examples presented in this report. When adequate data become available, proximity effects may be modeled as indicated in Figure 23. This figure illustrates the data processing required for simulation of the aerodynamic proximity effects listed in columns 1 and 2 of Table 10. Simulation of landing gear reactions may be accomplished as in Reference 13, and restraining system forces can be included with the landing gear reactions if desired.

---

36. Fozard, J. W., Sea Harrier - The First of the New Wave, Aeronautical J., January 1977, pp. 15-40.

37. Bryson, L. B., F. E. Heenan, C. A. Johnson, Helicopters in the Royal Navy, Aeronautical J., August 1972, pp. 469-500.

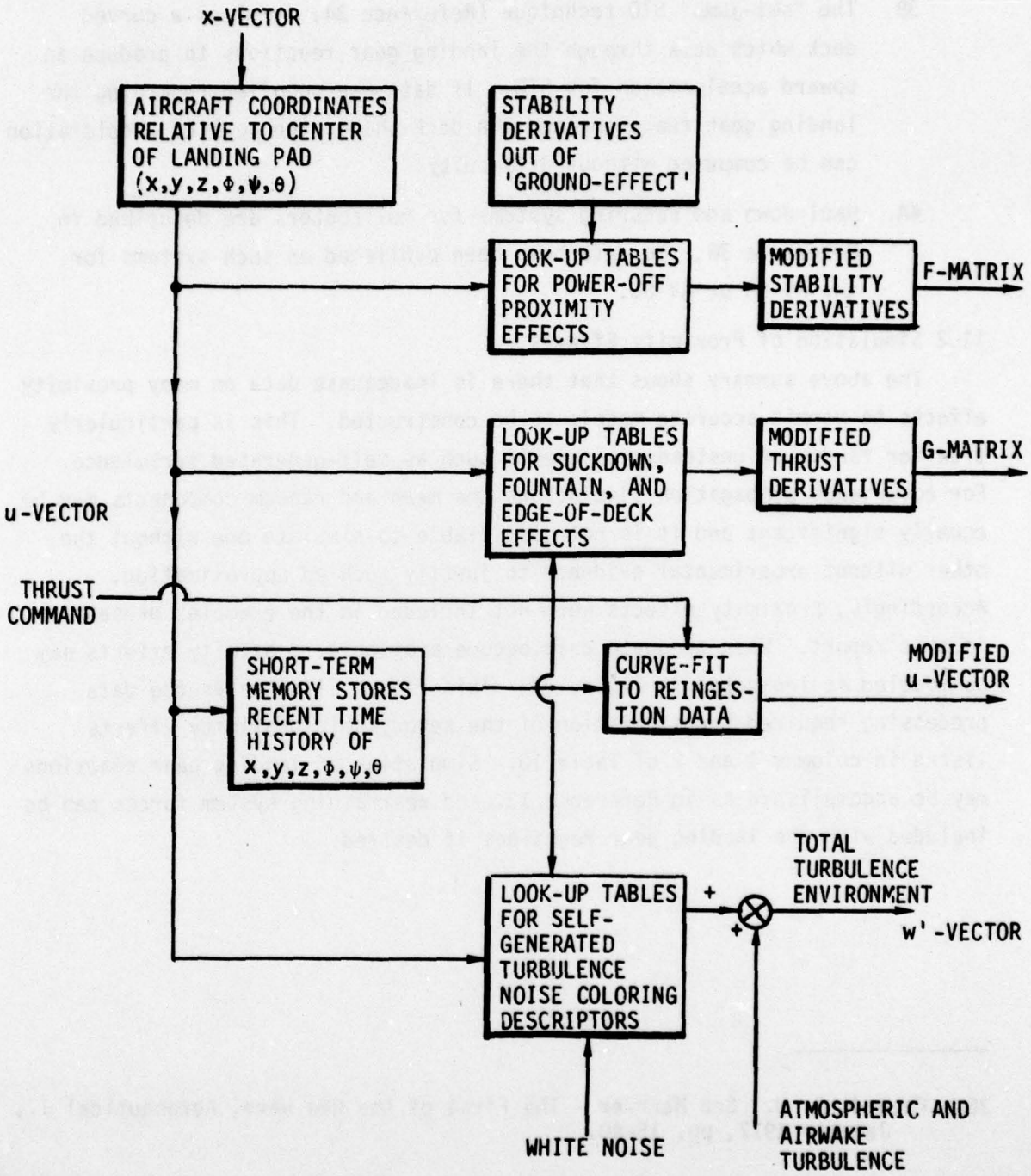


FIGURE 23 FLOW CHART FOR SIMULATION OF PROXIMITY EFFECTS

12.0 MISCELLANEOUS TOPICS

12.1 Introduction

This section discusses some topics which do not fit under any of the previous section headings. These include the use of probability ellipses to present the mean and variance information on a single graph and the simulation of launch, in addition to recovery.

12.2 Probability Ellipses

The results of the examples presented earlier in this report have been presented as graphs of the mean and standard deviation of appropriate state variables versus time. A disadvantage of this type of presentation is that two graphs are required to illustrate the time history of each state variable, one for the mean and one for the standard deviation of the random component. This disadvantage can be overcome by using the form of presentation sketched in Figure 24. This consists of a graph showing the mean values of two state variables (or output variables) x_1 and x_2, with the mean value denoted by $\bar{x}_1$, $\bar{x}_2$. As shown in Reference 30, the covariance matrix P of x_1 and x_2 can be related to the probability, p, that the vector x with components x_1 x_2 lies within an ellipse defined by the equation

$$(x - \bar{x})^T P^{-1} (x - \bar{x}) = L^2 \tag{12.1}$$

For jointly Gaussian distributions of x_1 and x_2 the above probability, p, is given by

$$p = 1 - e^{\frac{(-L^2/2\sigma_{x_1}\sigma_{x_2})}{(2\sigma_{x_1}\sigma_{x_2})}} \tag{12.2}$$

The ellipse axes are tilted because (in general) P is not a diagonal matrix. In other words the covariance or cross-correlation of x_1 and x_2 causes the ellipse axes to be nonparallel to the x_1 and x_2 axes.

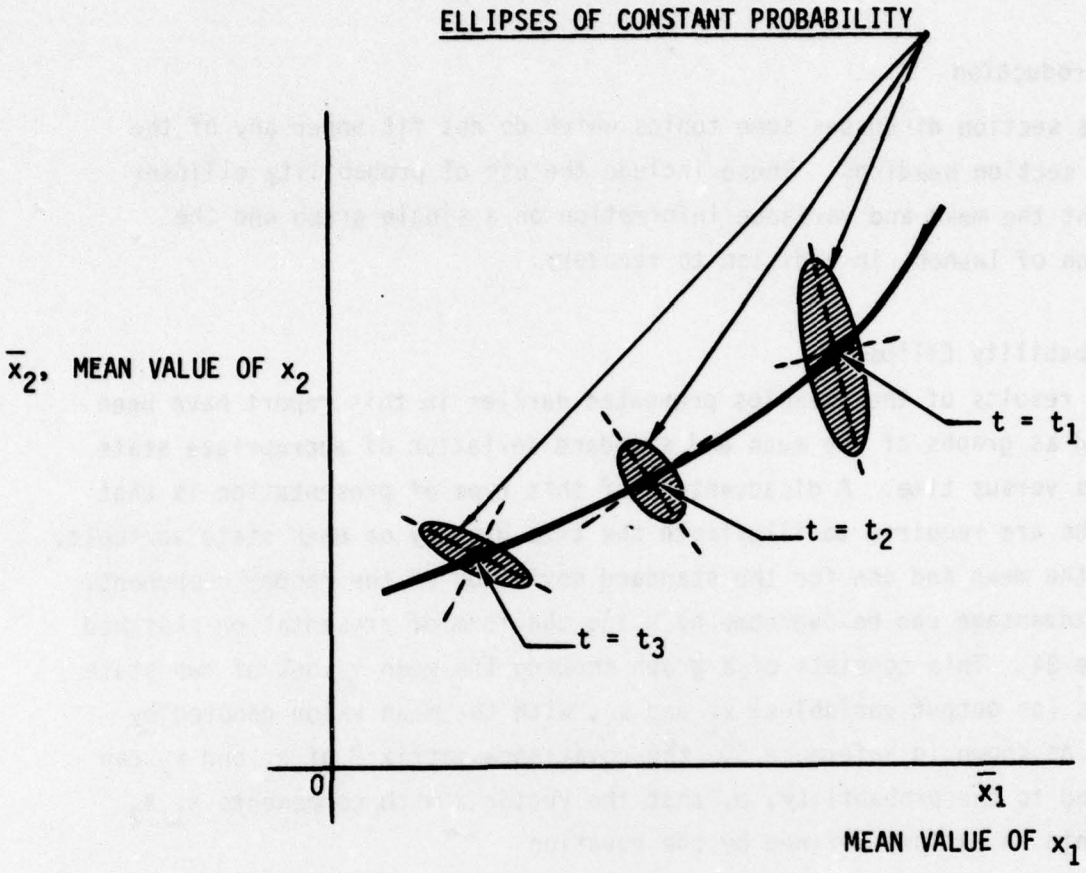


FIGURE 24 COMPACT PRESENTATION SHOWNING MEAN VALUES AND DEGREE OF RANDOMNESS OF TWO VARIABLES.

In principle, the form of presentation shown in Figure 24 is more compact than plotting $\bar{x}_1$, $\bar{x}_2$, σ_{x_1}, σ_{x_2} versus time on four separate graphs, as in the examples presented earlier. VOLAR includes the capability to output probability ellipses. Figure 25 shows a typical example generated by VOLAR. This example illustrates a practical problem that can occur with this type of presentation. The problem relates to scaling. It is often difficult to pick common scales for $\bar{x}_1$ and σ_{x_1}, and for $\bar{x}_2$ and σ_{x_2} that will not result in the ellipses becoming too small or too narrow. One can of course choose L to yield a large probability thus enlarging the ellipse, or one can employ a different scale for σ_{x_1}, retaining the original scales for $\bar{x}_1$, $\bar{x}_2$, and σ_{x_2}. The latter alternative changes the aspect ratio of the ellipse. It is a matter of user's choice whether this distortion is preferable to the lack of resolution implied by a very narrow but unscaled ellipse. In Figure 25 both the σ-axes are drawn to 5 times the common scale of the x-axes, distorting the scale of the ellipse but not its proportions.

12.3 Simulation of Launch

In the examples presented in this report VOLAR has been employed to simulate recoveries in various Sea States, but no launches have been simulated. The emphasis on recovery reflects flight experience that this is a more demanding task than launch. VOLAR may be applied to launch and indeed to any other maneuver that can be simulated by conventional Monte Carlo methods.

To simulate launch it is suggested that the landing gear dynamics should be neglected, and the aircraft position and velocity merely initialized at deck levels. If a more precise simulation is desired it will be necessary to model the landing gear dynamics.

Currently VOLAR does not include a subroutine for landing gear reactions. Such a subroutine could be added using the Monte Carlo program of Reference 13 as a guide. It would be desirable to formulate the landing gear reactions in a form that is sufficiently general to model ski-jump type launches. The comments of Section 11 regarding current deficiencies in analytic models of proximity (ground) effects should also be noted since such effects may be important during launch operations.

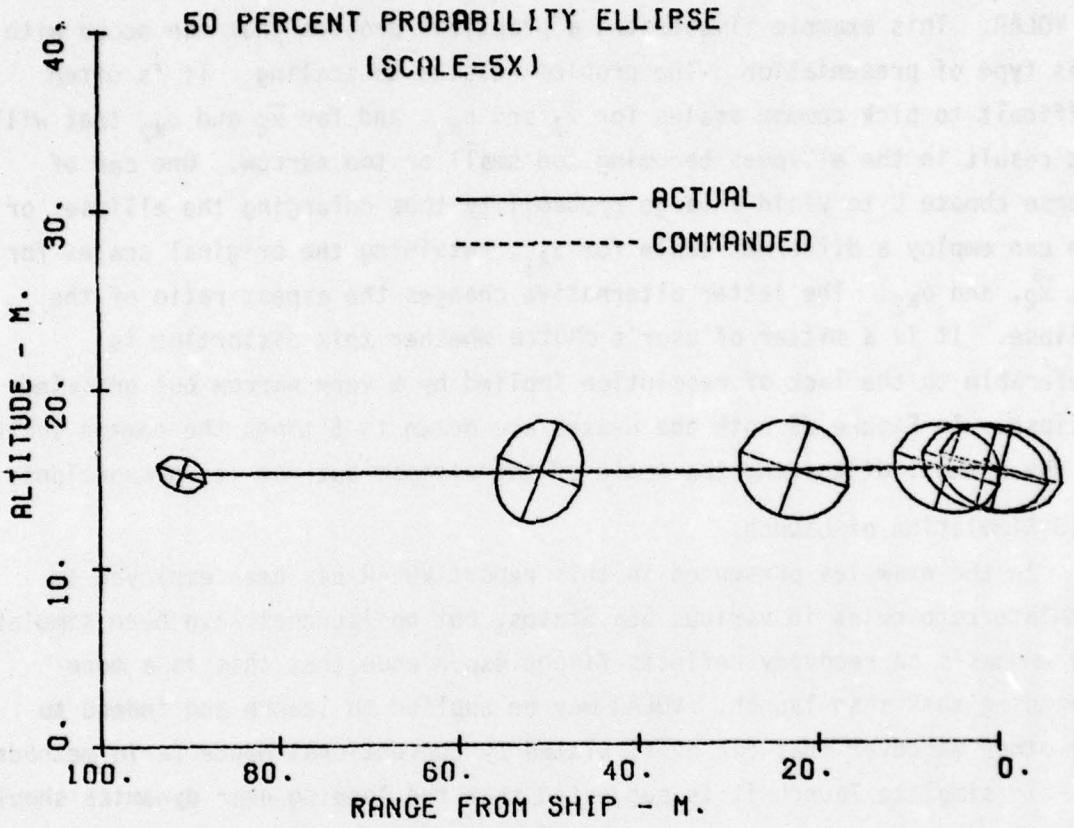


Figure 25 Example VOLAR Printout of Probability Ellipses

13.0 CORRELATION OF SIMULATED APPROACHES WITH FLIGHT TEST RESULTS

13.1 Introduction

In this section the results of the VOLAR simulations of Section 6, 8, and 10 are compared with flight data on the AV-8A. A quantitative data base for the flight tests is given in Reference 9 which reports AV-8A shipboard suitability trials. In these trials the operating envelope of the AV-8A was determined partly by performing VTO's and VL's but primarily by attempting to hover (i.e. stationkeep) over all portions of the deck of an LPD-class ship while varying the W.O.D. as much as possible. A boundary was established relating combinations of the W.O.D. magnitude and W.O.D. angle for which the pilot was able to stationkeep. This boundary is plotted on a polar graph with W.O.D. magnitude as the radial coordinate and W.O.D. direction relative to the ship centerline as the angular coordinate. Figure 26 shows this graph, which is known as a "dynamic interface chart". Figure 26 is taken from Reference 9.

In Figure 26 the shaded area represents the combination of W.O.D. magnitude and direction for which the above described AV-8A operations were found to be feasible for starboard approaches. The deck outline is indicated by the heavy lines, and the deck markings for the two landing pads are represented by lines of lighter weight. The direction of the approach flight path relative to the ship is not necessarily parallel to any of these deck lines. These lines are a useful reference to the pilot and may be used by him to establish a safe approach direction, but they do not indicate an "optimum" approach direction. (Even if such an optimum were known, it would vary with W.O.D. direction and hence could not be consistently indicated by fixed lines painted on the deck.) This point is emphasized because, for the examples in this report, the approach was made at 150 degrees to the ship centerline, with the flight path parallel to the wind over deck. As shown in Figure 26 this approach is approximately 15 degrees to port of the appropriate deck line. The heavy dots in Figure 26 denote the two flight conditions simulated by VOLAR. The 20 knot W.O.D. condition discussed in Section 8 is within the capabilities of the pilot-airframe-ship system. The 35 knot conditions discussed in Sections 6 and 10 lies outside the operational boundary.

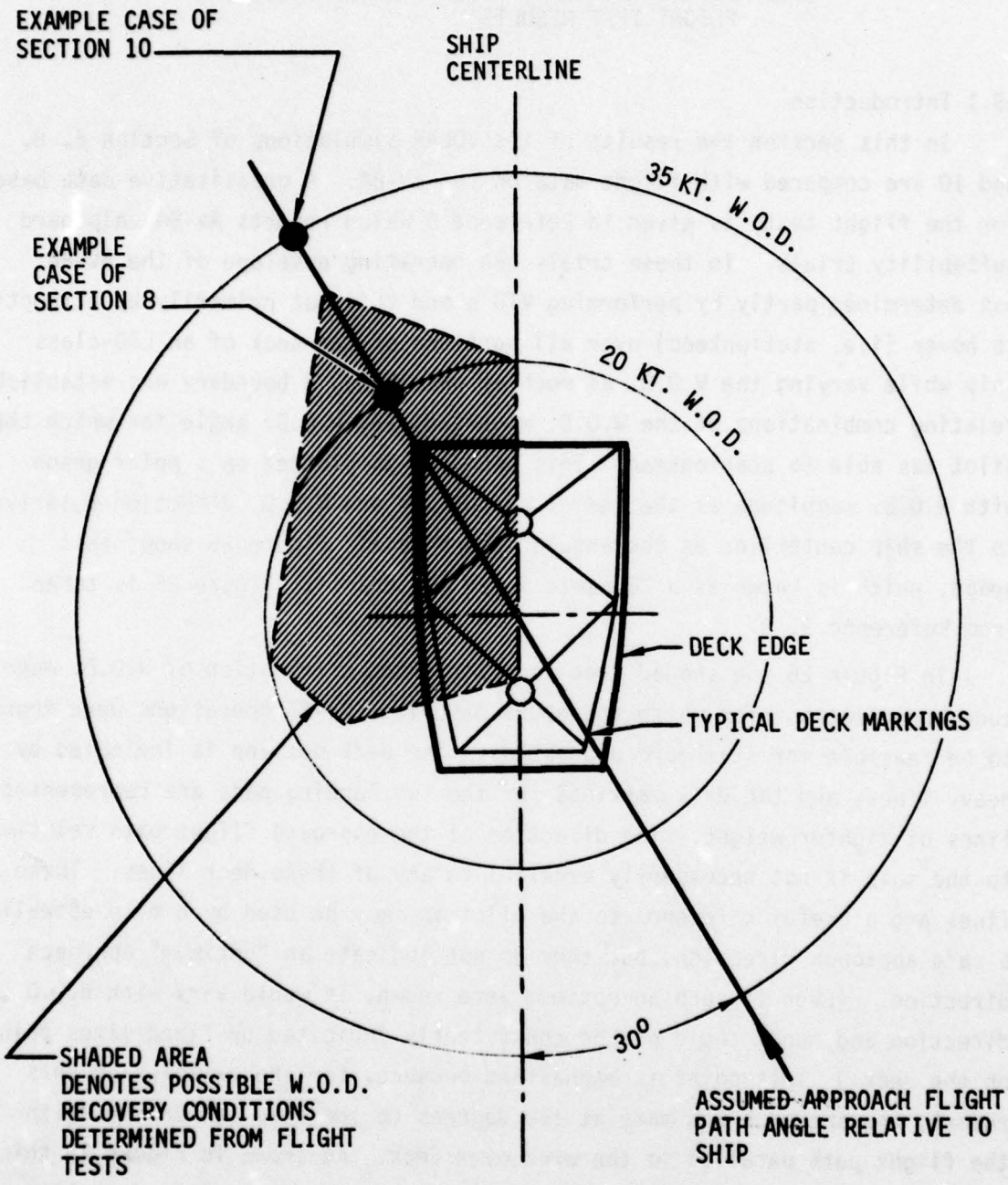


Figure 26 LPD Dynamic Interface Chart

The type of AV-8A used in the flight tests of Reference 9 was an early version of the MK. 50 Harrier - one of the first twelve AV-8A's. These aircraft had only a roll stability augmenter system which was of very limited authority, no head-up-display was employed,* and only daylight landings were performed. (Night landing attempts were made but these were not successful.) The AV-8A model employed for the VOLAR simulations did not include any S.A.S., since pilot comments indicated that the authority of the roll S.A.S. was so small that it was essentially ineffective.

13.2 Comparison with VOLAR results

The VOLAR simulations for the 20 knot and 35 knot W.O.D. conditions are directly compared on Figure 18, which shows the longitudinal state variables computed using the optimal pilot model. Figure 20 shows the lateral state variables computed using the classical pilot model.

It is evident from these figures that the pilot employs larger random control deflections for the 35 knot condition. Despite this, his control of the airplane is less precise. For example from Figure 18(h) the standard deviation of the airplane height relative to the deck near the instant of touchdown is 0.6m at 35 knots W.O.D. compared to less than 0.1m at 20 knots W.O.D. The pilot's random control activity has increased by a factor of approximately 6, as shown in Figure 18(d). In addition, the simulation of the lateral degrees of freedom for 35 knots W.O.D. (see Figure 10) indicated the lateral position error has a large random component with a standard deviation of 2.7 meters, even without including ship motion in the simulation. The trends computed by VOLAR are thus in agreement with the flight data.

The above correlation is encouraging, but it is clearly limited by the fact that the dynamic interface chart is more indicative of stationkeeping performance than of the complete recovery process. Definitive criteria for establishing safe operational boundaries are not known. Detailed flight test records are required to discover the quantitative limits on state and control variables that determine the boundary between acceptable and unacceptable approaches and for comparison to the simulated data.

*Subsequent AV-8A's incorporated a 3-axis S.A.S. similar to the AV-8B S.A.S. described in Reference 14, and also employed a head-up-display.

14.0 CONCLUSIONS

The VOLAR digital computer simulation program models the dynamics of launch and recovery of aircraft operating from ships. The program includes mathematical models for: the airframe and its control system, ship motion, the airwake, atmospheric turbulence, the display system and the human pilot. Helicopters or fixed-wing aircraft can be simulated. The current VOLAR ship motion airwake models have been specially developed for small ships but the program can simulate any type of aircraft and ship.

Using inputted statistical data on the airwake, ship motion and other disturbances, each VOLAR run computes time histories of the means and variances of all system state variables. The run time required is typically 7 percent of that required for a 200-run Monte Carlo simulation.

VOLAR simulations of AV-8A recoveries on a small LPD-class ship show good agreement with trends reported from flight experience. Variations of Sea State parameters and wind-over-deck were included in these simulations.

The VOLAR simulations presented here demonstrated the use of two alternative human pilot models. Both models are based on published data. One, the "classical" model involves a selection of parameters based on published verbal rules. It is therefore dependent to some extent on the user's interpretation of these rules. The alternative model, the "optimal pilot" model, is defined mathematically. This model is recommended because it is not subject to individual differences of interpretation. Currently, simulations using the optimal pilot model require approximately four times the run time required by the classical model. Simplification of the optimal pilot model should be explored in future work.

The work reported here was limited to developing the program and demonstrating its use by a few runs which were compared with AV-8A flight data. Further work should be directed at using the program to explore the effects on accuracy of variations in airframe characteristics, control power, approach direction and glideslope, ship size, displays, and piloting techniques.

REFERENCES

1. Houbolt, J. C., Atmospheric Turbulence, AIAA Paper 72-219, January 1972.

2. Kleinman, D. L., S. Baron, and W. H. Levison, An Optimal Control Model of Human Response, Part I. Automatica, Vol. 6, 1970, pp. 357-369.

3. Gelb, A., and R. S. Warren, Direct Statistical Analysis of Nonlinear Systems: CADET, AIAA J., Vol. 11, No. 5, May 1973, pp. 689-694.

4. Warren, R. S. and J. Siegel, SAM-D Performance Analyses Using CADET, Vols. I and II, TASC TR 268-1, -2, Contract DAAH01-72-C-0826, August 1973.

5. J. H. Taylor, "Handbook for the Direct Statistical Analysis of Missile Guidance Systems via CADET," The Analytic Sciences Corp., TR 385-2, ONR Contract No. N00014-73-C-0213, May 1975.

6. J. H. Taylor and C. F. Price, "Direct Statistical Analysis of Missile Guidance Systems via CADET, Final Report," ONR Contract No. N00014-73-C-0213, March 1976.

7. Abzug, M. J., User's Manual for FORTRAN COVAR Computer Programs, Aeronautical Consultant Associates, 14951 Camarosa Dr., Pacific Palisades, Ca. 90272, Rpt. ACA R-122, January 1976.

8. McRuer, D. T., I. L. Ashkenas, and F. D. Graham, Aircraft Dynamics and Automatic Control, Princeton University Press, Princeton, New Jersey, 1973.

9. Anon., AV-8A Shipboard Suitability Trials, Naval Air Test Center, Patuxent River, Md., Report No. FT-65R-73, 17 October 1973.

10. Hutchins, D. E., Review of U. S. Navy VSTOL Handling Qualities Requirements, Proc. Navy/NASA VSTOL Flying Qualities Workshop, April 1977, Naval Postgraduate School, Monterey, Ca., Published August 1977.

11. Fortenbaugh, R. L., A Math Model for the Airwake of a DE-1052 Class Ship, Vought Corporation, Report 2-53300/7R-3397, May 1977.

12. Fortenbaugh, R. L., Application of the Vought Small Ship Airwake Model for Starboard Approaches to DD-963 Class Ships, Vought Corporation, Report 2-55830/8AVO-153 (to be published in final report under Contract No. N62269-78-C-0129).

13. Nave, R.L., Progress Toward a Computerized VSTOL/Small Platform Landing Dynamics Investigation Model, NADC Report 77024-30, Naval Air Dev., Ctr., Warminster, Pa., 1977.

14. Anon., AV-8B Simulator Evaluation, VSTOL Performance, McDonnell Douglas Corp. Rept. MDC-A3922, Contract No. N00019-75-C-0487, March 1976.

15. Lebacqz, J. V., Summary Documentation of AV-8A Model Development and X-22A Simulation of AV-8B, Calspan Corp., Buffalo, N. Y., X-22A TM No. 98, W/A P63-054, July 1977.

16. Lacy, T. R., MIL-F-83300; View from an Aircraft Designer, Proc. Navy/NASA VSTOL Flying Qualities Workshop, April 1977, Naval Postgraduate School, Monterey, Ca., Published August 1977.

17. McRuer, D. T., and H. R. Jex, A Review of Quasi-Linear Pilot Models, Trans. 1.E.E.E., Vol. HFE-8, No. 3, September 1967.

18. Craig, S. J., and A. Campbell, "Analysis of VTOL Handling Qualities Requirements, Part I: Longitudinal Hover and Transition," AFFDL-TR-67-179, 1968.

19. Craig, S. J., A. Campbell, and R. H. Klein, "Analysis of VTOL Handling Qualities Requirements, Part II: Lateral-Directional Hover and Transition," AFFDL-TR-67-179, Part II, 1970.

20. Craig, S. J., I. L. Ashkenas, and R. K. Heffley, "Pilot Background and Vehicle Parameters Governing Control Techniques in STOL Approach Situations," FAA RD 72-69, June 1972.

21. Anderson, R. O., A New Approach to the Specification and Evaluation of Flying Qualities, AFFDL-TR-69-120, Wright-Patterson Air Force Base, Ohio: Air Force Flight Dynamics Laboratory, June 1970.

22. Dillow, J. D., The "Paper Pilot" - A Digital Computer Program to Predict Pilot Rating for the Hover Task, AFFDL-TR-70-40, Wright-Patterson Air Force Base, Ohio: Air Force Flight Dynamics Laboratory, March 1971.

23. Anderson, R. O., A. J. Conners, and J. D. Dillow, Paper Pilot Ponders Pitch, AFFDL-TM-70-1, Wright-Patterson Air Force Base, Ohio: Air Force Flight Dynamics Laboratory, November 1970 (Revised January 1971).

24. Nolting, D. L., Predicting Lateral Hover Flying Qualities with Paper Pilot, AFIT Thesis GA/MA-73A-2, Wright-Patterson Air Force Base, Ohio: Air Force Institute of Technology, December 1973.

25. Dillow, J. D., and D. G. Picha, Application of the Optimal Pilot Model to the Analysis of Aircraft Handling Qualities, AFIT-TR-75-4, Air Force Institute of Technology, Air University, Wright-Patterson Air Force Base, Ohio, 1975.

26. Baron, S., D. L. Kleinman, D. C. Miller, W. H. Levinson, and J. I. Elkind, Application of Optimal Control Theory to the Prediction of Human Performance in a Complex Task, AFFDL-TR-69-81, 1970.

27. Stengel, R. F., J. R. Broussard, P. W. Barry, and J. H. Taylor, Modern Methods of Aircraft Stability and Control Analysis, Report ONR-CR215-237-2, 1977.

28. Karmarkar, J. S., and J. A. Sorensen, Information and Display Requirements for Independent Landing Monitors, NASA CR-2687, 1976.

29. Phatak, A., H. Weinert, I. Segall, and C. N. Day, Identification of a Modified Optimal Control Model for the Human Operator, Automatica, Vol. 12, 1976.

30. Bryson, A. E., and Y. C. Ho, Applied Optimal Control, Blaisdell, Waltham, Mass., 1964.

31. Melsa, James L., and Stephen K. Jones, Computer Programs for Computational Assistance in the Study of Linear Control Theory, McGraw-Hill, Inc., 1973.

32. Brown, R. G., and F. A. Camaratta, Navairengcen Ship Motion Computer Program, Naval Air Engineering Center, Lakehurst, New Jersey, Report NAEC-MISC-903-8, 1977.

33. Fortenbaugh, R. L., Application of the NAEC Ship Motion Simulation Program for Starboard Approaches to DD-963 Class Ships, Enclosure to Vought Report 2-55830/8AVO-153, 1978.

34. Levey, H. C., The "Ground" Interference of a Carrier Deck, J. Roy. Aero. Soc., April 1957, pp. 276-281.

35. NATOPS Flight Manual, NAVAIR Rept. 01-AV8A-1, 1976.

36. Fozard, J. W., Sea Harrier - The First of the New Wave, Aeronautical J., January 1977, pp. 15-40.

37. Bryson, L. B., F. E. Heenan, C. A. Johnson, Helicopters in the Royal Navy, Aeronautical J., August 1972, pp. 469-500.